GLOBAL CHANGE AND ECOSYSTEM CHARACTERISTICS: SPATIAL/TEMPORAL VARIATIONS AND KEY CLIMATE/BIOLOGICAL DRIVERS OF NEE AND WSA IN THREE DISTINCT ECOSYSTEMS IN THE UNITED STATES

By

Zutao Yang

A DISSERTATION

Submitted to
Michigan State University
in partial fulfillment of the requirements
for the degree of

Geography - Doctor of Philosophy

2015

ABSTRACT

GLOBAL CHANGE AND ECOSYSTEM CHARACTERISTICS: SPATIAL/TEMPORAL VARIATIONS AND KEY CLIMATE/BIOLOGICAL DRIVERS OF NEE AND WSA IN THREE DISTINCT ECOSYSTEMS IN THE UNITED STATES

By

Zutao Yang

Ecosystem characteristics are continuously changing at a variety of spatial and temporal scales. Since ecosystems provide us essential services that are associated with ecosystem characteristics, it is critical to understand the spatial and temporal variations of ecosystem characteristics at different scales as well as their corresponding consequences and underlying drivers.

In this dissertation, I present three studies that investigate the temporal variations of NEE (net ecosystem exchange of CO_2) in a terrestrial ecosystem (i.e., Oak Openings in Ohio), of the temporal changes of water surface area (WSA) in a wetland ecosystem's (i.e., Prairie Pothole Region), and the spatial-temporal change of NEE and in an aquatic ecosystem (i.e., Western Lake Erie). I found that NEE in Oak Openings mostly varied at daily, seasonal, and annual time scales. At the daily scale, PAR is a more important meteorological driver than Ta (air temperature), while at the seasonal and annual scale, Ta is a more important meteorological driver than PAR. Additionally, vegetation phenology is another major driver of NEE variation at the seasonal and annual scales. The study in the Prairie Pothole Region (PPR) suggests that WSA is a linear function of the Palmer Drought Severity Index (PDSI). The PDSI of the year before last and the current year explain 79% of the annual variance of WSA. Also, past drought conditions were more important than current drought conditions in determining the current WSA of the potholes. Based on this model and future climate projection, WSA in PPR is predicted to lose over half of its current value by 2050s and retain less than one-third of itself by the 2080s. In western Lake Erie, neither strong diurnal course nor strong seasonal/ annual course of NEE were

found. However, monthly mean NEE and monthly mean chlorophyll-a were significantly correlated with 1-2 month lags, depending on the location. Chlorophyll-a was also found to affect the relationship between meteorological variables and NEE. During algal bloom seasons, daily PAR, Ta, wind speed, and VPD were significantly correlated with daily NEE; while during non-algal bloom seasons, no relationship was observed between them. Overall, studies in this dissertation suggest that NEE varied uniquely among different time periods, different frequencies, different ecosystems and locations, and WSA in PPR varied intra-annually and inter-annually. These variations were driven by a few key climatic and biological factors with long lasting or lagged effects.

This dissertation is dedicated to my parents, who give me endless love, support, and encouragement.

ACKNOWLEDGEMENTS

The author was supported by the Research Assistantship of Department of Geography at Michigan State University and the Teaching Assistantship of the Department of Environmental Science at University of Toledo. I would like to acknowledge my advisor – Dr. Jiquan Chen for his unconditional support and patient guidance through the research and PhD program. I thank Dr.Richard Becker at the University of Toledo for his full support when I was studying at the University of Toledo. I also acknowledge my doctoral committee members – Drs. Ashton Shortridge, Jiaguo Qi, Joseph P. Messina, and Peilei Fan for their valuable suggestions, advices, and assistances. I thank Carol Stepien, Kevin Czajkowski, Song, Qian, and Thomas Bridgeman from the University of Toledo, and Housen Chu, Changliang Shao, Ranjeet John, and all others in the LEES lab for valuable suggestions to improve the quality of my publication and for helping the field work and data collection. I appreciate Sharon Ruggles, Jean Lepard, Kathleen Mills, and Alan Arbogas for helping me transfer smoothly from University of Toledo to Michigan State University, and for logistical assistance during my PhD program. I also thank Gabriela Shirkey for editing my manuscripts and this dissertation.

TABLE OF CONTENTS

LIST OF TABLES

LIST OF FIGURES

KEY TO ABBREVIATIONS

AIC ……Akaike Information Criterion

CDOM …….....Color Dissolved Organic Material

COI …….....……Cone of Influence

CPA ……...Color Producing Agent

CSAT3 ……..... 3-dimensional Sonic Anemometer

CWT ……..Continuous Wavelet Transformation

CZCS …….Coastal Zone Color Scanner

EC ……..Eddy Covariance

ETM+ ……Enhanced Thematic Mapper Plus

Fc …….. Turbulent Exchange of CO_2

FT …….....Fourier Transformation

GHG ……..Greenhouse Gas

GLEON …….The Great Lake Ecological Observatory Network

GRACE ……Gravity Recovery and Climate Experiment

HAB ……..Harmful Algal Bloom

HTT ……...Hilbert-Huang transform

IPCC ……..Intergovernmental Panel on Climate Change

IRGA …….Infrared Gas Analyzer

LAI ……Leaf Area Index

MNDWI …… Modified Normalized Difference Water Index

MODIS ……..Moderate Resolution Imaging Spectroradiometer

NDVI …….Normalized Difference Vegetation Index

NDWI ……....Normalized Difference Water Index

NEE …….. Net Ecosystem Exchange

NEON ……The National Ecological Observatory Network

PAR …….. Photosynthesis Active Radiation

pCO_2…….. Partial Pressure of Carbon Dioxide

PDSI ……..Palmer Drought Severity Index

PPR ……Prairie Pothole Region

PWC ……..Partial Wavelet Coherence

RH …….Relative Humidity

SeaWIFS …….. Sea-Viewing Wide Field-of-View Sensor

SWC…….. Soil Water Content

Ta …….. Air Temperature

TM …….Landsat Thematic Mapper

U ……Horizontal Wind Velocity

USCCC ……. US-China Carbon Consortium

USDA ……U.S. Department of Agriculture

VPD …….. Vapor Pressure Deficit

WSA ……..Water Surface Area

WTC ……..Wavelet Coherence

XWT ……..Cross Wavelet Transformation

CHAPTER 1 INTRODUCTION

1.1 Overview

Ecosystem characteristics (i.e., processes/functions and properties/structures) are continuously changing at a variety of spatial and temporal scales. The rate of such change can either be dramatic and/or abrupt, as exemplified by geo-hazards and fire hazards, or subtle and/or gradual such as phenological changes and biomass accumulation. Both kinds of changes are important to our understanding of ecosystem resilience and our sustainable perspective (Landres et al. 1999, Coppin et al. 2004, Folke 2006, Pachauri et al. 2014).Ecosystems provide us essential services that benefit humankind; yet, the change of ecosystem characteristics alters these services. Causes and consequences of these changes can be both natural and human-related, or a combination of the two (Coppin et al. 2004). Because of this, it is critical to understand the change of ecosystem functions and structures at different spatial and temporal scales, as well as their corresponding causes and consequences. Moreover, accurate and continuous knowledge related to these changes are required for sustainable ecosystem management (Landres et al. 1999, Coppin et al. 2004).

Various aspects of ecosystem characteristics do not stand alone, but instead interact with, drive the change of, or respond to other internal characteristics or external variables at multiple temporal and spatial scales (Jones 2002). Ecosystem functions (e.g., net ecosystem exchange (NEE)), for example, are by definition related to the matter and energy cycles within the ecosystem, which could vary substantially in space and time. The functions are regulated by different biotic and abiotic components (e.g., vegetation properties, water availability, soil properties, climate conditions, etc.) that operate in a hierarchy of temporal and spatial scales (Chapin et al. 2002). On the other hand, ecological processes or functions also change ecosystem

properties in many ways (Jones 2002). To give a few examples, NEE is directly related to existing biomass in growing seasons within temperate forests (Maselli et al. 2009, Garrity et al. 2011, Xie et al. 2014a); lateral inputs of nutrients to coastal water can lead to an algal bloom that further alters both the biotic and the abiotic conditions of the water (Livingston and Prasad 1997, Anderson et al. 2002); and evaporation, an important ecosystem processes in lakes and wetlands, can reduce surface water and wetlands and can therefore change many services and characteristics of wetland ecosystems (Zedler and Kercher 2005, Reis and Yilmaz 2008, Tong et al. 2014). Ecosystem characteristics present spatial and temporal variations within all these complex interactions and changes; thus, there needs to be more research to improve our overall understanding of these dynamics.

Global change (e.g., climate warming, land use/land cover change, population increase, etc.) has in some way magnified changes within ecosystems. These rapid changes will have both direct and indirect effects on global ecosystems, and in return, will affect the services humankind receives (Pachauri et al. 2014). As a result, temporal and spatial variations of many important ecosystem characteristics have recently received wide attention. Published studies have considered the temporal and spatial variations of many important ecosystem characteristics, such as ground water quality and level (Ahmadi and Sedghamiz 2007, Schot and Pieber 2012), vegetation biomass and yield (Schmer et al. 2010, Meng et al. 2013), chlorophyll-a and water quality in coastal and lake water (Xu et al. 2004, Ali et al. 2014), productivity and evapotranspiration/evaporation in both land and water (Assouline and Mahrer 1996, Mainuddin and Kirby 2009, Sun et al. 2013), soil moisture and respiration (Epron et al. 2004, Wilson et al. 2004, Khomik et al. 2006, Avila et al. 2011), to name a few. Long-term observation networks (e.g., NEON,GLEON, and FLUXNET) are developed for network science as a tool to facilitate

the study of spatial and temporal variability of ecosystem characteristics. The knowledge of spatial and temporal changes of ecosystem characteristics gained from all local and regional studies is important for future human adaptation to global changes (Pachauri et al. 2014). In this dissertation, a focus on spatial and temporal change of NEE and WSA, as well as their climate or biological drivers will be presented within three case studies. NEE is an important ecosystem function or process in both terrestrial and aquatic ecosystems, while WSA is an important ecosystem property or structure especially for wetlands. NEE is one of the most important components of carbon cycling, and offers important feedback on climate change. Commonly, NEE is taken as the starting point in the construction of more complete GHG (Green House Gas) balances of an ecosystem (Jacobs et al. 2007). Knowledge about its temporal change at different scales of individual ecosystems is critical to modeling efforts that quantify the global carbon cycle (Stoy et al. 2009). WSA, on the other hand, is critical for a wetland ecosystem to maintain its diversity of ecosystem services and plant and animal life. Losing WSA leads to a reduction of wetland ecosystems (Zedler and Kercher 2005).To increase and update our knowledge related to changes of NEE and WSA, I conducted three case studies. The first investigates the variation of NEE at different time scales and some of its important biotic/abiotic drivers in a rare terrestrial ecosystem (i.e., Oak Openings in Ohio). The second study examines the variation of WSA in an important wetland ecosystem (i.e., Prairie Pothole Region) and its sensitivity to drought. The last one to investigate the changes of NEE in an unique aquatic ecosystem (i.e., Western Lake Erie with its infamous algal blooms) and the biophysical and climate drivers of the change. The location and a landscape overview of each of these three ecosystems are shown in Figure 1.1.

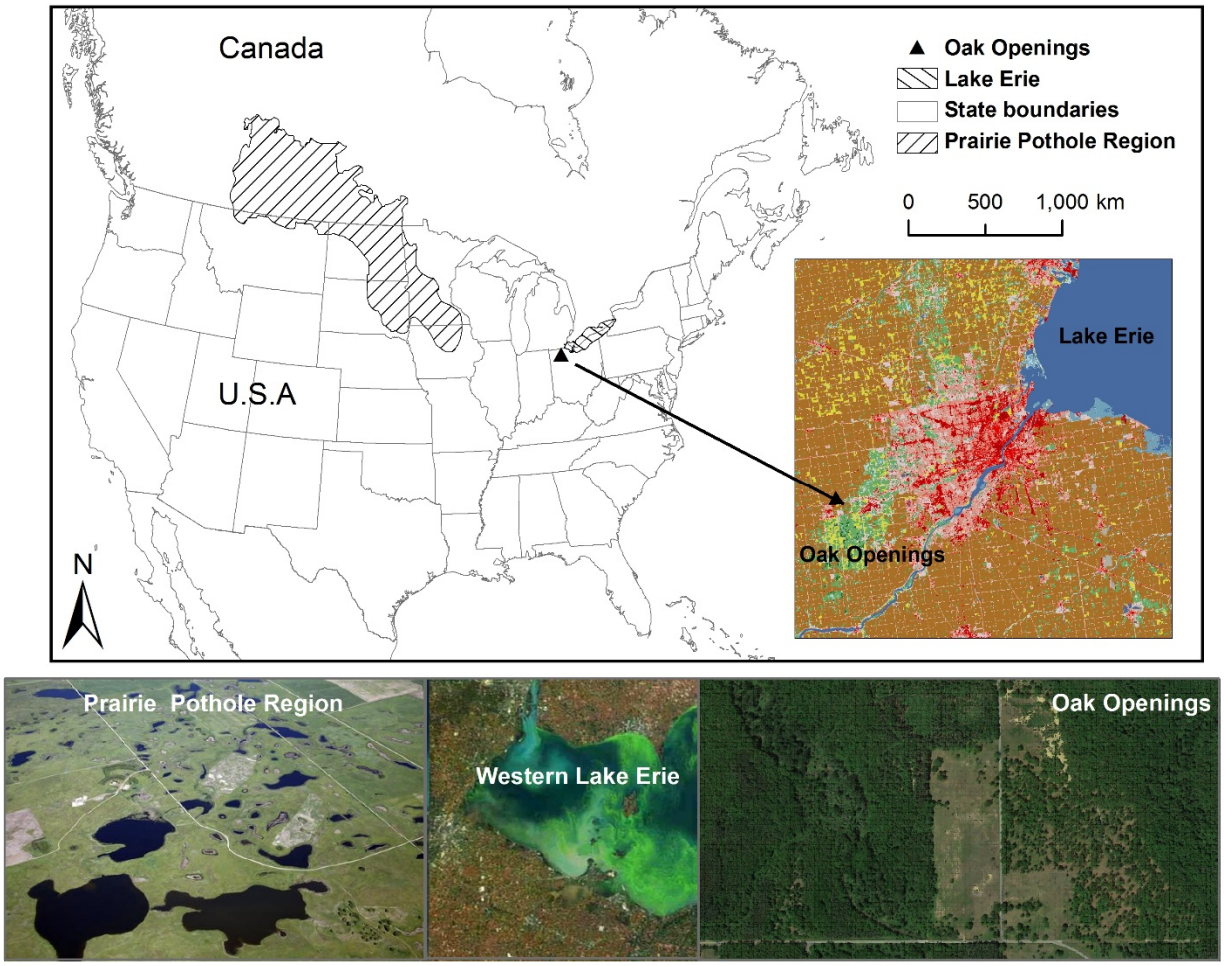

Figure 1.1, The location of the three ecosystems studied in this dissertation and their landscape views from aerial photographs or satellite images.

These three case studies strongly rely on available long-term data and large-scale spatial data to examine spatial and temporal variations. Remote observation of the earth via satellite has been available for decades at varying spatial and temporal resolutions. Weather stations that record daily meteorological conditions have been used in climate observation for over half a century in most countries. Recently, eddy covariance (EC) towers have provided direct measures of NEE over a diverse group of ecosystems at 30-min intervals for years. These data and

techniques provide us with a great opportunity to study temporal-spatial variability, especially long-term variability of some important ecosystem functions and structures, and the related drivers. In this dissertation, we take advantage of the integration of multiple remote sensing products, climate data measured from weather stations, and flux data measured by EC towers, to study ecosystem processes and properties that relate to water and carbon.

1.2 Objectives and hypotheses

This dissertation targets three contrasting ecosystems: Ohio Oak Openings, Western Lake Erie, and the Prairie Pothole Region (PPR). Oak Opening is a rare land ecosystem, Lake Erie is a unique water ecosystem, and PPR include precious wetland ecosystems linking the land and the water. These three ecosystems were all formed by the last glacial retreat, but now are rare and unique ecosystems with a substantially reduced area. They are all sensitive to global changes, especially climate change and intense human activities. PPR contains thousands of shallow wetlands known as potholes, but over half of these potholes have been drained and converted to agriculture. As these potholes has few natural drainage systems, they also tend to dry up as climate is warming. Most original parts of the Oak Openings have been lost by human destruction; more so, this land type is rare now that just over 130 square miles are left across the globe. These openings are also sensitive to climate change due to the sandy soils and frequent wildfires. Anthropogenic activities has caused eutrophic problems for Lake Erie for decades. Lake Erie is the southernmost and shallowest lake among the five Great Lakes, thus it is more vulnerable to climate change.

The main goal is to examine temporal and spatial variations of NEE and WSA as well as their driving mechanisms, including the biological and climate drivers. Climate drivers are highlighted in this dissertation because NEE and WSA have important feedback useful to global carbon/water cycling and climate change research. Biological properties are highlighted because they respond to and affect climate change by changing carbon cycling.

Climate change is reported as an important driver for the change of both wetland size (Hayal et al. 2012) and NEE (Huxman et al. 2004, Liu et al. 2005, Urbanski et al. 2007, Kwon et al. 2008). In terrestrial ecosystems, climate and meteorology can regulate NEE directly or

indirectly through the phenology of vegetation (Chapin et al. 2002). In aquatic systems, processes related to NEE, such as the growth of algae, the mixture of different water layers, and the community respiration, etc., are all associated with the change of weather and climate (Wetzel 2001, Dodson 2004). Aside from effects caused by agriculture and urbanization, wetlands are also sensitive to climate change, especially temperature increases and decreased precipitation, which reduce essential waters for a wetland ecosystem (Johnson et al. 2005).

Biological properties (e.g., the green biomass) is directly related to the amount and variation of NEE though photosynthesis and respiration (Goulden et al. 2004, Xiao et al. 2004, Richardson et al. 2009). In lakes, algae that contains chlorophyll-a could be the main producer. Algae take in dissolved CO_2 through photosynthesis in water, and may change the CO_2 balance between surface water and the above atmosphere (Wetzel 2001, Dodson 2004).

As a result, the general questions in this dissertation investigate how important carbon/water related ecosystem characteristics (i.e., NEE and WSA) change over space and time and how meteorological/climatic variables (e.g., radiation, temperature, moisture, etc.) and biological variables (e.g., LAI and chlorophyll-a) could cause these variations. Herein, I also structure the specific sets of more detailed hypotheses and research questions that I attempt to answer through three case studies.

First, I examined the carbon process NEE in a land ecosystem, Ohio's Oak Openings. Specifically, I examined the variations of NEE at many temporal scales and the confounding effects of meteorological drivers, PAR (photosynthesis active radiation), and Ta (air temperature) (Chapter 2) at these scales. I aim to address questions: 1) what are the most variable time scales of NEE; and 2) how do Ta and PAR affect NEE differently at these main temporal scales? I hypothesize that the variations of NEE are distributed unevenly at different time scales,

and that PAR and Ta play different roles at different time scales. Addressing such questions is important for understanding carbon cycling because NEE is not stationary or composed of components varying at different frequencies (time scales) that are regulated by different processes and because the major signals and the corresponding drivers need to be captured for accurately modeling NEE.

I then investigated one of the most important water and carbon related characteristics, WSA, in the Prairie Pothole Region wetland ecosystem. In particular, the inter-annual and intra-annual change of WSA in the pothole wetlands and the climatic drivers were examined (Chapter 3). I aim to address how drought can reduce the WSA of these precious wetlands, how such a loss of wetland will affect regional water and carbon processes, and other as environmental processes. The hypotheses are: wetlands in the Prairie Pothole Region are highly sensitive to the drought and that drought could have long lasting effects on these wetlands.

Lastly, I investigated a water ecosystem known as western Lake Erie. I examined the variations of NEE at many temporal scales, the potential effects of meteorology and chlorophyll-a on NEE, but focused ultimately on the possible influences of algal blooms on carbon processes NEE (Chapter 4). The following questions are addressed: 1) Does NEE and chlorophyll-a vary both spatially and temporally; 2) Does algal bloom affect NEE directly and indirectly? I hypothesized that both NEE and chlorophyll-a would present some seasonal patterns, chlorophyll-a would vary substantially in space, and that NEE would also differ between sites. I also hypothesized that chlorophyll-a, which served as a proxy of algae biomass, would only have a relationship with NEE at long time scales (i.e., month-season) and that the relationship between meteorological drivers and NEE would change under different concentrations of chlorophyll-a at short time scales (i.e., daily).

In summary, I studied three contrasting and unique ecosystem ranging across land, wetlands, and water in this dissertation in order to understand spatial-temporal changes in two important carbon/water ecosystem characteristics, NEE and WSA, and to understand the key climate and biological drivers by analyzing long-term time series records and large scale spatial data (Figure 1.2).

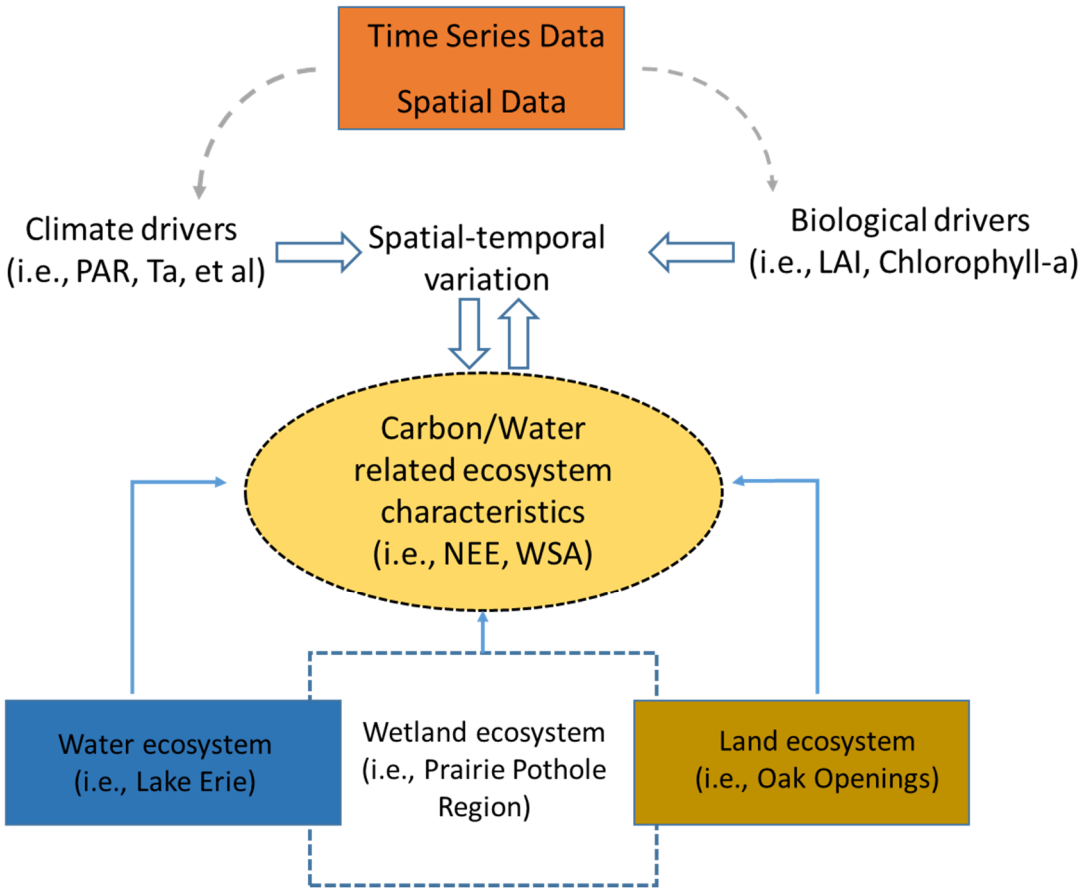

Figure 1.2, A conceptual diagram of the study framework of this dissertation.

CHAPTER 2 DISENTANGLING THE CONFOUNDING EFFECTS OF PAR AND AIR TEMPERATURE ON NET ECOSYSTEM EXCHANGE AT MULTIPLE TIME SCALES

Abstract

Net ecosystem exchange of CO_2 (NEE) in temperate forests is modulated by multiple microclimatic factors. The effects of these factors vary across time scales, with some correlated to produce confounding effects. PAR and air temperature (Ta) are among the two most important drivers of NEE in temperate forests and are highly correlated because of their similar diel and annual cycles. In this chapter, I attempted to disentangle the confounding effects of them on NEE at multiple time scales. I applied innovative spectral analysis techniques, including the Continuous Wavelet Transformation (CWT), Cross Wavelet Transformation (XWT), Wavelet Coherent (WTC), and Partial Wavelet Coherence (PWC), on a seven-year time series (2004-2010) of PAR, Ta, and NEE from the Ohio Oak Openings Ameriflux site (N 41.5545°, W 83.8438°), USA. I found that PAR was the primary driver of NEE oscillation at short time scales (e.g., multi-hour and daily), while Ta dominated as the driver of NEE oscillation at long time scales (e.g., seasonal to annual). At the daily scale, PAR co-varied with NEE without time lag, while Ta lagged NEE for 2-3 hours during growing seasons, which could be explained by the strong dependence of NEE on photosynthesis anda time lag of 2-3 hours of daily course Ta to that of PAR. At the daily scale during the non-growing seasons, NEE varied little and co-varied with Ta and PAR with none high common power. At the annual scale, Ta co-varied with NEE with no time delay, but PAR lead NEE by about one month. This can be explained by the strong dependence of leaf area index (LAI) on Ta as well as the lag between the LAI/biomass development and the progress of sunlight. I also found that NEE distributes most of its variation

at seasonal and annual scales, suggesting that Ta is more important than PAR in determining the annual and long-term carbon budget.

Keywords: Carbon Flux, Wavelet Analysis, Temperate Forest, Environmental Drivers

2.1 Introduction

Our knowledge about the variability of the net ecosystem exchange (NEE) of CO_2 in terrestrial ecosystems at multiple time scales remains poor yet it is critical to global modeling analyses for quantifying the terrestrial carbon cycle(Stoy et al. 2009). NEE is simultaneously modulated by multiple physical and biological forcing factors that constantly change over time with unique magnitudes and frequencies(Baldocchi et al. 2001, Baldocchi and Wilson 2001, Stoy et al. 2005, Stoy et al. 2009). The daily and seasonal progression of sunlight and temperature, precipitation events, the seasonal changes of plant structure, and the decadal succession of plants are obvious examples. Ecosystem functions (*e.g.*, NEE) respond to these forcing factors and their variability are the transferred variability of these drivers.

The response of NEE to each environmental driver varies by time scales. At the hourly scale, NEE variations are likely to be forced by changes in photosynthesis, stomatal conductance, and respiration that are controlled by sunlight and temperature (Baldocchi et al. 2001) and precipitation events (Stoy et al. 2005). At the daily scale, they are forced mostly by daily rhythms of solar radiation, air and soil temperature, humidity, and atmospheric CO_2 concentration (Jarvis et al. 1997, Baldocchi et al. 2001). Weather patterns/changes associated with the passages of high- and low-pressure systems, fronts, and precipitation can cause weekly fluctuations in NEE (Baldocchi and Wilson 2001, Stoy et al. 2005). At monthly, seasonal, and annual scales, NEE experiences the effects of seasonal changes in sunlight, temperature, soil water balance, leaf dynamics, phenology, drought/wet events, and growing season duration(Baldocchi et al. 2001, Goulden et al. 2004, Stoy et al. 2005, Stoy et al. 2009). At multi-year scales, long-term climatic changes (*e.g.*, *El Nino, La Nina* cycles) and ecological dynamics (e.g., succession) and environmental changes (e.g., N deposition, CO_2 fertilization) may be more

responsible for the NEE variations (Baldocchi et al. 2001, Stoy et al. 2005). Despite this general knowledge, few efforts have been made to thoroughly examine the changes of variations in NEE and its drivers across multiple time scales.

Ecosystem models synthesizing terrestrial carbon exchange often represent an explicit hypothesis on how an ecosystem transfers variability from microclimatic drivers to ecological responses, such as NEE and energy fluxes. However, Stoy et al. (2013) evaluated the wavelet coherence between measurements and several NEE models at multiple time scales and found that the mechanisms for diurnal and annual NEE variability require further improvement to correctly simulate the magnitude of fluxes. This suggests some of the explicit hypotheses might be wrong or not accurate enough, due partially to the fact that the modulating effects of the microclimatic drivers may vary across time scales, and drivers might be correlated to produce confounding effect. Temperature (*e.g.* Ta), radiation (*e.g.* photosynthetically-active radiation, PAR), and water (*e.g.*, precipitation) are among the most important microclimatic drivers that modulate the magnitude and frequency of carbon flux in temperate forests (van Dijk et al. 2005) and have always been important variables in ecosystem models (Liu et al. 1997, Xiao et al. 2004, Urbanski et al. 2007). However, among the three, PAR and Ta are highly correlated at multiple time scales because they have similar diurnal and seasonal cycles and thus may produce strong confounding effects. This inspired us to further confirm, refine, and adjust the effect of Ta and PAR on NEE across time scales (especially daily, seasonal, and annual scales). Here, I collected seven years of meteorological and flux measurements at the Oak Openings site in northwest Ohio with the objectives to explore the variability of NEE at multiple temporal scales and to disentangle the effects of Ta and PAR on regulating NEE. This site is ideal for disentangling the confounding relationship between Ta and PAR, because it is a mature forest without any severe

disturbance to cause long-term directional changes of NEE, and data records is long and complete. I excluded precipitation in our analysis because: 1) its effects have been reported in our previous studies (Noormets et al. 2008, Xie et al. 2014a), 2) it is a stochastic event and lacks regular daily and seasonal patterns, and 3) it is weakly correlated to Ta and PAR. Soil moisture and air humidity could also be an important drivers of NEE at our targeted ecosystem, but this chapter aim to disentangle the effect so of PAR and Ta, and thus I exclude soil moisture too, but included some figures into the supplemental materials to show its effects (APPENDIX A, Figure A.5 and A.6). However, I included leaf area index (LAI) to assist our analysis because it is the most important biological driver of NEE and is highly correlated with PAR and Ta at seasonal to annual scales (Chen et al. 2002).

A spectral analysis of NEE and its driving force are especially well-adapted to achieve our study objectives. The Fourier transform (FT) technique can be applied to analyze the frequency spectrum of the time series and determine the magnitude of frequencies, but not on the timing of particular frequency components (Massel 2001). Thus, the FT is only appropriate for stationary signals with constant frequency components present throughout the records. The non-stationarity nature of the flux measurements requires time-varying statistics that can decompose signals into the time-scale domain. A recently-developed method, Hilbert-Huang transform (HHT), does a good job to tackle non-stationary and nonlinear data (Huang and Wu 2008), but it is only empirically based and is at its early stage with difficulties in dealing with two or more time series simultaneously. Alternatively, a suite of wavelet analysis tools is ideally suited to the analysis of multi non-stationary signals (Torrence and Compo 1998, Grinsted et al. 2004, Cazelles et al. 2008). Continuous wavelet transform (CWT) that employs a finite basis function, aka “mother wavelet”, which is translated (shifted) and dilated (expanded and contracted) across a signal, can

quantify the time series signal variance across both time and frequency. In addition, cross-wavelet analysis (XWT) is able to expose the common power and relative phase in time-frequency space of two time series. The wavelet coherence (WTC), a measure of wavelet coherence, can detect the significant coherence against noise, even when the common power is low between the two time series. The partial wavelet coherence (PWC), a technique similar to partial correlation, can identify the resulting wavelet coherence between two time series after eliminating the influence of a third common dependence (Ng and Chan 2012). Because of these unique features, I chose to employ them in this case study to achieve our study objectives. I hypothesized that PAR is the major driver at short scales (*e.g.*, hours, day) and Ta is the major driver at long scales (season, year). Specifically, I: (1) quantified the variability of NEE across multiple time scales (2) investigated the scale-dependent relationships between Ta/PAR and NEE.

2.2 Methods

2.2.1 Site characteristics

Our study site is located in a 70-year-old oak-dominated forest within Oak Openings Preserve Metropark near Toledo (N 41.55°, W 83.84°) in northwest Ohio, USA. The forest comprises a mosaic of oak (*Quercus spp*.) woodlands, maple (*Acer spp*.) floodplains, remnants of oak savanna, and barrens and prairie (Brewer and Vankat 2004). The topography is flat with an elevation range of 200–205 m. The long-term mean annual air temperature is 9.2 °C and the annual total precipitation is 840 mm (Noormets et al. 2008). The height of the dominant trees is ~24 m, with an average canopy height of ~20 m. An open path eddy-covariance (EC) system was mounted on the top of a 34-m tower surrounded by uniform canopy in all directions with similar species and age composition(Xie et al. 2014a).

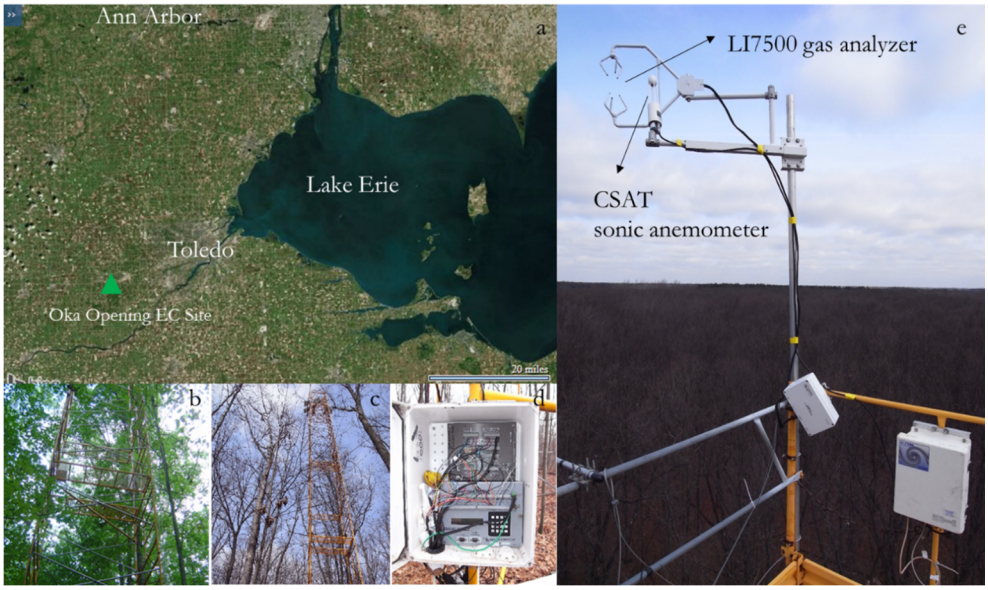

Figure 2.1, The location of the study site (a), side views of the EC tower in both summer (b) and winter (c) , the CR5000 data collection logger (d), and EC systems (LI-7500 and CSAT3, e)

2.2.2 Flux measurement

Turbulent exchanges of CO_2 (Fc) between the forest and the atmosphere were measured using the EC method (Lee et al. 2004) since November, 2003. The EC system consists of a LI-7500 infrared gas analyzer (IRGA; Li-COR Biosciences, Lincoln, NE, USA) that measures high frequency CO_2 densities and a 3-dimensional sonic anemometer (CSAT3; Campbell Scientific, Inc. (CSI), Logan, UT, USA) that measures wind speed/directions. Raw data spikes (>6 standard deviations) were removed; wind coordinates were rotated to mean streamline plane calculated from wind data over an entire year(Wilczak et al. 2001); and temperature was corrected for changes in atmospheric humidity and pressure(Schotanus et al. 1983). Each 30-min mean flux value was then calculated as the covariance of vertical wind speed, air temperature, and CO_2 densities using the Webb–Pearman–Leuning correction(Webb et al. 1980, Massman and Lee 2002). The warming of the IRGA above air temperature was corrected to 30-min fluxes(Grelle and Burba 2007). The 30-min NEE ($umol CO_2\ m^{-2}\ s^{-1}$) was calculated as the sum of turbulent flux and the CO_2 storage estimated as mean rate of 30-min change in CO_2 concentrations measured within the canopy.

To exclude outliers and bad data, all 30-min flux data from the EC tower were quality checked, including stationarity, integral turbulence characteristics, and friction velocity thresholds (Noormets et al. 2008). As a result, gaps exist for long time series NEE (Table 2.1).

Table 2.1, The gap percentage of NEE, PAR and Ta time series in each year of the whole year (before the slash) and of the growing season (after the slash) as defined from May to October here.

	2004	**2005**	**2006**	**2007**	**2008**	**2009**	**2010**
NEE	48.4/50.0	43.2/31.6	46.7/41.2	46.7/46.8	41.8/24.0	37.1/29.2	44.5/33.1
PAR	35.5/3	2/0	5/0	31.4/27.0	19.8/2	9.5/3	0/0
Ta	34.0/0	4/0	5/0	24.7/21.1	0/0	0/0	0/0

The gaps were filled using a dynamic parameter process model (Moffat et al. 2007). First, a respiration model was parameterized from nighttime data to fill nighttime NEE (e.g. ER, the respiration):

$$ER = R_{10} e^{E_a / R(1/R_{ref} - 1/(T_a + 273.15))} \qquad (1)$$

where R_{10} is the reference respiration (μmol CO_2 m^{-2} s^{-1}), E_a is the activation energy (kJ mol^{-1} K^{-1}), R is the universal gas constant (8.3134 J mol^{-1} K^{-1}), and T_a is the air temperature above the canopy (°C). Daytime ER was then estimated from Eq. (1), assuming consistency of temperature sensitivity between nighttime and daytime gas exchanges. The daytime NEE was then filled with:

$$NEE = ER + (\alpha \cdot PAR \cdot P_{max}) / (a \cdot PAR + P_{max}) \qquad (2)$$

where α is the apparent quantum yield (μmol $CO_2 \mu mol^{-1}$ PAR), PAR has a unit of $\mu mol m^{-2}$ s^{-1}, and P_{max} is the maximum apparent photosynthetic capacity of the canopy (μmol CO_2 m^{-2} s^{-1}).

2.2.3 Meteorological and vegetation measurements

Ta (°C) was measured by a HMP45AC probe (Vaisala, Finland) and PAR ($umol m^{-2} s^{-1}$) by a LI-190SB Quantum sensor (Li-COR) above the canopy at the same height as the IRGA every 20 s, which were then used to calculate the 30-min means. The original Ta and PAR 30-min series also included gaps due to sensor failure (Table 2.1). Short gaps (<1.5 h) were filled by linear interpolation and longer gaps (≥1.5 h) were filled using the Mean Diurnal Variation method (Falge et al. 2001). The LAI 8-day composite as a proxy of vegetation ($m^2 m^{-2}$) was obtained from the 1-km resolution MODIS LAI/FPAR Collection 5 (http://daac.ornl.gov/MODIS/modis.shtml) with an online subset output of a 3 km × 3 km pixel matrix centered on the flux tower. The average value of the nine pixels who passed data quality control were used to compose the LAI time series.

2.2.4 The Continuous Wavelet Transform (CWT)

The wavelet transform analyzes time series that contain non-stationary power at many different frequencies (Daubechies 1990). A wavelet is a function with a zero mean localized in both frequency and time and characterized by localized time (Δt) and frequency (Δw or the bandwidth). According to the classical Heisenberg uncertainty principle, there is always a tradeoff between localization in time and frequency. One particular wavelet, the Morlet wavelet (with $w_0 = 6$), provides a good balance between the localization of time and frequency. I applied it as the mother wavelet in our analyses. The Morlet, consisting of a plane wave modulated by a Gaussian, is defined as:

$$\psi_0(\eta) = \pi^{-1/4} e^{iw_0\eta} e^{-\eta^2/2} \qquad (3)$$

where w_0 is dimensionless frequency and η is dimensionless time.

The idea behind the CWT is to apply the wavelet as a band pass filter to a time series. The mother wavelet is stretched in time by varying its scale and normalizing it to have unit energy. Therefore, CWT can be thought of as a consecutive series of band-pass filters applied to a time series. The CWT of a time series X with uniform time steps (δ_t) is defined as the convolution of X with the scaled and normalized mother wavelet:

$$W_n^X(s) = \sqrt{\frac{\delta_t}{s}} \sum_{n'=1}^{N} x_n \psi_0[(n'-n)\frac{\delta_t}{s}] \qquad (4)$$

where n=1, . . ., N, s is the set of scales used. The wavelet power is defined as $|W_n^X(s)|^2$. Because the mother wavelet cannot be completely localized in time, the CWT has edge artifacts. It is therefore a Cone of Influence (COI) that was introduced as the area where errors will occur to the wavelet power at the beginning and end of the wavelet power spectrum (Torrence and Compo 1998). Many geophysical time series have distinct red noise characteristics; thus, a 5% significant level against red noise needs to be tested. The method for significance tests were described in Grinsted et al. (2004). I adopted the ecosystem spectral transfer function (EST) from Stoy et al.(2009), which is defined as:

$$EST_{X_1,X_2} = \log \frac{W^{X_1}(s)}{W^{X_2}(s)} \qquad (3)$$

X_1 is "amplified" ("dampened") by X_2 if EST_{X_1,X_2} is positive (negative). The concepts of amplifying and dampening come from signal processing literature, which need not imply causality in systems that respond to many factors (Stoy et al. 2009) but are useful to ascertain or deduce the simplest driver-response relationships across scales of time.

2.2.5 The Cross Wavelet Transform (XWT)

The XWT of two time series X and Y is defined as $W^{XY} = W^X W^{Y*}$, where * denotes complex conjugation. The cross wavelet power is defined as $|W^{XY}|$. The XWT reveals areas with high common powers for two time series but does not necessarily suggest a high coherent or cause and effect relationship unless the two time series are phase-locked. The complex argument arg (W^{XY}) can be interpreted as the local relative phase between X and Y and drawn in the time frequency space of XWT (*e.g.*, Figure 2, 3 and 4) as arrows. Arrows pointing down are interpreted as X leading Y by 90° or lagging Y by 270°. Arrows pointing up are interpreted as X lagging Y by 90° or leading Y by 270°. Arrows pointing left and right can interpreted as anti-phase and in-phase, respectively.

2.2.6 The Wavelet Coherence (WTC)

I used the WTC to quantify the coherence of the two time series of XWT in time-frequency/scale plane. High coherence between two time series can happen at frequencies and time periods where their common wavelet power is not necessarily high. The WTC is a tool for identifying possible relationships between two processes by searching frequency bands and time intervals during which they co-vary (Ng and Chan 2012). The WTC squared of two time series X and Y is defined as (Grinsted et al. 2004):

$$R_n^2(x,y) = \frac{|S(s^{-1}W_n^{XY}(s)|^2}{S(s^{-1}|W_n^X(s)|^2) \cdot S(s^{-1}|W_n^Y(s)|^2)} \qquad (4)$$

where S is a smoothing operator and W is the WTC operator. This definition closely resembles the traditional correlation coefficient and is useful to think of the WTC as a localized correlation coefficient in time frequency space (Grinsted et al. 2004). When there is real significant

relationship between two phenomena, it is shown in the WTC time frequency space. The S operator can have varying forms and produce a large impact on the significant level. I followed the form of Torrence and Webster (1998) for the Morlet wavelet.

2.2.7 The Partial Wavelet Coherence (PWC)

The PWC is a new wavelet analysis technique recently introduced by Mihanovic et al. (2009) to the field of marine science together with another new wavelet tool of multiple wavelet coherence (MWC). The idea of the PWC is to calculate the resulting WTC for two time series after removing their common dependent factors. The PWC is a technique similar to partial correlation that helps find the resulting WTC between two time series Y and X_1 after eliminating the influence of the time series X_2 when X_1 and X_2 are not independent (Ng and Chan 2012). The PWC square is defined as:

$$RP^2(y, x1, x2) = \frac{|\, R(y, x1) - R(y, x2) \cdot R(y, x1)^* \,|^2}{[1 - R(y, x2)]^2 [1 - R(x2, x1)]^2} \qquad (5)$$

where R is the WTC operator.

2.2.8 Wavelet analysis

I used non-gap-filled data for wavelet analysis because gap-filing can bring artificial correlations that will contribute to wavelet common power or coherence. However, a tradeoff is that we will lose information at time scales shorter than the length of the gaps during periods with the gaps; gaps will sometimes bias wavelet calculation at scales longer than the length of the gaps. Additionally, when three time series were analyzed together by the PWC, gaps are more likely to cause problems and confound the results. Therefore, WTC were also used on gap-filled data for the interpretation and PWC was only applied to gap-filled data. The WTC analysis

related LAI to NEE, PAR, and Ta was also conducted to clarify the effects of PAR and Ta at seasonal scales. Each time series was normalized to have zero means (with zeroes in gaps when gapped data were used) and unit variances for cross comparison. MATLAB codes distributed by Ng and Chan (2012) (http://www.cityu.edu.hk/gcacic/wavelet/) were modified for all wavelet analysis. A 5% significant level against red noise was tested through the Monte Carlo simulations (Grinsted et al. 2004)

2.3 Results

2.3.1 Oscillations of NEE in time and scale

The magnitudes of NEE oscillation varied across time scales but were mainly at four scales: the diurnal (*i.e.*, ½ day), the daily, the seasonal, and the annual (Figure 2.2). At the annual scale, significant oscillations appeared constant throughout the entire measurement period. Significant oscillations were also observed at seasonal scales and peaked at *c.a.* 170-180 day (i.e., equivalent to the growing season length) continuously throughout the 7-year study period, except the significant oscillations at scales from *c.a.* 40 days to *c.a.* 150 days in 2006, likely because of a large number of short gaps during the growing season. At the daily scale, however, significant oscillations were found during the growing seasons. Oscillations at the diurnal scale were also obvious during the growing seasons (Figure 2.2a), but the average oscillation power is much lower than that at the daily scale (Figure 2.2b). Oscillations at scales from weekly to monthly were also apparent as a few hotspots (i.e., red areas in the time-scale half-plane with high wavelet power enclosed by thick contours, which represent 5% significance level against the red noise) in some years. Generally, more variance was distributed at the long scales (the seasonal and annual) than at the short scales (the diurnal and daily).

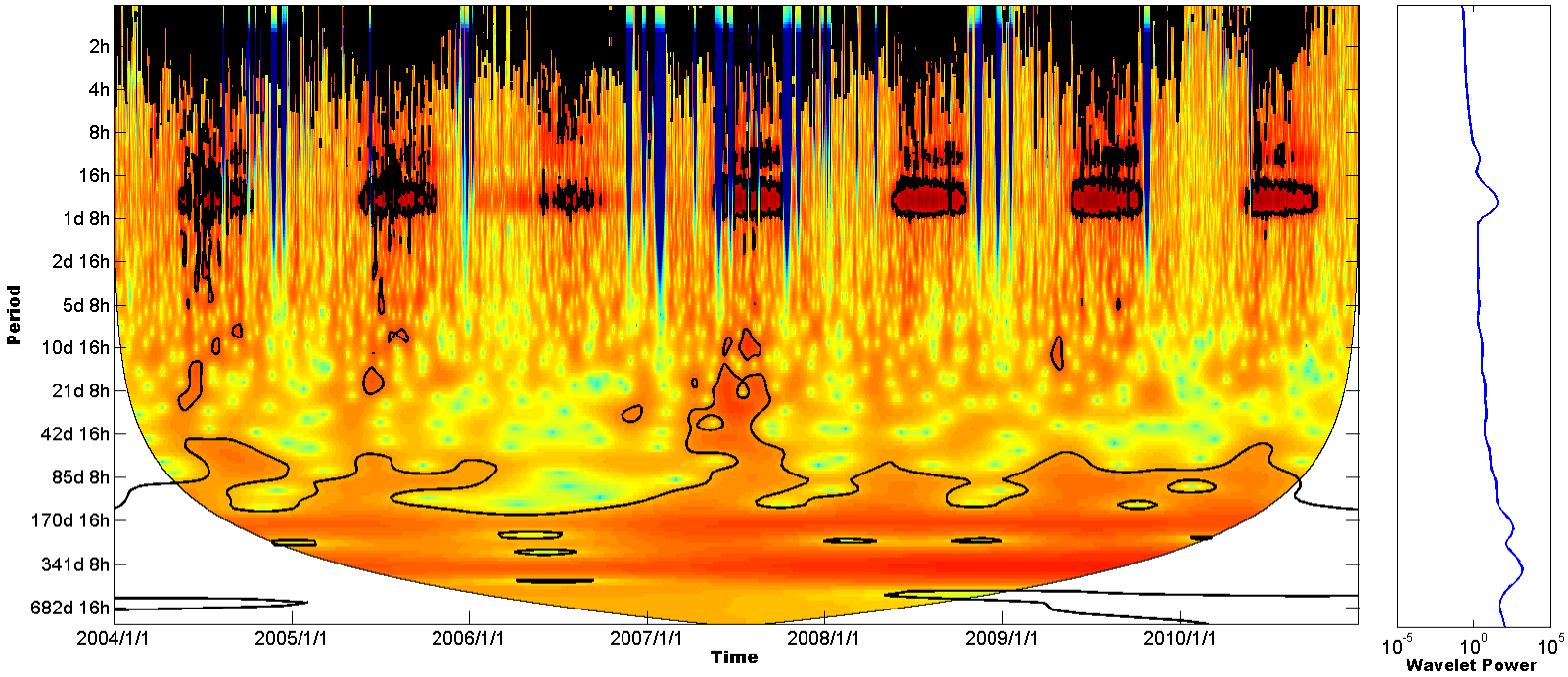

Figure 2.2, Continuous wavelet transform for NEE time series. The left axis is the Fourier period for the scaleogram timescale half-plane and the right plot is the scale-wise wavelet power spectra. The 5% significance level against red noise is shown as a thick contour. The cone of influence is shown as a thin line. The blue vertical stripes are caused by long data gaps. The redder the color, the higher is the wavelet power

2.3.2 Common power between Ta/PAR and NEE

High and significant common power was found at some scales, mainly diurnal, daily, seasonal, and annual, from the XWT time-scale half-planes (Figures 2.3 and 2.4). Ta & NEE and PAR & NEE had significantly high common power centered at the daily scale during the growing seasons and annual scale throughout the entire period. PAR & NEE also showed high common power at the diurnal scale, while Ta & NEE showed much fewer pixels on the time-scale half-plane with high common power at this scale. The highest common wavelet power for PAR & NEE happened at the daily scale while the highest common wavelet power for Ta & NEE were found at the annual scale. Significant common oscillations at seasonal scale were present but not continuous. From weekly to monthly scale, regions with significant common power were only observed in 2004 and 2007.

2.3.3 Coherence between Ta/PAR and NEE

The time scales and time periods for the significant coherence were consistent with the high common power and stable phase relationships detected in the time-scale half-planes in the XWT (Figures2.3-2.8). Both Ta and PAR oscillation were significantly correlated with NEE at the daily scale during the growing season and at the annual scale throughout the time series. At the diurnal scale, the results were not clear due to the influences of data gaps. However, for the last four years with less number of short gaps (Figures2.5 and 2.6) and gap-filled data (Figures2.7 and 2.8), PAR & NEE were tightly correlated during the growing seasons at diurnal and daily scale, while the coherence between Ta and NEE was weak. At intermediate scales (multi-days, multi-weeks, and multi-months), significant coherent regions emerged discontinuously and occasionally for both WTCs.

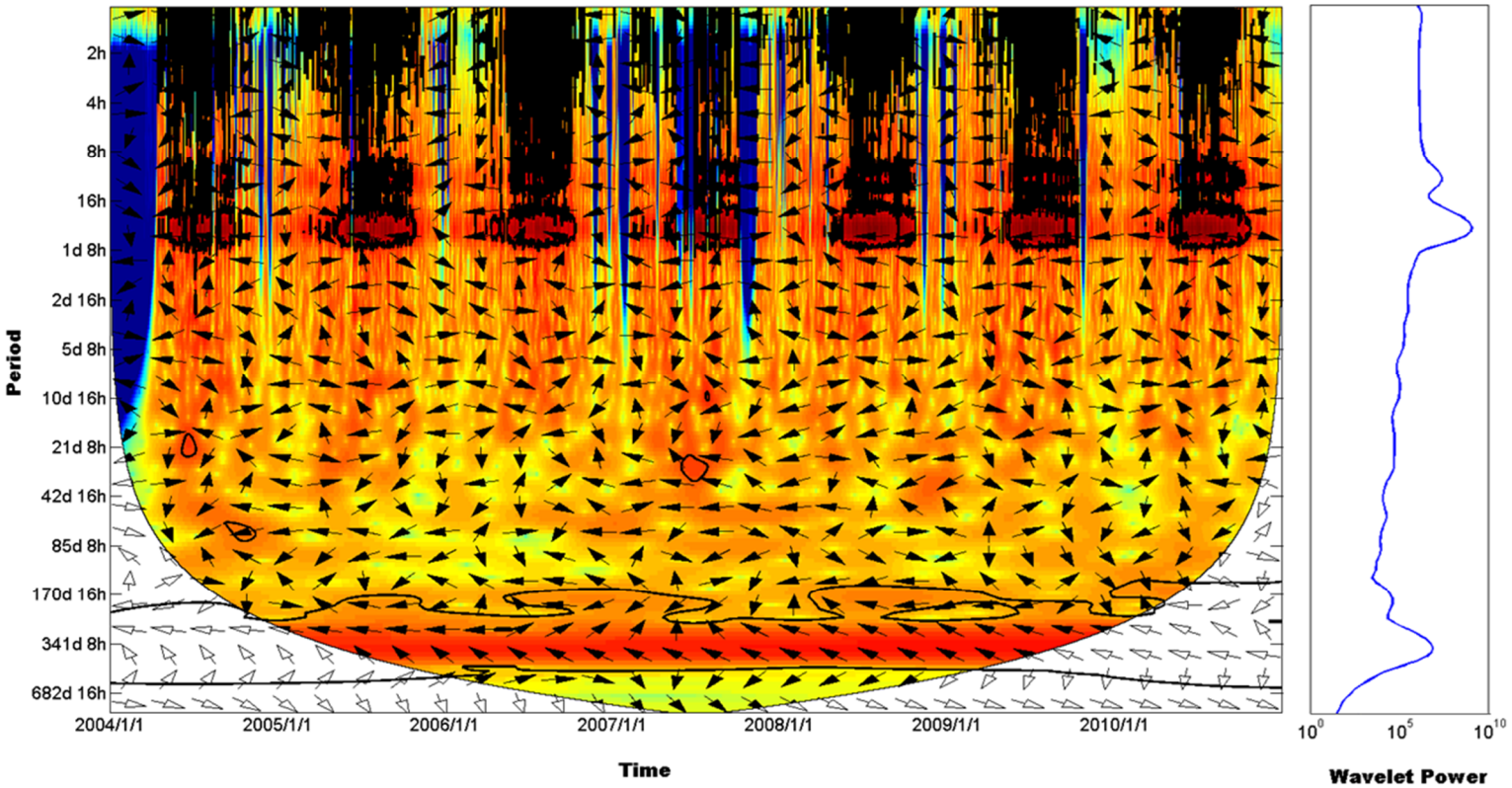

Figure 2.3, Cross wavelet transform for PAR and NEE. The XWT finds regions in time frequency space where the two time series have high common power. The 5% significance level against red noise is shown as a thick contour. The cone of influence (COI) is shown as a thin line. The redder the color, the higher is the common wavelet power. The relative phase relationship is shown as arrows

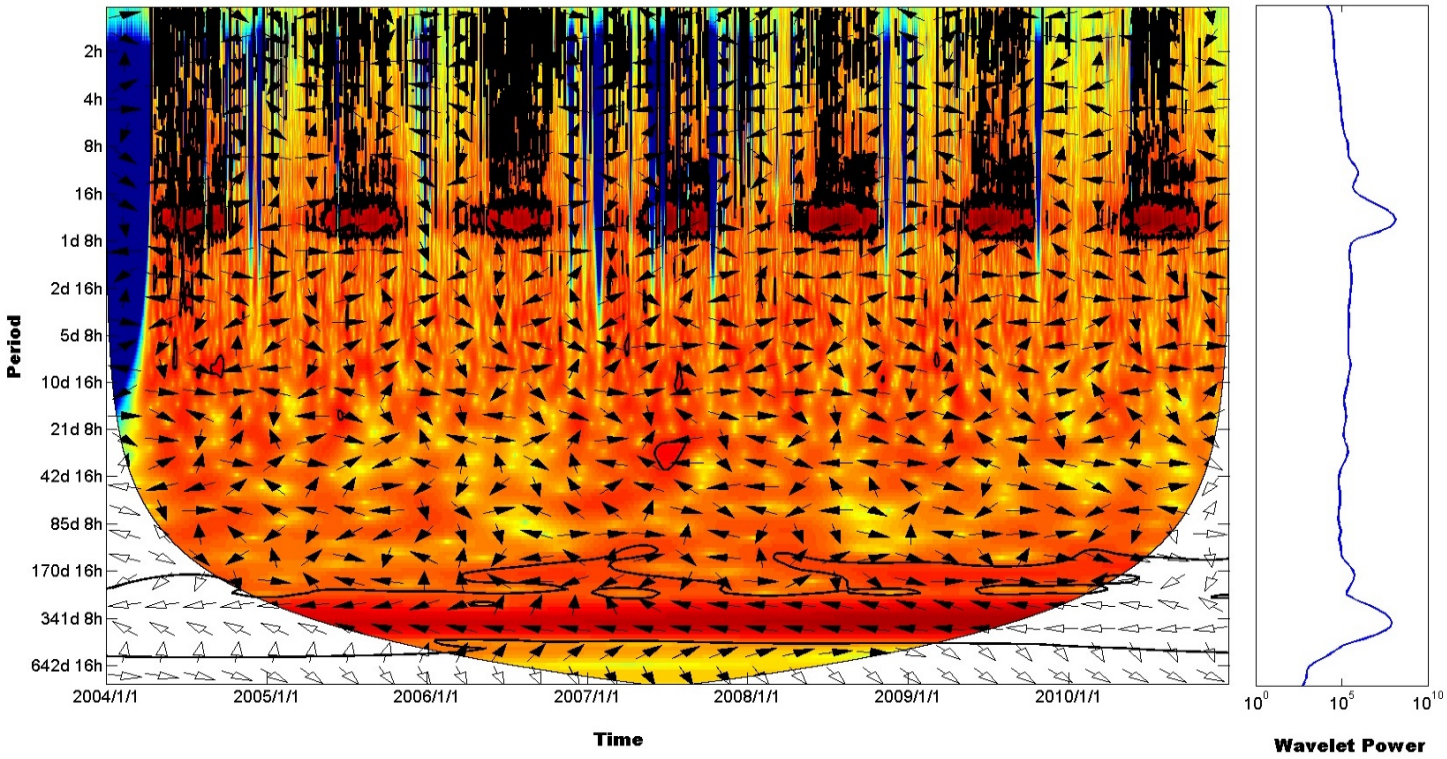

Figure 2.4, Cross wavelet transform for Ta and NEE (XWT (Ta, NEE)). The XWT finds regions in time frequency space where the two time series have high common power. The 5% significance level against red noise is shown as a thick contour. The cone of influence (COI) is shown as a thin line. The redder the color, the higher is the common wavelet power. The relative phase relationship is shown as arrows.

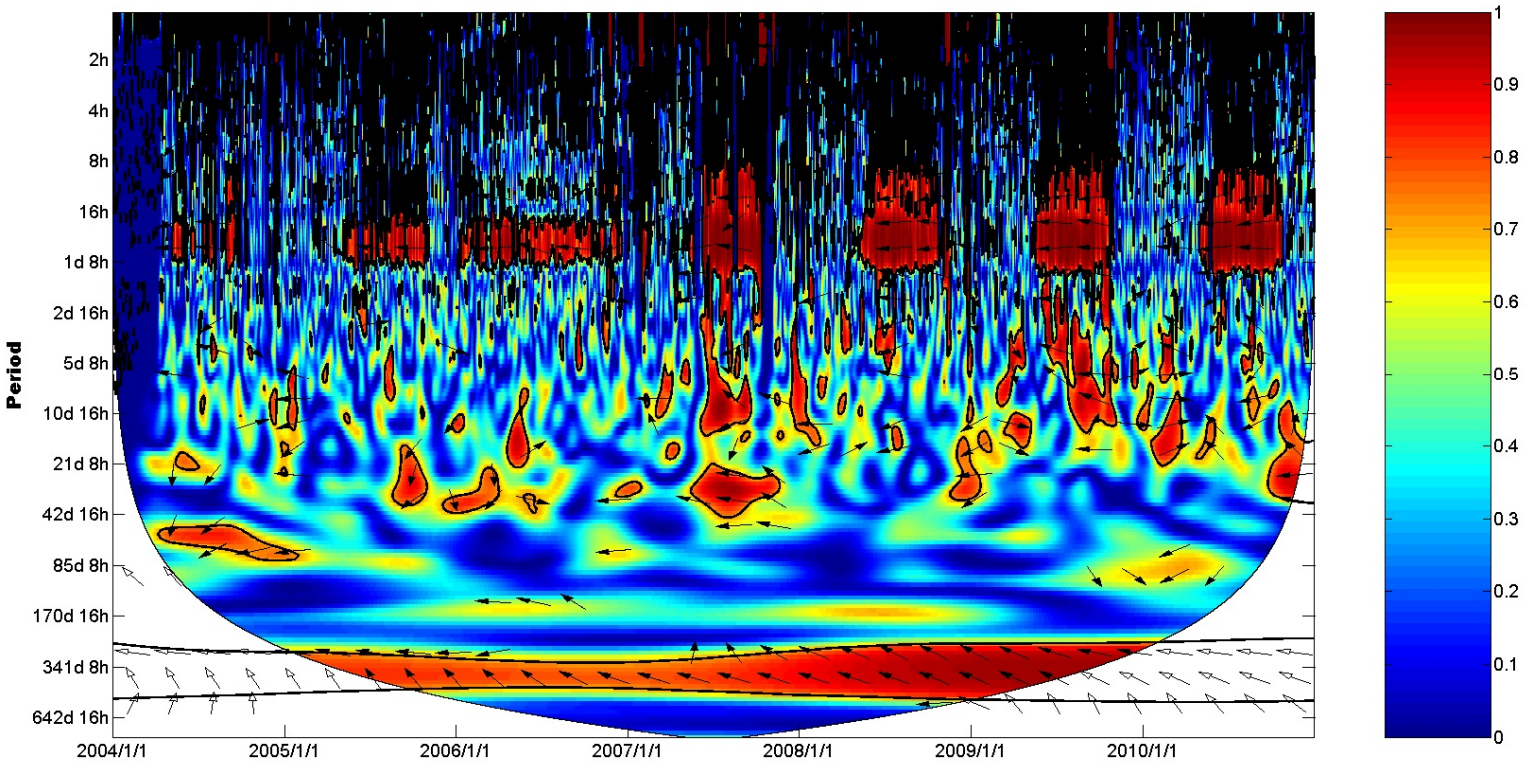

Figure 2.5, WTC between PAR and NEE. The WTC finds regions in the time frequency space where the two time series have high wavelet coherence (e.g., high correlation of the oscillation). The 5% significance level against red noise is shown as a thick contour. The cone of influence (COI) is shown as a thin line. The relative phase relationship is shown as arrows.

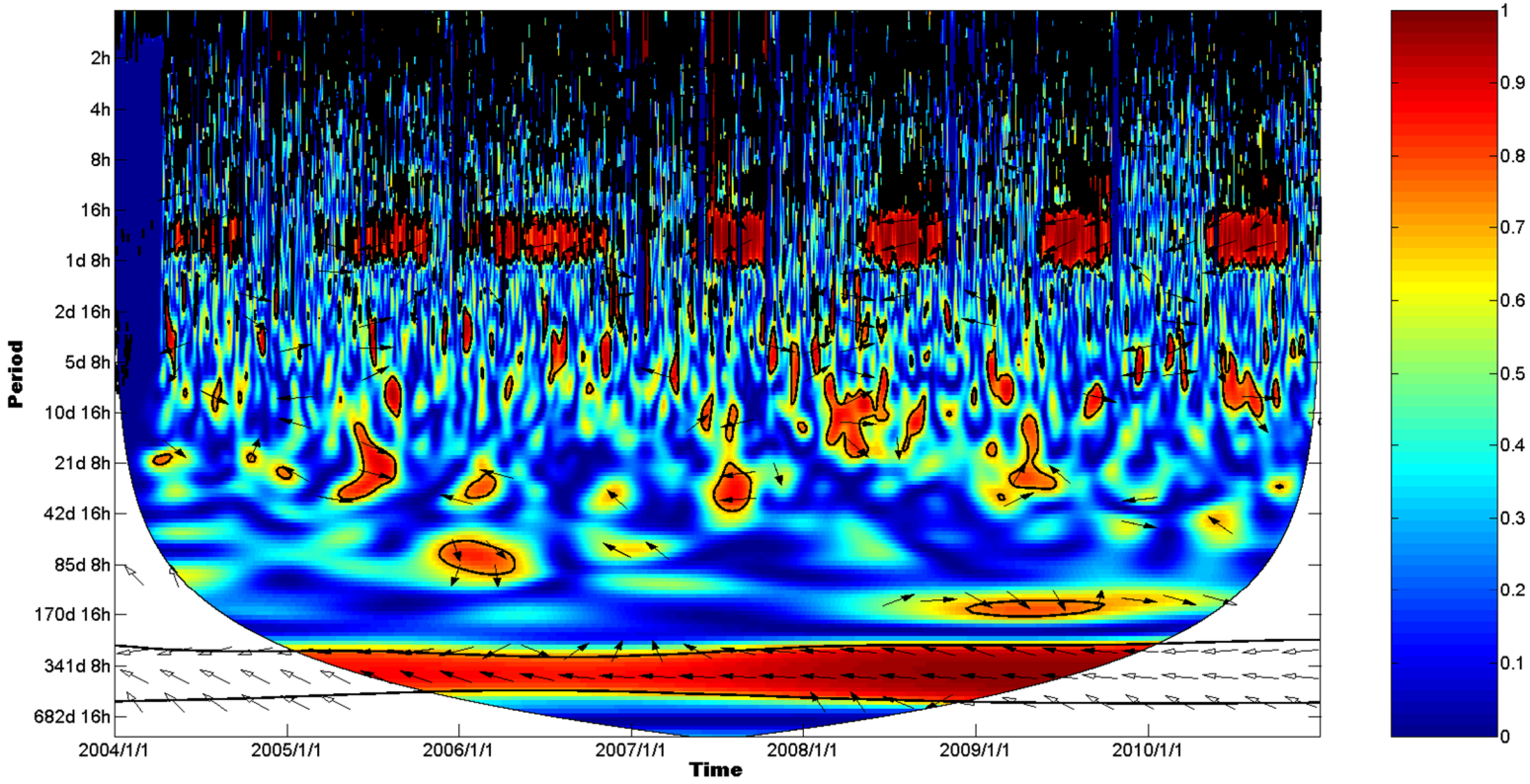

Figure 2.6, WTC between Ta and NEE. The WTC finds regions in the time frequency space where the two time series have high wavelet coherence (e.g., high correlation of the oscillation). The 5% significance level against red noise is shown as a thick contour. The cone of influence (COI) is shown as a thin line. The relative phase relationship is shown as arrows.

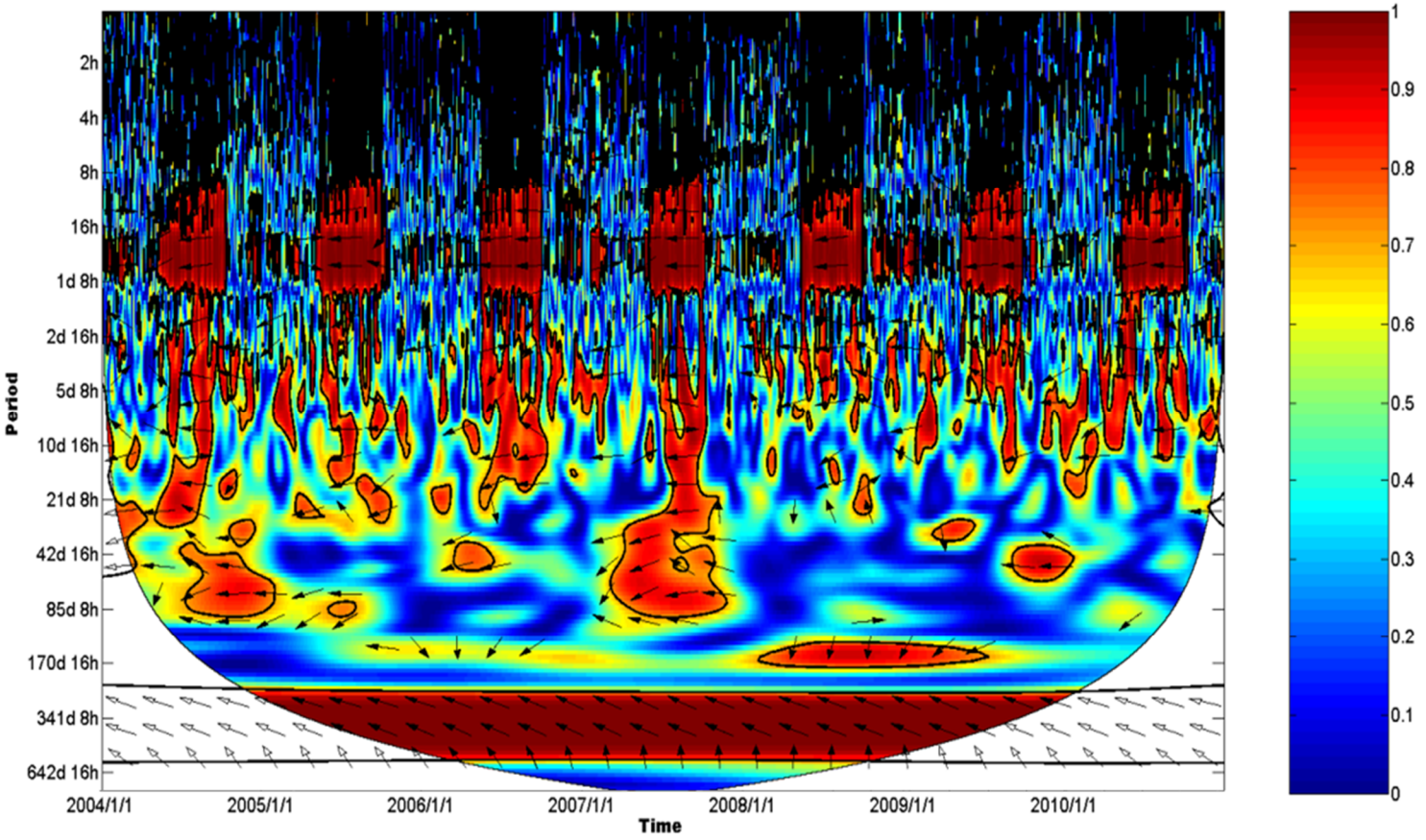

Figure 2.7, WTC between PAR and NEE of gap-filled data. The WTC finds regions in the time frequency space where the two time series have high wavelet coherence (e.g., high correlation of the oscillation). The 5% significance level against red noise is shown as a thick contour. The cone of influence (COI) is shown as a thin line. The relative phase relationship is shown as arrows.

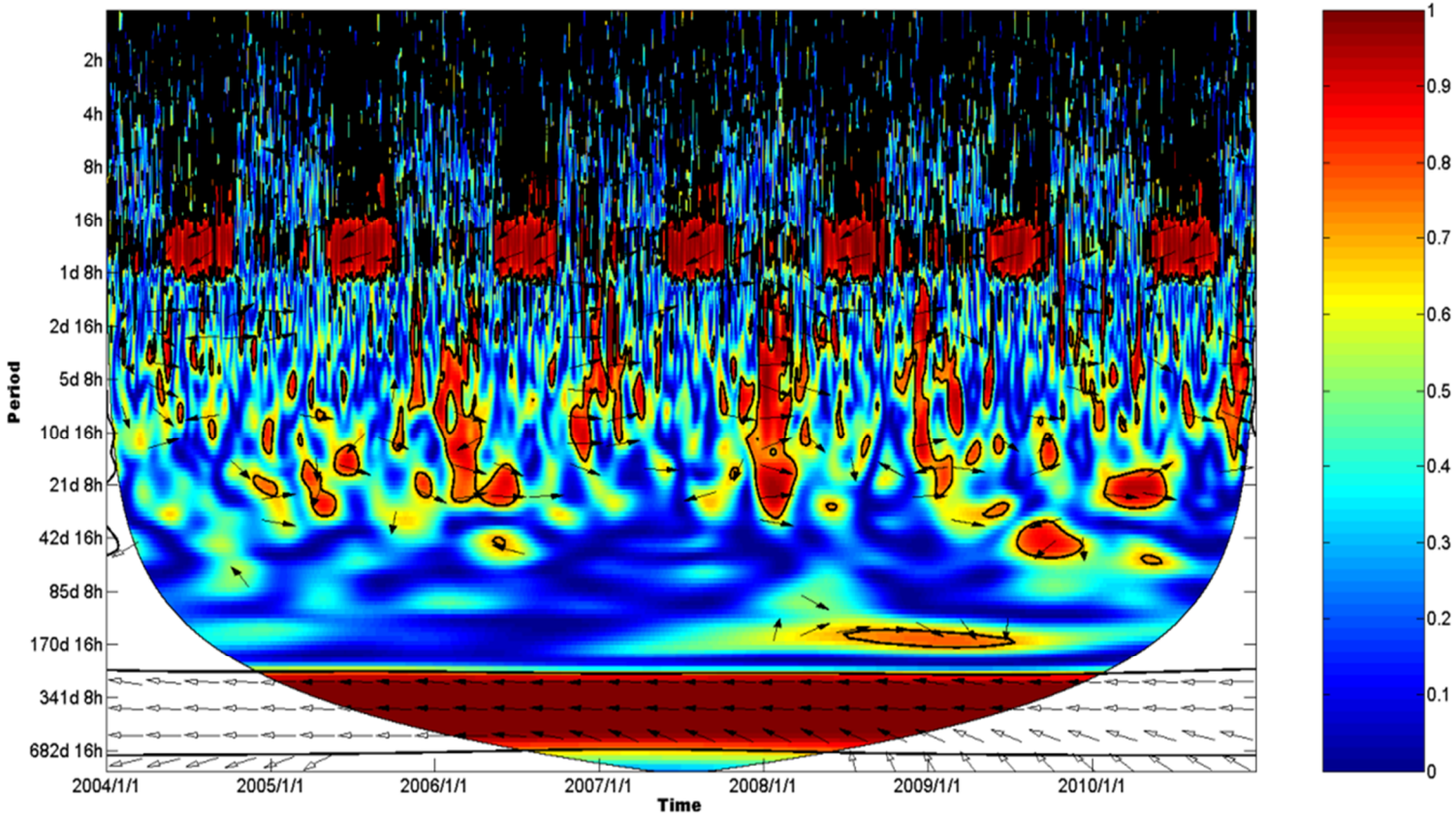

Figure 2.8, WTC between Ta and NEE of gap-filled data. The WTC finds regions in the time frequency space where the two time series have high wavelet coherence (e.g., high correlation of the oscillation). The 5% significance level against red noise is shown as a thick contour. The cone of influence (COI) is shown as a thin line. The relative phase relationship is shown as arrows.

2.3.4 Spectral transfer across scales

The tendency of NEE to have less variation (dampen) or more variation (amplify) than the variability of PAR and Ta varied across scales (Figure 2.9). At ≤8 h scale, the NEE variability tended to be greater than that of Ta and PAR. Between scales of 10-32 hours (i.e., equivalent to diurnal and daily scales), NEE seemed less variable than PAR. However, NEE was more variable than Ta at these scales. The NEE oscillated more than PAR and Ta from the scale of ~ 2 days to one year, except at scales approaching the growing seasonal scale. NEE oscillated more than Ta and PAR at time scales longer than a year.

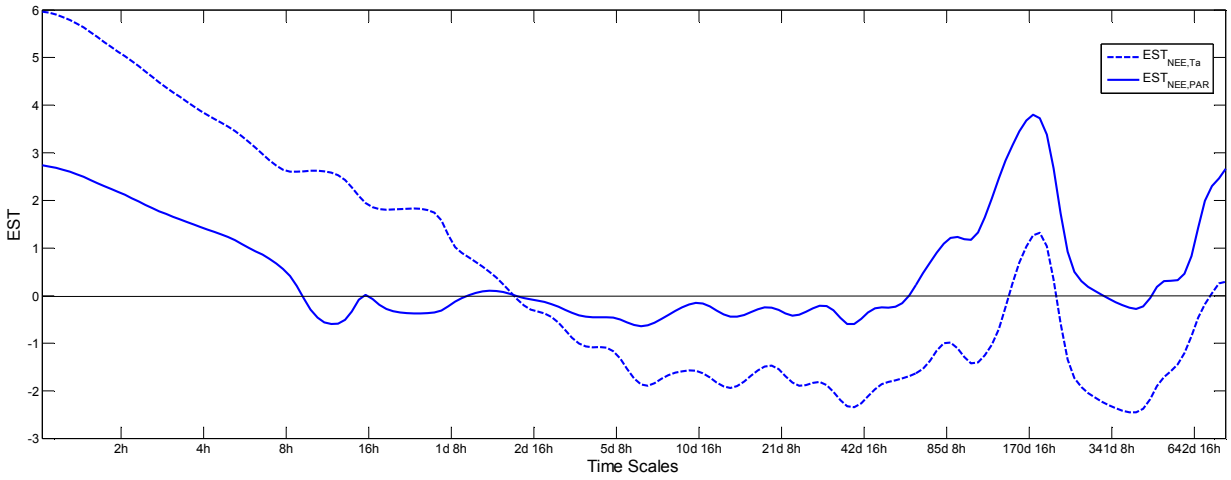

Figure 2.9, Ecosystem spectra transfer (EST) of NEE for PAR and Ta averaged throughout the 7 years across different time scales. The EST shows the tendency of NEE to dampen (less variation) or amplify (more variation) the oscillation of Ta and PAR.

2.3.5 Partial coherence across scales and phase relationship

Partial wavelet coherence had fewer significant oscillations across all scales in the time-scale half-plane, but the observed areas with significant coherence were still mostly located at the daily and annual scales (Figure 2.10). Out of the COI, Ta & NEE was continuously and significantly high at the annual scale after removing the effects of PAR. At the daily scale, however, no regions with significant coherence could be detected for Ta & NEE. In contrast, after removing the common dependence on Ta, PAR & NEE was only significant at the daily scale during growing seasons in all years, but not at the annual scale. Additionally, at intermediate scales (multi-day, multi-week, and multi-month), significant PWC regions for PAR & NEE and Ta & NEE were observed for some time durations.

Locked-phase angles often suggest significant correlation between phenomena recorded in the two time series. The phase angles provided by the XWT/CWT time-scale half-plane at the daily scale during the growing season and at the annual scale throughout the entire time series were stable (Figures 2.3-2.8). The phase angles based on data with gaps often deviated from the average trend, or sometimes totally shifted the average trend, due likely to data gaps affecting the phase angle calculation that is based on an entire cycle. Thus, we describe the phase angles and interpret them based on analysis of gap-filled data (*e.g.*, Figures2.7 and 2.8). At the daily scale, the phase angles for PAR & NEE are locked nearly anti-phased, while the phase angle for Ta & NEE were locked at *ca.* 146° (Table 2.2). At the annual scale, the phase angle for PAR & NEE was locked at -147°, while the phase angles for Ta & NEE were locked nearly anti-phased (Table 2.2). At the diurnal scale, however, PAR & NEE were approximately anti-phased, while the phase-angles for Ta & NEE were very changeable

(Figures 2.7-2.8). These differences could be caused by PAR and photosynthesis – the major component of NEE – that were not detectable at nights. We thus made two groups of artificial time series: daytime series (06:00 – 18:00 h) and nighttime series (18:00 – 06:00 h), respectively, performed the WTC analysis, and calculated the statistic of phase angles again. It turned out that Ta was locked with NEE in-phase in the nighttime series, and locked with NEN at *c.a.*124°, while PAR was locked with NEE anti-phased in the daytime series. Based on the NEE sign convention and the facts more sunlight corresponds well with more CO_2 withdrawal from the atmosphere by photosynthesis, and the rising temperatures are associated with more CO_2 release by respiration, our the interpretation is that: at the daily scale, PAR synchronizes with NEE without time lag while NEE lagged NEE for 2-3 hours. At the annual scale, Ta synchronized with NEE without time lag, while PAR lead NEE *ca.* 34 days. At the diurnal scale, there is no time lag between the oscillations of PAR and NEE while Ta lagged NEE during cycles where daytime dominated and synchronized with NEE during nighttime cycles.

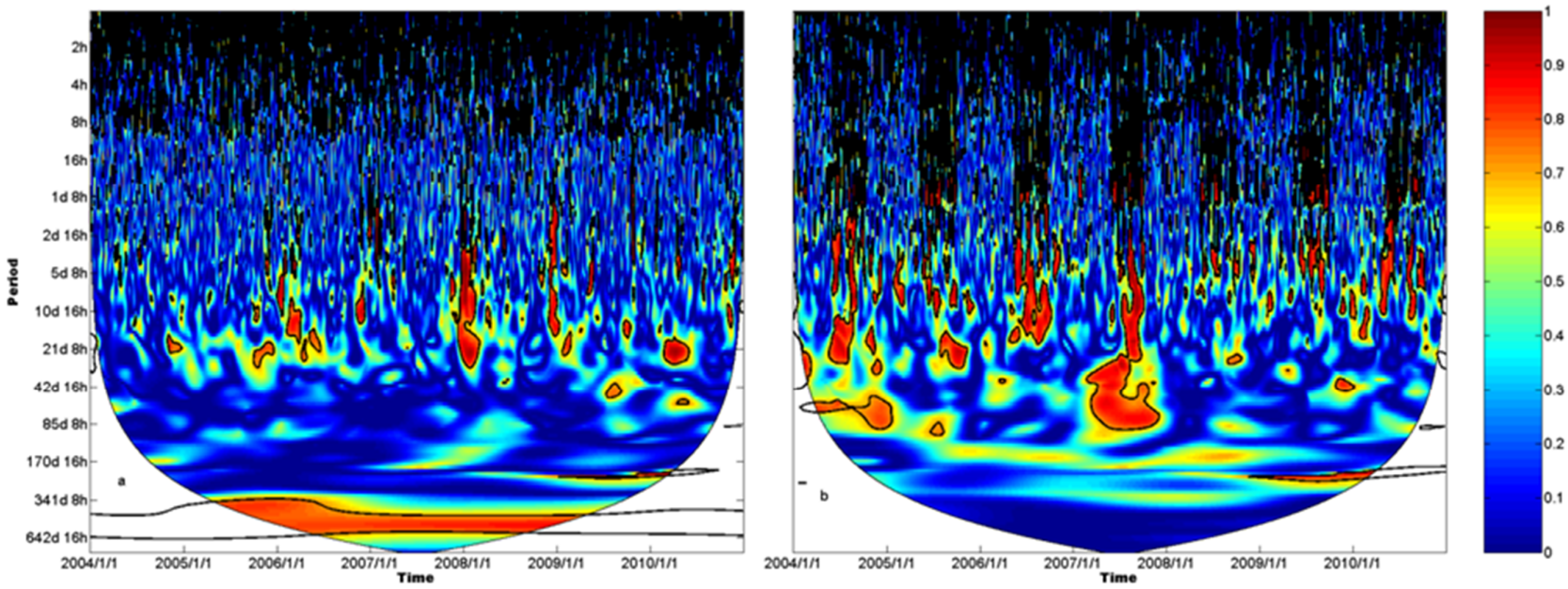

Figure 2.10, PWC (NEE, Ta, PAR) (a) and PWC (NEE, PAR, Ta) (b) on data with gaps. The 5% significance level against red noise is shown as a thick contour. The cone of influence (COI) is shown as a thin line.

Table 2.2, The mode phase angles of oscillations for Ta and NEE, and for PAR and NEE at diurnal, daily, and annual scale. All angles were rounded to integral angels before statistics. The mode angles for diurnal scale were derived from two artificial daytime and night time series. We did not use mean values here, because when the actual angles are at *ca.* ±180°, they are easily being changed from a positive angle to a negative angle by noises, and vice versa, leading to misunderstanding mean values.

Scale	Ta and NEE	PAR and NEE
Diurnal (12h)	-179 °(Nighttime) 124 °(Daytime)	-179 ° (Daytime)
Daily	146 °	-179 °
Annual	-179 °	-150 °

2.3.6 Wavelet coherence and phase relationship for LAI to Ta/PAR and NEE

LAI was highly correlated with NEE at seasonal-annual scales, with Ta and PAR in the growing season scale (e.g., the 170-180 day) and the annual scale. LAI was anti-phased (*i.e.*, no time lag) with NEE at the growing season and at the annual scale (Figure 2.11), in-phased (no time lag) with Ta and but locked at ~ -68° with PAR (a time lag of *ca.*34 days at the annual scale) at the growing season and the annual scale (Figure 2.11).

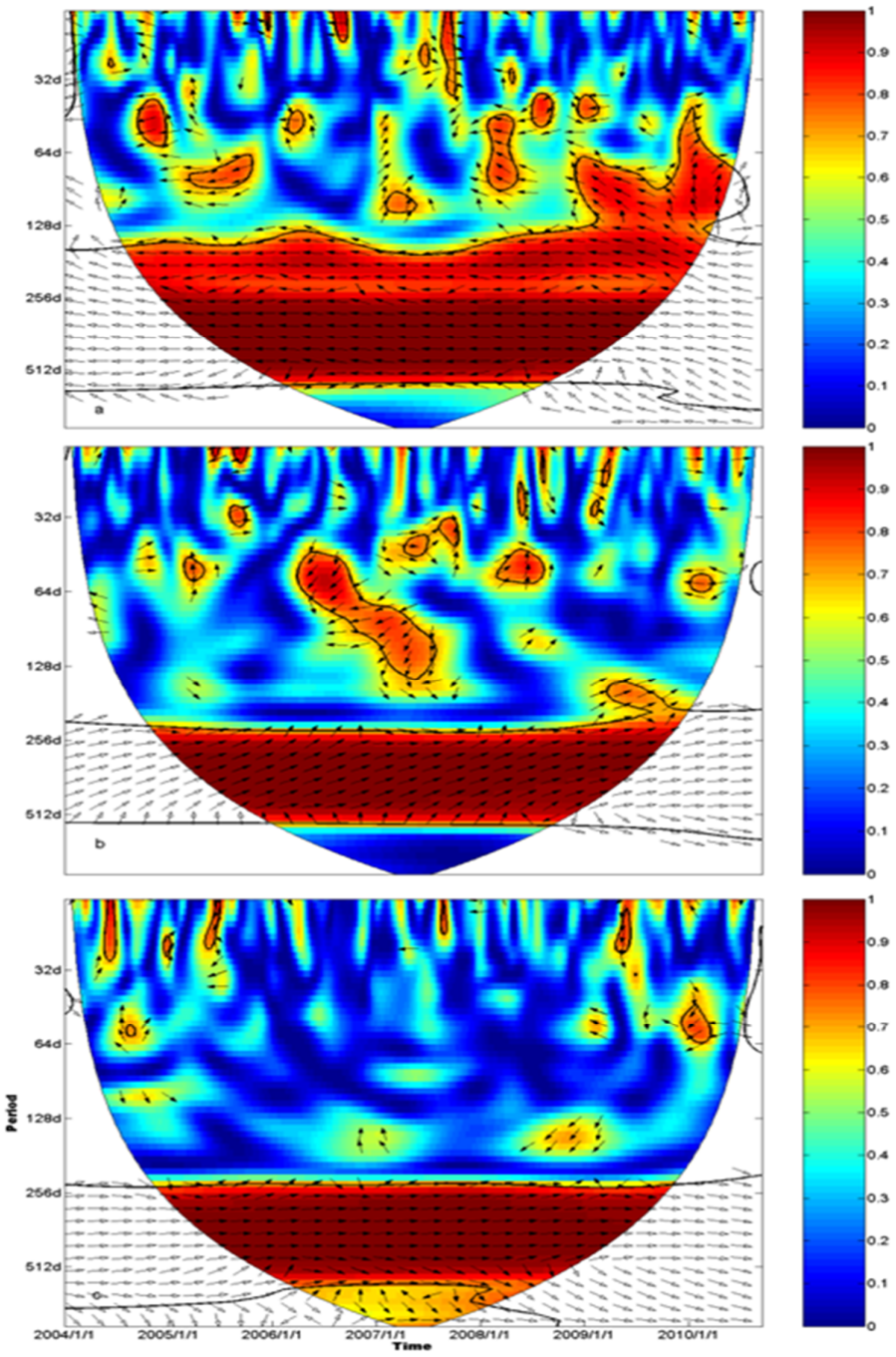

Figure 2.11, WTC for MODIS 8-day composite LAI and NEE (a), PAR (b), and Ta (c). The 5% significance level against red noise is shown as a thick contour. The cone of influence (COI) is shown as a thin line. The relative phase relationship is shown as arrows.

2.4 Discussion

2.4.1 NEE variations and regulations

Spectral peaks at daily, seasonal, and annual time scales are the general features in a global NEE time series(Stoy et al. 2009), with more pronounced pattern for temperate forests(Baldocchi et al. 2001, Katul et al. 2001, Braswell et al. 2005, Richardson et al. 2007). Our wavelet analysis is in consistent with their reports.

Climatic variability (e.g., Ta, PAR) centered at the diurnal, daily, and annual scales plays a dominant role in controlling the total variability in measured flux (Figure 2.3-2.5). However, less driving forces of Ta and PAR were observed at the seasonal scales. At this scale, significantly high common power was occasionally observed between NEE and the two climatic drivers (Figures 2.3 and 2.4), without any significant coherence (Figures2.5 and2.6). The EST analysis (Figure 2.9) further suggested that NEE is more variable than both Ta and PAR at the growing season scale. This indicates that other variables, either physical or biological, might have also contributed to the variance of NEE at this scale. Our analysis on LAI suggests that LAI is likely the main driver for NEE at seasonal scales (Figure 2.11; also see Stoy et al., (2005), Baldocchi et al., (2001)). The average growing season length at our site is *ca.* 180 days, indicating a LAI dynamic/cycle of 180 days. This explains why wavelet power also peaks at a scales at *ca.* 170-180 day (Figure 2.2). However, LAI responds to climatic variability and is highly correlated with Ta and PAR at growing season to annual scales (Figure 2.11). Therefore, we cannot exclude the regulating effect of Ta and PAR at the seasonal scales.

At other scales (*i.e.*, hours, weekly, monthly, 2-3 months, and >1 year), Ta and PAR were not likely the major drivers for NEE oscillations, as suggested by that significant common powers and coherence were rarely found at these scales (Figure 2.3-2.3). The dynamics of LAI could be responsible for the observed successional oscillation at scales from ca. 42-150 days (Figure 2.11a), while turbulences at hourly scales and irregular precipitation events may have played more important roles at scales of a few hours (Baldocchi et al. 2001, Stoy et al. 2005). However, drought events and synoptic weather changes that affect PAR, Ta, humidity, and wind direction maybe responsible for hotspot NEE at weekly to monthly, and even longer time scales (Baldocchi et al. 2001, Stoy et al. 2005). We suspect that the wavelet power hotspots from weekly to seasonal scales in 2007 were likely caused by the heat waves in the summer (http://www.ncdc.noaa.gov/oa/climate/research/2007/jul/jul07.html). At scales longer than a year, NEE seemed more variable than Ta and PAR (Figure 2.9). Aggregation at longer time scales from model predictions and long-term measurement have both suggested that variations in environmental drivers (e.g., PAR, Ta, VPD, soil water content, etc.) become progressively less important while variations in the biotic response become progressively more important in determining the carbon flux(Richardson et al. 2007, Urbanski et al. 2007). Factors causing such biotic responses may include ecosystem succession, nutrient availability, and disturbances that need years for ecosystems to recover or large-scale climate cycles (e.g., El Nino, La Nina cycles)(Baldocchi et al. 2001, Stoy et al. 2009). We did not observe any significant oscillations at multi-year scales because our site has been stable as a mature forest and experienced no serious disturbance during 2004-2010.

2.4.2 The unique effects of PAR and Ta across scales

The dominant oscillations or variations of NEE happened at the diurnal, daily, growing seasonal and annual scales (Figure 2.2). Both PAR and Ta are highly related to the NEE variations at these scales. However, PAR and Ta played different roles at each of these scales.

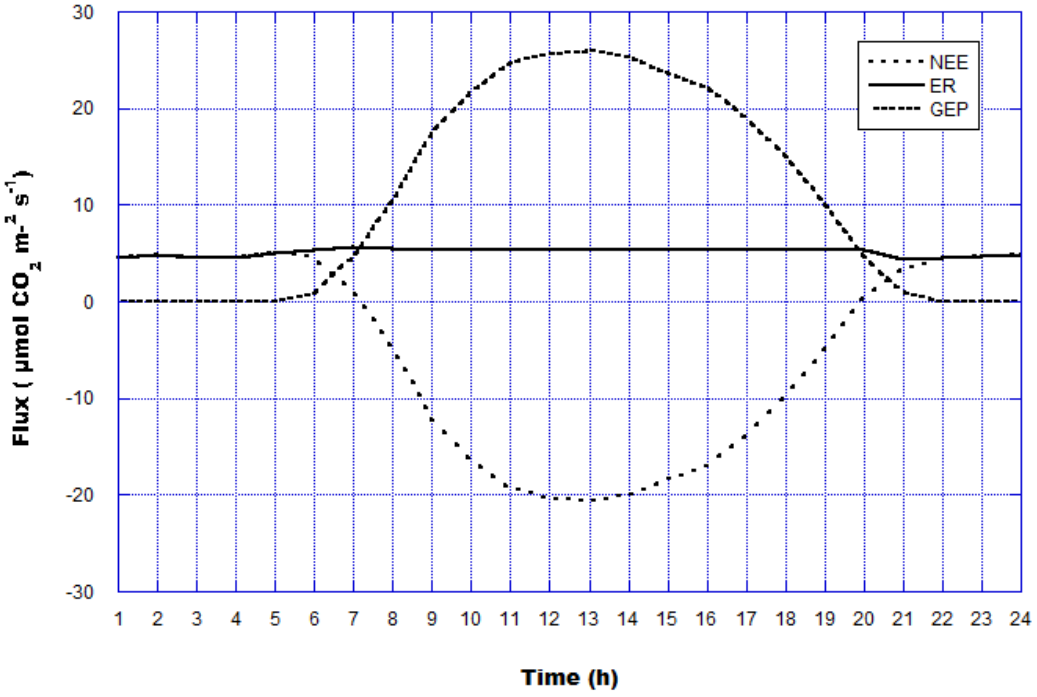

Figure 2.12, The daily cycle of NEE, ER (ecosystem respiration) and GEP (gross ecosystem productivity) at our study sites. Data were from gap-filled 30-mean flux of NEE, ER, and GEP averaged by hour based on June to September measurements in 2010. This figure shows that GEP (photosynthesis) dominates the daily cycle of NEE and contribute the most variation.

PAR is the primary regulator for NEE compared to Ta at the daily scale. First, the co-varying powers for PAR & NEE are stronger than those for Ta & NEE at this scale (Figure 2.3). PAR has more oscillating power than Ta at the daily scale (Figure 2.9), which probably transfers more variation to ecosystem functions. More importantly, there is no delay between the oscillations of NEE and PAR, while Ta lags NEE for ~2-3 hours. We speculate that photosynthesis, instead of respiration, dominates the variation of NEE (Figure 2.12;Yuan et al. 2010). Photosynthesis is a function of PAR while respiration is a function of temperature (Kull and Kruijt 1998, Tjoelker et al. 2001, Mueller et al. 2010). Therefore, PAR and photosynthesis productivity should theoretically be oscillating synchronously whereas Ta and respiration change at similar pace. However, the daily course of Ta often lags the daily course of sunlight, and thus the daily course of photosynthesis often leads the daily course of respiration (Baldocchi et al. 2001, Tang et al. 2005). During the growing season at our ecosystem, NEE variation depends strongly on photosynthesis that respiration has contributed less to NEE, resulting in PAR's dominancy.

At the diurnal scale, PAR remained as the primary driver for NEE compared to Ta during growing seasons. Higher common power and more regions with significant coherence are for PAR & NEE than for Ta & NEE (Figures 2.3-2.6). Though PAR only functioned as a driver during daytime, most NEE variation happened during daytime when photosynthesis dominated (Figure 2.12). During daytime, PAR co-varied with NEE synchronously while Ta still lags NEE 2-3 hours. Only during complete nighttime when photosynthesis was not possible, Ta was the primary driver and co-varied with NEE with no time lag. Daytime

length changes throughout a year but is longer than nighttime during the growing seasons in our ecosystem, further highlighting the importance of PAR in driving NEE at this scale.

At the seasonal scale, Ta replaced PAR as the major driver for NEE. Both Ta and PAR have significant common wavelet power with NEE occasionally, but no significant coherence for the entire series. However, LAI, the major direct driver for the NEE oscillations at this scale, is primarily determined by temperature rather than PAR, as suggested by the lag of both LAI and Ta to PAR. Though PAR is also commonly thought as an important driver of Ta as energy source, LAI seems to respond mostly to temperature. For example, the leaf out/off time is determined by Ta rather than PAR.

At the annual scale, Ta remained the primary regulator for NEE as compared to PAR. The oscillation of PAR led NEE *ca.* one month but there is no delay between NEE & Ta oscillations. This could be explained by the strong dependence of LAI/biomass dynamics on Ta; the *ca.* one month lag of the LAI biomass (*e.g.* LAI) development to the progress of sunlight (*e.g.* PAR) (Figure 2.11); and vegetation characteristics (*e.g.*, phenology and LAI) determine the magnitude and dynamics of gross productivity (Penuelas and Filella 2001, Griffis et al. 2003). Numerous studies reported that it is Ta, but not PAR, that served as an important control of the variation of annual carbon flux in temperate forests both in time and space (Law et al. 2002, Yu et al. 2013).

The results from the PWC analysis further prove the different roles played by Ta and PAR across temporal scales. The PWC is powerful to provide the "stand-alone" relationship between two time series after removing the effect of a third factor (Ng and Chan 2012). We observed insignificant partial coherence for Ta & NEE at the daily scale and for PAR & NEE

at the annual scale (Figures2.7 and 2.8), suggesting little "stand-alone" effect of Ta at the daily scale and of PAR at the annual scale on NEE oscillations. In contrast, we observed significant partial coherence for Ta & NEE at the annual scale and for PAR & NEE at the daily scale (Figures 2.7 and 2.8), suggesting significant "stand-alone" effect of Ta at the annual scale and of PAR at the daily scale on NEE oscillations.

2.4.3 Measurement uncertainty, nonlinear characteristics, and spectral leakage

Measurement uncertainty could be considered as part of noise. Ta and PAR could be measured directly with guaranteed accuracy as long as the sensors function normally (±0.2 °C and ±5% respectively at 20 °C and normal humidity). The accuracy of LAI from MODIS collection 5 is *ca.* 0.66-1.0 (*i.e.*, RMSE) when all biomes are taken in account (Fang et al. 2012, Ryu et al. 2012). The NEE is often contaminated from both random and systematic errors that may mask out some oscillating patterns. There is a growing recognition within the EC community that more attention must be paid on quantifying NEE uncertainties. However, it remains a challenging task. The conventional QA/QC protocols for processing the EC data, such as Webb–Pearman–Leuning corrections, focuses on systematic errors, but not random errors. Yet, it is well known that random error is not normal and linearly scaled with the magnitude of fluxes(Richardson et al. 2006). We thus have assumed the remaining error terms being red noise, and applied the Monte Carlo simulations to just report the significant results.

Another uncertainty involved in quantifying the regulatory mechanisms is the nonlinearity embedded in our time series, where wavelet is not a powerful tool for the

processes. For example, ecosystem respiration is usually described as an exponential function of Ta (Eq. (1)), whereas canopy photosynthesis is considered as a hyperbolic function of PAR. To partly solve the problem, we ran XWT (lg (NEE),Ta), WTC (lg (NEE), Ta), XWT(sqrt(NEE), PAR), and WTC(sqrt(NEE), PAR) to linearize these variables (FiguresA.1-A.4 in the APPENDIX A). The new results from transformed data are consistent with our original results found in this paper (Figures2.3 and 2.4*vs.* Figure A.1 and A.2 and Figures2.5 and 2.6*vs.* FiguresA.3 and A.4). Therefore, our findings are robust to some potential nonlinear characteristics.

Spectral/energy leakage is inherent of wavelet analysis, thus we must consider its effect. Our analysis has reveal significant powers and coherence at four bands that peak at diurnal, daily, growing season, annual scales. Significant results within each band beyond the peak might be caused by energy leakage from the central time scales, though none of these central time scales owned a dyadic frequency in terms of the time resolution (half-hour) of data, which reduces energy leakage (Peng et al. 2009). Therefore, there is no guarantee that all significant frequencies within each band are real components of the data. However, the significant results located at exactly the four central time scales is unlikely caused by energy leaking for neighboring frequencies. Firstly, it is unlikely for energy leakage to produce higher energy than where it is leaked from even with multiple source frequencies. Secondly, the original data have clearly revealed the significant cycles at these scales (Figure 2.12, Figure A.7). Finally, this is in consistent with previous study that frequencies related to these four scales are major components of NEE or microclimatic time series(Baldocchi et al. 2001, Goulden et al. 2004, Stoy et al. 2009).

2.4.4 The implication to ecosystem modeling

Lessons learned from this study suggest that we should consider the proper primary drivers by time scale. Recognizing the time lag between Ta and NEE/photosynthesis at the daily scale and between PAR and NEE at the annual scale in ecosystem modeling will likely improve the estimation of NEE(Dietze et al. 2011, Stoy et al. 2013). Appropriate representation of ecosystem state variables (e.g., LAI, vegetation type) that respond to climatic variables is also pivotal for modeling NEE variation across seasonal-annual scales because they are important regulators of NEE at those scales. At other intermediate scales, it is always a challenge for ecosystem modelers to simulate the NEE variations (Baldocchi et al. 2001, Siqueira et al. 2006, Dietze et al. 2011, Stoy et al. 2013) due to the irregular and unpredictable events (e.g., precipitation, drought, frontal passages, etc.) that play important roles (Baldocchi et al. 2001, Stoy et al. 2005). Though the proportion variation of NEE at the intermediate sales is relatively small (Figure 2.2), careful records of these events would improve models' performance.

2.5 Conclusions

I employed innovative wavelet tools for spectral analysis at different time scales for seven years of EC measurements. We found that Ta and PAR played different roles at a given time scale. At the daily scale during the growing seasons, both PAR and Ta co-varied with NEE with high common powers and coherence. However, PAR co-varied with NEE with no time delay and is the primary driver for NEE, while Ta is the minor one and lagged NEE for 2-3 hours. This could be explained by the strong dependence of NEE on photosynthesis, the strong dependence of photosynthesis on PAR, and a lag of 2- 3 hours of the daily course of Ta to PAR. Significant coherence and high common power between Ta and NEE were detected at this scale, due likely to their common dependence on PAR. At the diurnal scales during the growing seasons, PAR is also the major climatic driver as daytime NEE variations overwhelm nighttime NEE variation, except for complete nighttime cycles where Ta became as the primary driver for NEE. At diurnal and daily scales during the non-growing seasons, both the oscillations of Ta and PAR are not significantly correlated with the oscillations of NEE. At the annual scale, high common powers and coherence were observed for Ta & NEE and PAR &NEE throughout a year. However, Ta appeared to be primary driver for NEE and co-varied with NEE synchronously, while PAR leaded NEE by *ca.*one month with insignificant influence on NEE after the common dependence on Ta was removed. At the seasonal scale, both Ta and PAR were not directly correlated with NEE, but Ta is likely more important than PAR for regulating NEE, because Ta determines LAI and other biological properties.

My results supported my hypothesis that PAR is the primary climatic driver at short time scales (*e.g.*, hours to days) and Ta is the primary climatic driver at long time scales (*e.g.*, seasonal/annual). The unique influences of Ta and PAR on NEE by time scale will have important implications for future ecosystem modeling on ecosystem NEE.

2.6 Acknowledgements

This study was supported by the USDA FS Southern Global Change Program (cooperative agreements 03-CA-11330147-073 and 04-CA-11330147-238), the Toledo Area Metroparks, and the US-China Carbon Consortium (USCCC). We thank the Department of Environmental Sciences of the University of Toledo for supporting the study through a teaching assistantship. We appreciate Asko Noormets, Qinglin Li, Mike Deal, Jared DeForest, and Housen Chu for maintaining the EC tower. We also thank Lisa Taylor for language proof.

CHAPTER 3 EVALUATING THE SENSITIVITY OF WETLANDS TO CLIMATE CHANGE WITH REMOTE SENSING TECHNIQUES

Abstract

Wetlands are valuable ecosystems that provide many valuable services, yet many of these important ecosystems are at risk because of current trends in climate change. The Prairie Pothole Region (PPR) in the upper-Midwest of the United States and south-central Canada, characterized by glacially sculpted landscapes and abundant wetlands, is one such vulnerable region. According to regional/global climate model predictions, drought occurrence will increase in the PPR region through the 21st century and thus will probably cause the amount of water in wetlands to decline. WSA (water surface area) of Kidder County, ND, from 1984–2011 was measured by classifying TM/ETM+ (Landsat Thematic Mapper / Enhanced Thematic Mapper Plus) images through the modified normalized difference water index. I then developed a linear model based on the WSA of these wetlands and historical climate data and used this to determine the wetland sensitivity to climate change and predict future wetlands' WSA in the PPR. My model based on Palmer drought severity index (PDSI) of the current year ($PDSI_{t-0}$) and of the previous second year ($PDSI_{t-2}$) can explain79% of the annual wetland WSA variance, suggesting a high sensitivity of wetlands to drought/climate change. I also predictedthe PPR wetlands' WSA in the 21st century under A1B scenario (a mid-carbon emission scenario) using simulated PDSI based onIntergovernmental Panel on Climate Change AR4 22-model ensemble climate. According to our prediction, the WSA of the PPR wetlands will decrease to less than half of the baseline WSA (defined as the mean wetlands' WSA of the 2000s) by the mid of the 21st century, and

to less than one-third by the 2080s, and will then slightly increase in the 2090s. This considerable future wetland loss caused only by climate change provides important implications for future wetland management and climate adaptation policy.

Keywords: Wetlands, Climate Change, Ecosystem, Sensitivity, Drought

3.1 Introduction

Wetlands were once considered to be 'nuisances' to early European settlers, in that they were obstacles impeding agricultural development. Because of this view, the USA experienced a significant wetland net loss in the late 19th century. One example of this is found in the Prairie Pothole Region (PPR) of the northern Great Plains (Mitsch and Gosselink 2007). The PPR is a vast area (approximately 715 000 km2) that contains thousands of shallow depressions known as potholes created by the last glacial retreat approximately 12 000 years ago (Figure 1) and is renowned for providing habitats for large proportions of the North America continental waterfowl populations because of its large amount of wetlands (Batt et al. 1989). However, because of agricultural development, over half of the original 8 million ha wetlands in the PPR have been lost (Council 1982, Dahl 1990). Fortunately, more recently, the great value of wetlands for water supply, flood control, fisheries, waterfowl breeding, habitats and biodiversity enhancement have been realized, and the importance of wetlands has since been recognized. Thus, concerns over the fate of varying wetland ecosystems are widespread presently, and many programmes have been implemented to protect, restore and reserve them from further loss by human activities (Knutsen and Euliss 2001, Gleason et al. 2011).

In addition to the influences of direct human activities on the PPR wetlands climate change presents a new threat to those precious wetlands. Their unique geographical and geological characteristics make them particularly sensitive to climate variables. First, there are few natural drainage systems (e.g. streams) in the region and thus the majority of these wetlands have no stream inlets or outlets. Also, many of them are underlain by glacial till that

has low permeability and restricts their interaction with groundwater. As a result, the water balance of these potholes greatly depends on water exchange with the atmosphere, e.g. precipitation is the largest source of water (Winter and Rosenberry 1998, Johnson et al. 2005)and evaporation is the largest loss of water(Winter and Rosenberry 1998, Rosenberry et al. 2004). This great dependence on atmospheric water makes the wetlands particularly sensitive to climate variability in terms of temperature and precipitation (Winter and Rosenberry 1998, Johnson et al. 2005). Previous studies have suggested that spatiotemporal climate variation and the corresponding drought/deluge cycles are common in the PPR, and they affect the dynamics of wetland water surface levels and the corresponding ecosystem services (Huang et al. 2011). For example, field measured water levels and the number of pothole wetlands were reported to have good correlation with climate variables such as drought index and wet–dry cycles (e.g., Larson 1995, Winter and Rosenberry 1998, van der Valk 2005, Withey and van Kooten 2011). These well-established relationships imply the sensitivity of prairie wetlands to climate change. Climate change is expected to increase severity of drought conditions in the PPR under nearly all global circulation model scenarios (Johnson et al. 2005). The Intergovernmental Panel on Climate Change (IPCC) predicts that global surface temperature could rise by between 1.1 and 6.4 C by 2100 (Solomon et al. 2007), whereas regional climate models also predict a rise between 1.8 to 4 ° C in the PPR (Johnson et al. 2010). Although precipitation has moderately increased in recent decades, predicted drought conditions caused by warmer temperature will have important impacts on the PPR by reducing water levels/surface area of pothole wetlands, because the water level

fluctuation, the inter- annual and intra-annual water surface change is a key factor in regulating many ecosystem services and maintaining the ecosystem (Huang et al. 2011).

Because of the importance of wetlands in the PPR, as well as the importance of water surface, the dynamics of the PPR wetlands or their water dynamics instead have been studied by many researchers. Field surveys are conducted to measure water level fluctuations but have been limited to only a few individual wetlands (Rosenberry et al. 2004, Niemuth et al. 2010). As an alternative, remote sensing data is widely used in monitoring programmes to map PPR wetlands and lake areas, especially Landsat images and aerial photographs (Frazier and Page 2000, Beeri and Phillips 2007, Zhang et al. 2009). Although those spatial data can very effectively capture the spatial extents of the wetlands/lakes at certain points, satellite records are only available since the 1970s with limited coverage annually, mainly because of cloudy weather. Aerial photographs are even more spatially and temporally limited, making them less useful in determining the long-term temporal change. Climate data are temporally more available than remote sensing data with less spatial information, thuscombining climate data and remote sensing data could make up for each other to provide more information to wetland monitoring programmes. If a robust relationship between climate variables and spatial extent variables concerning wetland dynamics derived from remote sensing can be established, it can be used to fill temporal and spatial gaps, predict into the future, as well as estimate the causal effect of climate change on wetlands. For example, Withey and van Kooten (2011) employed linear regression analysis with temperature, precipitation and the standard precipitation index to predict the effect of potential climate change on wetlands of Western Canada. They predicted that future climate change could decrease Western

Canadianwetlands by between 7% and 47% from the baseline climate. Sorenson et al. (1998)found that in the Northern Great Plains, Palmer drought severity index (PDSI) is strongly correlated with annual counts of both pond numbers in May and breeding duck populations and used this relationship to project future pond and duck numbers under two general circulation model scenarios. In addition, Huang et al. (2011) simulated wetland water surface from 1910 to 2009 in Cottonwood Lake area of North Dakota, by integrating PDSI and remote sensing data.

In this research, we estimated the sensitivity of the PPR wetlands to climate change in terms of water surface area (WSA) and thus explored the impact that a changing climate might have on those wetlands. We use PDSI as our climate change proxy, because PDSI is a commonly used drought index based on water balance conception, which takes into account precipitation, temperature, evapotranspiration, stored soil moisture and runoff, as well as previous PDSI (Dai, 2011) and thus contains important information of climate change. The purpose of this chapter is (1) to determine the accuracy using Landsat images for characterizing the spatial variability in Prairie Pothole wetlands, (2) to establish a simple linear model between WSA and PDSI so that the sensitivity of wetlands to climate change could be estimated, (3) to take this model to predict wetland WSA in the 21st century based on PDSI series simulated under A1B climate change scenario and (4) to discuss the influence of climate change on the PPR wetlands based on our results.

3.2 Study area

My study area is the Kidder County, North Dakota, USA, located in the northeast of the PPR and covering an area of about 3800 km^2 (Figure 3.1). Kidder County is situated above unique geological and hydrological characteristics due to the last glacial retreat. Most of its subsurface is glacial till or unconsolidated ice-contact deposits of gravel, sand and silt. However, lacustrine deposits (silt) and fluvial deposits (cross-bedded sand and sand) are also present. Grassland, agricultural land, and lakes and potholes are the main land cover types. The topography is relatively flat, with elevation ranging from roughly 500 to 700 m and a mean elevation about 560 m above sea level. Also, as several major air masses from the Arctic, Pacific Ocean and the Gulf of Mexico converge in the atmosphere overhead, Kidder County represents an area of great climate variability in air temperature and moisture (Winter and Rosenberry 1998). Kidder County serves as a good candidate for studying the sensitivity of wetlands particularly on glacial moraine in the PPR to climate change with thousands of wetlands and variable climate.

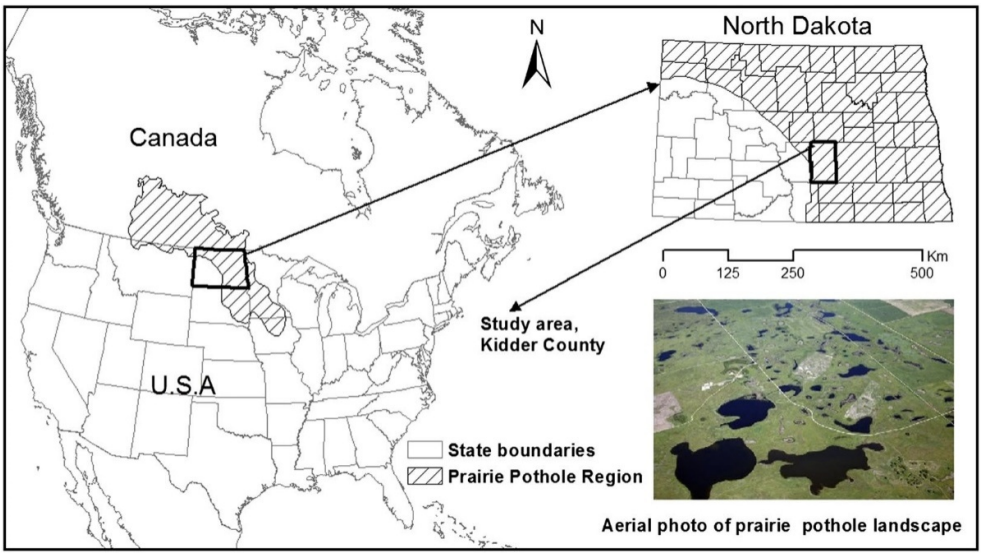

Figure 3.1, The study area, Kidder County, North Dakota, USA, is located in the Prairie Pothole Region (PPR). An aerial photograph on the lower right shows the wetland landscape

3.3 Datasets

Sixty seven cloud-free and high-quality Landsat TM/ ETM+ scenes between 1984 and 2011 were collected for classifying water surface (Table 3.1). High-resolution aerial photographs were downloaded from the USDA (http://www.fsa.usda.gov) for visual interpretation of wetland water surface.

As stated earlier, PDSI was used as the climate change proxy. Therefore, I downloaded monthly PDSI of the North Dakota climate division 5 from 1895 to 2011 from the National Climate Data Center (http://www.ncdc.noaa.gov/oa/ncdc.html) (Figure 3.2). The PDSI is the most prominent index of meteorological drought used in the United States and has been used to quantify long-term changes in aridity over global land in the 20th and 21st century (Dai 2011). Palmer (1965) originally developed PDSI intending to measure the cumulative departure in surface water balance in each climate division (The US climate divisions are available at http://www.esrl.noaa.gov/psd/data/usclimdivs/ data/map.html). PDSI is based on the water balance equation, which takes into account the water supply (precipitation and stored soil moisture) and demand (potential evapotranspiration, water storage and runoff), as well as previous conditions (i.e. wetness in one month is related to the previous month) (Huang et al. 2011). PDSI is also a standardized measure, ranging from +10 to -10(Dai 2011). However, it typically falls into the range from +4 to -4, which defines the extreme drought (-4) and extreme wet (+4) thresholds of the index (Huang et al. 2011).

Table 3.1, Landsat dataset (Path 32, Row 27) used in this study. The dataset in group 1 was used for model development, while the dataset in group 2 was used for model validation. The asterisks denote ETM+ images, while the others are TM images.

Group 1 for model development		Group 2 for model validation	
Year	Dates	Year	Dates
1986	20/5 5/6 23/7 8/8	1984	19/9
1987	21/4 7/5 30/10	1989	31/7
1988	23/4 9/5 29/8 30/9	1990	4/9
1991	31/3 22/8	1995	1/8
1992	20/5 27/10	1996	29/4
1993	21/4 28/9	1997	23/9
1994	26/5 14/8	1999	21/9 31/10
1998	5/5 25/8 10/9 28/10	2002	3/7
2000	2/5 18/5 9/10	2003	9/4 *
2001	25/8* 26/9* 20/10 5/11	2008	7/10
2005	6/4 22/4 15/10		
2006	25/4 11/5 28/6 14/7 19/11		
2007	28/4 2/8 3/9 19/9		
2009	3/5 19/5 4/6 20/6 22/7		
2010	20/4 25/7 13/10		
2011	12/7 13/8 14/9		

To explore the likely influence of future climate change on the PPR wetlands WSA by prediction, I also downloaded simulated monthly PDSI layers (2.5×2.5° resolution) in the 21st century from Climate and Global Dynamic (http://www. cgd.ucar.edu/cas/catalog/climind/pdsi.html), which were computed using multi-model ensemble-mean monthly data of precipitation, surface air temperature, specific humidity, net radiation, wind speed and air pressure from 22 coupled climate models participated in the IPCC AR4 (Dai 2011).

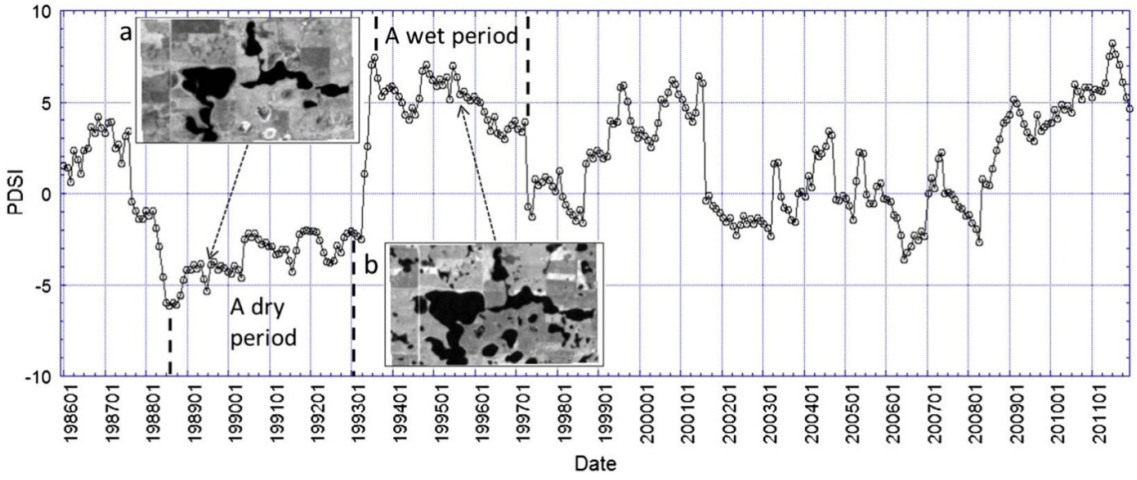

Figure 3.2, The monthly Palmer Drought Severity Index (PDSI) from 1986 to 2011 of Kidder County, ND showing the climate variation. A dry period with low PDSI and a wet period with high PDSI are illustrated. Two representative Landsat image subsets show less WSA in the dry period (a: band 5 subset of the TM image acquired on 31 July, 1989; b: band 5 subset of the TM image acquired on 1 August, 1995)

3.4 Methodology

I established a simple linear model between WSA and the PDSI climate index, and then used the model to simulate temporal change of WSA in the future under A1B climate change scenarios (a scenario with medium carbon emission assumption). First, water surface features were classified from the 67 Landsat images. In addition, temporally proximal aerial photographs of selected Landsat images were visually interpreted for water surface area, and the results were used determine the accuracy of Landsat extracted surface water area. Second, Iaveraged WSA and PDSI on different date to have annual mean values, divided the data into two groups, and used one group for linear model development and the other group for model validation. Finally, I used our linear model to predict the future WSA of the PPR using the simulated PDSI data.

3.4.1 Extracting water surface from remote sensing images

Geo-referenced Landsat images were firstly converted to top-of-atmosphere reflectance using the QUAC model built-in ENVI 4.8 (Bernstein et al. 2005) before classification. Ithen calculated the Modified Normalized Difference Water Index (MNDWI) with the green (band 2) and the Short Wavelength Infrared (SWIR, band 5) bands for water surface classification:

$$MNDWI = (Green - SWIR)/(Green + SWIR) \quad (1)$$

Using the SWIR band instead of the near-infrared band that is used in Normalized Difference Water Index (NDWI), MNDWI can considerably improve the enhancement of open water features and quickly discriminate water from non-water features (Xu 2006). A threshold of zero was applied on MNDWI images in a decision tree schedule to distinguish

water surface from non-water surface (Figure 3.3). I found that each classified images actually extracted the water surface as expected through careful visual check, except that a few un-planted agricultural lands with wet soils were also detected in some scenes during some wet periods. These fields were treated as false water surface and were excluded because no wetland was contained. However, to further confirm our water surface classification, two aerial photograph mosaics, made up of images which were acquired in 2006 (a relative dry year) and 2009 (a relative wet year) respectively, were visually interpreted, and their SWA was calculated and compared to classified Landsat images that were acquired on dates as close to them as possible (Table 3.2). The comparison validated that high accuracy was achieved by classifying WSA from TM/ETM+ images though slightly underestimated the actual WSA.

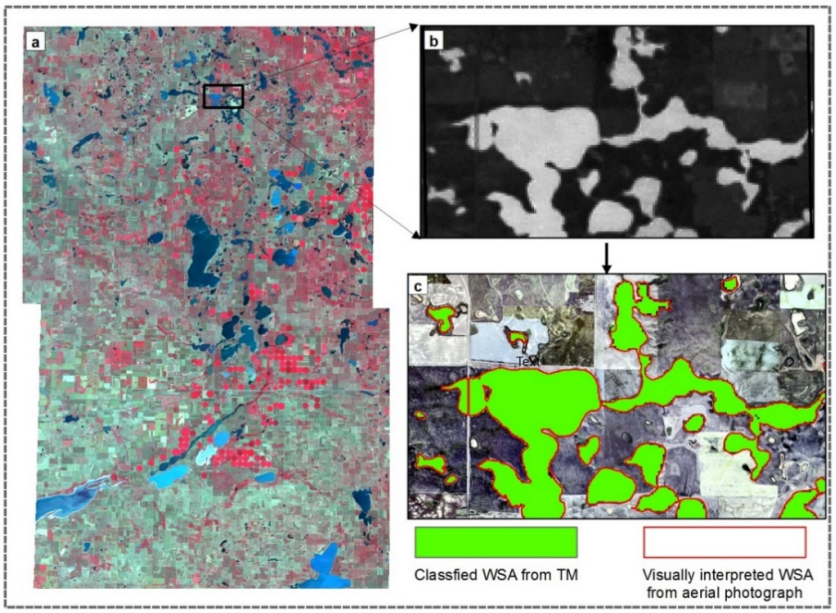

Figure 3.3, An example of water classification from the Landsat TM image acquired on 14 July 2007. a: false color composite of the image with band 4,3 and 2; b: MNDWI of a subset of the image; c: classified WSA from the image overlaying on the aerial photograph acquired on close date and the visually interpreted WSA from it.

Table 3.2, Visually interpreted aerial photographs were used to assess WSA classified from Landsat images acquired on dates close to the photographs. The Landsat image acquired on 14 July, 2006 was compared with the mosaic of aerial photographs acquired from 08 July to 14 July, 2006, and the Landsat image acquired on 22 July, 2009 was compared with the mosaic of aerial photographs acquired from 25 August to 30 August, 2009.

Coefficients	2006	2009
WSA from the aerial photograph/WSA from the TM image	98.4%	99.5%
Producer's accuracy	95.3%	86.9%
User's accuracy	93.7%	86.5%

3.4.2 Regression analysis, validation, and prediction

Though I collected 67 high quality and cloud free Landsat images spanning 28 years from 1984 to 2011, the number of scenes in each year varies. As there is intra-annual climate variance, the surface water also changes during different months or seasons within a year (Figure 3.4). All the Landsat images collected were acquired in spring, summer, or fall. However, the three seasons contribute most of the precipitation and evapotranspiration of the year, making the lack of winter data less important. For the total 28 years, I have 2 years (1985 and 2004) with no Landsat data and other years with varying number of TM/ETM+ scenes (Table 3.1). Thus, I divided the total 26 years having Landsat images into two groups: group 1 that has two or more images acquired in different seasons, and group 2 that only has images acquired in single season (Table 3.1). Since the existence of seasonal variation, I

expected the mean WSA of multi-seasons in years of group 1 on average to be closer to their annual mean WSA than years with single-seasonal images in group 2. Thus, Group 1data was used for regression analysis to establish a linearwhile group 2 data was used for the model validation. Since studies have stated that wetland WSA in the PPR are dependent upon water availability over previous years (Zhang et al. 2009, Niemuth et al. 2010), I put much attention into exploring the relationship between WSA and PDSI of lagged time steps (In this case, the time step is 1 year). I thus defined $PDSI_{t-0}$ as the PDSI value of the current year, $PDSI_{t-1}$ as the PDSI value one year previous, $PDSI_{t-2}$ as the PDSI value two year previous, and $PDSI_{t-3}$, $PDSI_{t-4}$, and so on accordingly. I did simple linear regressions between WSA and both lagged ($PDSI_{t-1}$, $PDSI_{t-2}$ … until $PDSI_{t-10}$) and non-lagged ($PDSI_{t-0}$) PDSI series. Autocorrelation between PDSI series was also explored. I then found that only $PDSI_{t-0}$, $PDSI_{t-1}$, $PDSI_{t-2}$, $PDSI_{t-3}$are significantly correlated to WSA and that PDSI has significant autocorrelation with one year lag. A stepwise multivariable regression analysis was thus done between WSA (the dependent variable) and $PDSI_{t-0}$, $PDSI_{t-1}$, $PDSI_{t-2}$, $PDSI_{t-3}$ to establish our final linear model. Subsequently, I validated my linear model using two methods. First, I took out any two years of data within group 1 (so that I have 120 cases as 16 years were contained by group 1), and fitted the model again by stepwise regression, in order to test sensitivity and stability of my model to fit the samples. Second, the WSA of the years within group 2 were predicted and compared to classified WSA from Landsat images to test the model's ability for prediction. After the model was validated, I predicted the temporal change of wetlands WSA in the PPR from 2020 to 2099 using simulated PDSI series by Dai (2011) under A1B climate change scenario assuming that the water area dynamics of the PPR region responds to PDSI the same

way as Kidder County. However, instead of modeling the actual WSA, I predicted it as the percentage relative to the mean WSA of the first decade in the 21st century, due to the lack of a validated full WSA dataset. I also did not do the prediction under other climate scenarios due to unavailable simulated PDSI series.

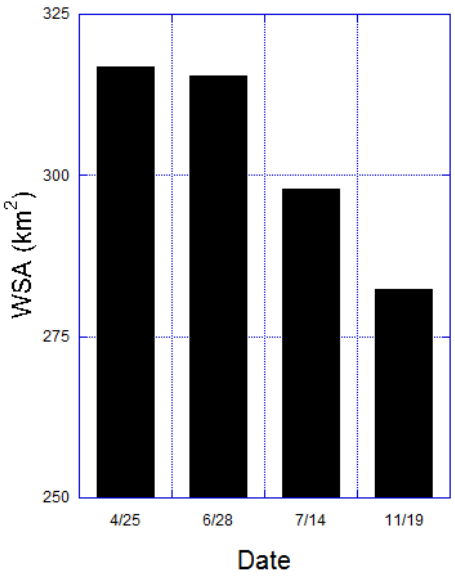

Figure 3.4, An example showing the 2006 seasonal WSA (water surface area) change due to intra-annual climate variation and other factors. The WSA was classified from Landsat images acquired in 2006 listed in table 3.3.1.

3.5 Results

3.5.1 Modeling

Significant correlation was only found between WSA and $PDSI_{t-0}$, $PDSI_{t-1}$, $PDSI_{t-2}$, $PDSI_{t-3}$, respectively (Figure 3.5). Among the single variables, $PDSI_{t-1}$ has the highest correlation with WSA (R^2=0.63), while $PDSI_{t-3}$ has the lowest correlation (R^2=0.26). As previous PDSI is also included in the calculation of current PDSI, I also explored the autocorrelation of PDSI. For annual mean PDSI, I only found significant correlation between $PDSI_{t-0}$ and $PDSI_{t-1}$ which is one year separated (Figure 3.6).

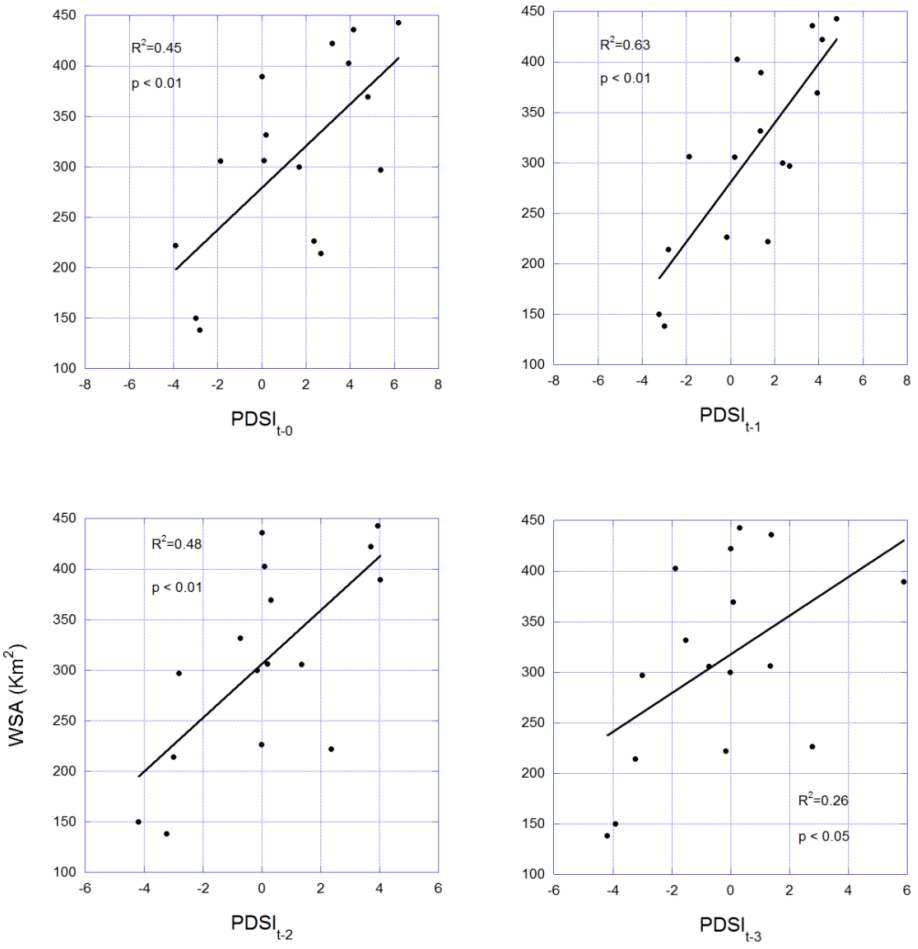

Figure 3.5, The simple linear regression relationship between WSA and $PDSI_{t-0}$, $PDSI_{t-1}$, $PDSI_{t-2}$, and $PDIS_{t-3}$ respectively. WSA data were classified from group 1 dataset listed in table 1 and then averaged for each year (total of 16 years included).

Since $PDSI_{t-0}$, $PDSI_{t-1}$, $PDSI_{t-2}$, and $PDSI_{t-3}$ have significant correlation with WSA and PDSI is auto-correlated with one year separation, Idid a stepwise multiple variable regression to establish our final linear model. The final model from stepwise regression was decided by minimizing the information loss with Akaike Information Criterion (AIC) that is the measure

of the relative fit goodness of a statistical model (Akaike 1981). The equation of our final linear model is:

$$WSA = 281.82 + 17.4 \times PDSI_{t-0} + 22.6 \times PDSI_{t-2} \quad (2)$$

Where WSA, $PDSI_{t-0}$, and $PDSI_{t-2}$ are the same as they have been defined before. The model has good R^2 equaling to 0.79, and all the coefficients are statistically significant (Table 3.3).

Table 3.3, Estimation and statistical test on equation (2).

Variable	Estimated coefficients	P value of T- test/F-test
(Intercept)	281.8	<0.001
$PDSI_{t-0}$	17.4	<0.001
$PDSI_{t-1}$	22.6	<0.001
R-Square	0.79	<0.001

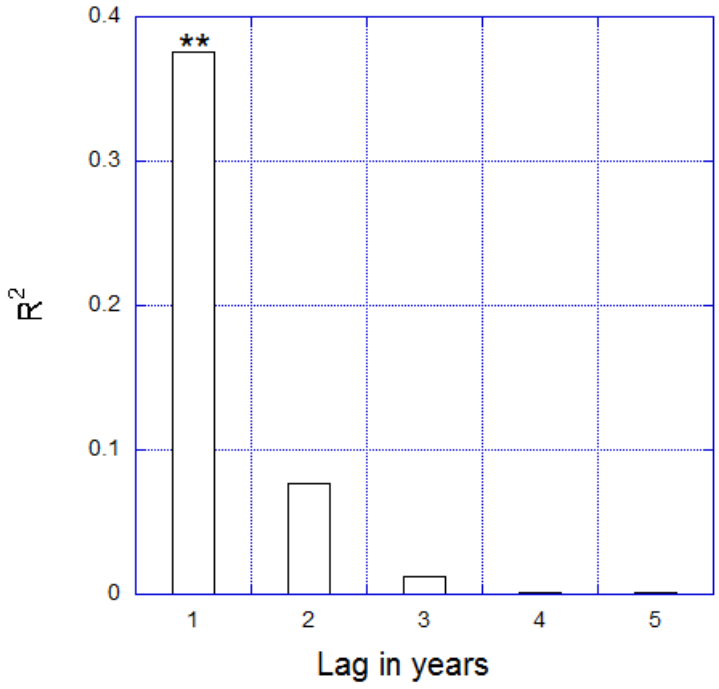

Figure 3.6, The autocorrelation of 100 year (1910-2010) annual mean PDSI time series with varying lag in years (lag longer than 5 years were not shown) shows that current year mean PDSI is only significantly correlated to that of last year. "**" above the bar indicates statistical significance with P value<0.01.

3.5.2 Validation

To develop our model, Iused data in years (16 years in total) covered by group 1 (Table 3.1). I then took out any two years and redid the regression. In this way, another 120 linear models were regressed by fitting $PDSI_{t-0}$ and $PDSIt_{-2}$ to WSA. The results are summarized in table 3.4. None of the coefficients change much within the 120 models, and the mean values of all coefficients are very close to those of the original model with no sample deduction. This suggests our model is not driven by a small number of outliers, and is not fitting the samples due to coincidence and is robust to fit the samples.

To further validate the model, we compared the predicted WSA of years in group 2 using equation (2) with WSA of the same years derived from Landsat images. As shown in figure 3.7, the predicted WSA and the remote sensing classified WSA matches very well. As uncertainty of WSA from seasonal variation could not be canceled out at all from group 2 remote sensing data (because having only one scene or two scenes of the same season for each year), the correlation between them could have been better.

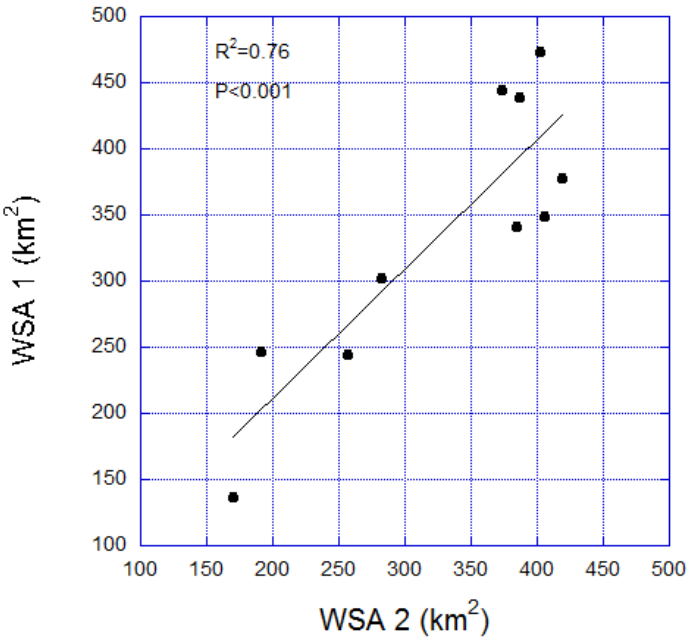

Figure 3.7, The validation of our model (Equation 2) by comparing WSA calculated from annual mean PDSI (WSA 1) with remote sensing derived WSA (WSA 2) in Kidder County, ND. The R^2 value is 0.76 with a slope of 0.98. The Landsat dataset group 2 listed in table 1 was used for the comparison and validation here.

Table 3.4, Basic statistics of some coefficients of the 120 linear models by taking any two years out of group 1 data.

Coefficients	(Intercept)	$PDSI_{t-0}$	$PDSI_{t-2}$	R^2	RSME
Min	272.7	12.6	18.7	0.67	33.1
Max	295.9	20.3	26.6	0.88	48.3
Mean	282.1	17.4	22.7	0.79	44.5
SD	5.0	1.6	1.6	0.04	3.6

3.5.3 Prediction

I modeled the WSA of the whole PPR in the 21st century using simulated PDSI based on IPCC AR4 22-model ensemble mean climate under the 20th century forcing and A1B scenario as described in the method section. Due to the variability in local geology, this prediction will be most accurate on similar glacial moraine, and there may be variability between sub regions in the PPR. The modeled WSA of the PPR in the 21st century as a percentage to the average WSA of the first decade (which serves as the baseline WSA and is derived from remote sensing) was plotted in figure 8. Based on our prediction, WSA in the PPR will have a decreasing trend with some oscillation, and local minimums will be found at the end of 2030s, the end of 2060s and beginning of 2070s, and the beginning of 2090s. Table 5 lists the mean modeled WSA of every decade as a percentage of the baseline WSA, which suggests that we could lose more than half of the wetland WSA in the PPR by 2050s, lose

more than two-thirds of the wetland WSA in the PPR by 2080s, and have a slight recovery of the PPR wetland WSA in the 2090s.

Table 3.5, The predicted WSA of every decade as a percentage of the baseline WSA (the mean of first decade) in 21st century.

	2020s	2030s	2040s	2050s	2060s	2070s	2080s	2090s
Percentage to the mean of 2000s	60.7	53.5	48.9	44.7	31.0	33.0	29.1	34.0

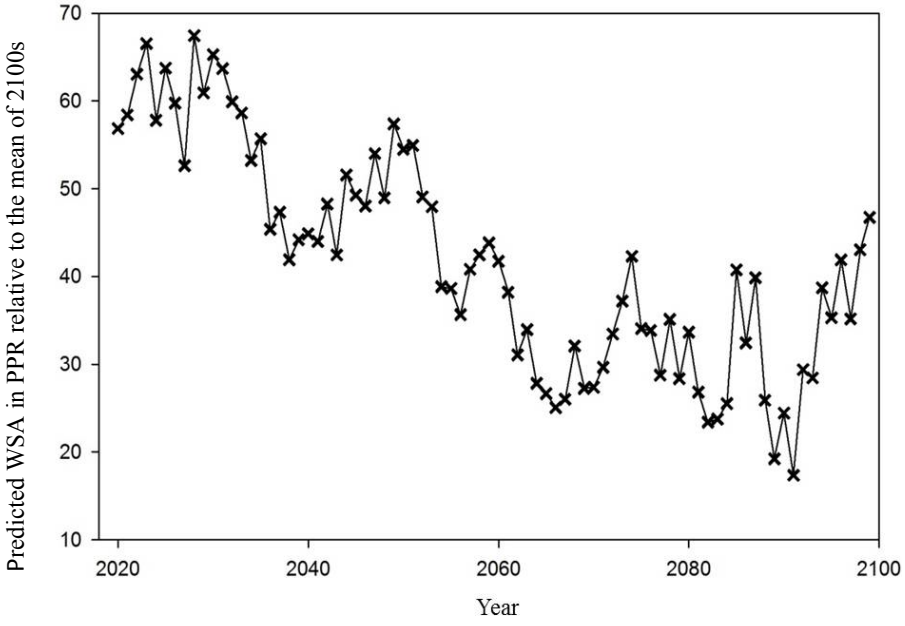

Figure 3.8, Predicted WSA of the PPR based on equation 2 from 2020 to 2099 as percentage of the mean WSA of the 2100s according to the 21st century PDSI monthly series simulated from 22 coupled climate models participated in the IPCC AR4 under A1B scenario.

3.6. Discussion

3.6.1 Sensitivity of the PPR wetlands to climate change

The water levels of PPR wetlands are not only influenced by climate variables of temperature and precipitation, but comprehensively by other factors like wetland size, basin morphometry, soil permeability, land use, catchment size, topographic position, groundwater flow, wetland and drainage patterns (Niemuth et al. 2010). However, climate is the most important among them. Precipitation and temperature explained more than 60% of the variation in number of wet basins throughout the Prairie Pothole Region (Larson 1995). PDSI was principally developed based on water balance concept and contain the important information reflecting climate change especially in terms of precipitation and temperature. Thus, PDSI is supposed to explain most WSA variation of the PPR wetlands. In our established linear model, $PDSI_{t-0}$ together with $PDSI_{t-2}$ can explain 79% of the WSA variance, and the slopes of $PDSI_{t-0}$ and $PDSI_{t-2}$ are large (17.4 and 22.6 respectively) for Kidder County, suggesting the high sensitivity of the PPR wetlands to climate change. For example, if both $PDSI_{t-0}$ and $PDSI_{t-2}$decrease by 1, Kidder County will lose 40$km^2$of wetland WSA, which is about 13% of the 28 year (1984-2011) average WSA. PDSI early three years prior has a slight influence on any given year's WSA (Figure 3.5). $PDSI_{t-1}$has the highest correlation with current year WSA by explaining 63% of the WSA variance when a single independent variable was used in the regression (Figure 3.5), because $PDSI_{t-1}$includes information from $PDSI_{t-0}$, $PDSI_{t-2}$, and itself due to the autocorrelation of PDSI series (Figure 3.6). However, $PDSI_{t-1}$ is also excluded from the final multi-variable linear model because of this redundant information it contains. Many studies have stated that wetlands WSA in the

PPR is dependent upon water availability over previous years (Larson 1995, Withey and van Kooten 2011). My results also support this point, suggesting that drought or wet condition in one year can not only influence WSA of the same year, but also can influence future WSA. The inertia and lagged influence is even larger than the no-lagged influence, as the coefficient of $PDSI_{t-2}$ is larger the $PDSI_{t-0}$ (Equation 2). This multi-year large inertia influence of PDSI suggests that minor dry periods or alternatively dry and wet periods may not alter the wetland WSA very much, but droughts lasting several years will dramatically decline the water surface in the wetlands.

3.6.2 Influence of climate change on wetlands of the PPR

Though there is less agreement regarding precipitation changes in the PPR, almost all model projection suggest that with no net change or even a modest increase in precipitation, drought frequency and severity are likely to increase during the 21st century due to, greater atmosphere demand caused by warmer temperatures(Sorenson et al. 1998). This drought trend will decrease the region's wetland WSA and accordingly all wetland surfaces, and impact their ability to support waterfowl and provide other ecosystem services. To provide some quantitative indication of the expected changes, we developed the linear regression model (Equation 2) that uses PDSI as proxy to determine how climate change will impact wetland WSA in the PPR. I then predicted the WSA in the 21st century using simulated PDSI under the projected A1B scenario. The A1B scenario is projected under medium carbon emission assuming balance across all energy sources (where balance is defined as not relying too heavily on one particular energy source) (Parry et al. 2007). Based on my prediction

under the A1B climate change scenario, the WSA of the PPR will decrease to less than half of the baseline WSA by the middle of this century, and to less than one-third by 2180s, though there may be a slight recovery at the end of the century (Table 3.5). This considerable decrease of WSA will not only just dry out the wetlands, but also have cascading influence on other features of the whole landscape. For example, it is simulated that the optimal numbers of waterfowls and ducks that the wetlands can support will fall at a much higher rate than wetland themselves (Withey and van Kooten 2011). Moreover, since wetlands have been drained for over a century to be a historical low level and continue to be drained for agricultural development (Withey and van Kooten 2011), important policy implications are provided from these results regarding the major influence of just climate change on wetlands. The practice of turning pothole wetlands into agricultural land must be very carefully considered as future climate change will also decrease both their size and abundance. Also, as wetlands have been identified as to be important carbon pools(Brander et al. 2006), the decrease of wetlands caused by climate change will have a positive feedback on itself by reducing their carbon uptake and triggering further carbon release. This must be considered in future adaptation to climate change. My predictions are made based on the "moderate" A1B climate scenario; however, we must be aware that there are different expectations of warming and drought magnitude over PPR region under other climate scenarios. For example, a more serious dry trend is simulated under the A2 climate scenario (a high carbon emission scenario) (Burke et al. 2006). Thus, according to the conceptual model, we would lose even more wetlands if future climate change underwent as the A2 climate scenario projects.

3.6.3 Model applications and uncertainties to be considered

My model could be useful for applications ranging from waterfowl management to climate change adaption in the PPR region, and my model conception could be applied to other wetland regions sensitive to climate change. If the users assume or predict the climate of the coming years reasonably, the WSA can be predicted from our model by calculating the corresponding PDSI. However, there are some assumptions made which reduce the certainty of the model results.

The first error source is about the inherent drawbacks of PDSI itself. PDSI is widely used and sufficient in many applications as a drought index; however, it is not perfect. For example, the assumption that no runoff is allowed to take place until the water capacity of the top soil layers is saturated is simplified and may lead to an underestimation of runoff (Huang et al. 2011). The drawback of PDSI most related to this study might be that all precipitation is treated as rainfall and snow storage is not accounted, resulting in inaccurate timing of PDSI values in the winter and spring months (Dracup 1991). For example, the observed spring WSA is larger than fall WSA in the study area in most years due to spring snow melting, which is an important component of PPR wetland hydrology, but the PDSI in not always higher in spring and cannot reflect it. Furthermore, the PDSI may have a slow response to drought of several months due to its dependence on soil moisture. This inaccuracy of PDSI is transferred to the model and thus influences its ability for prediction, though its influence is minimized by using annual mean PDSI values.

The second source of error in the model is related to scale. In terms of temporal scale, the basic time step of my model is one year, thus it is unable to account for short-term

weather events. For example, a severe thunderstorm may rapidly increase the water surface in a short time, which obviously cannot be reflected in our product. However, the influence of a likely single storm or other short events on the annual products is minimized by using a high number of satellite images. In terms of spatial scale, there are three sources of uncertainty. First, I used PDSI defined on a climate division which is close to but still larger than Kidder County where WSA is derived for model development. Since the American climate divisions are defined according to drainage basin or major crop, their boundaries do not necessarily delineate areas of climatological homogeneity(Guttman and Quayle 1996). This might influence the correlation between PDSI of a climate division and the WSA derived from just part of the division. If the PDSI and WSA were defined exactly the same spatial scale, an even higher correlation relationship between them could be expected. The second source of uncertainty related to spatial scale is about extrapolating from Kidder County to the entire PPR. We predicted the PPR wetlands WSA in 21st century by extrapolation (Figure 3.8) based on assumptions of homogeneity over the PPR landscape. However, the area of PPR is vast and exhibits considerable spatial and temporal climate variability as a result of convergence of multiple air masses. For example, drought or deluges do not always appear to be synchronous over the PPR and the spatial distribution of wetlands are not uniform but with varying sizes and types across the PPR (Kantrud et al. 1989). The assumption of homogeneity over the PPR make the extrapolation likely for the entire region due to the opposite variability between sub regions can compensate each other, but for any specific small sub section of the PPR (not include the Kidder County), the accuracy to model the temporal change of wetlands WSA may be reduced. Future improvements could be made to develop

individual models for each climate division in the PPR according to my conceptual model (i.e. acquiring WSA from remote sensing dataset, collecting PDSI series at similar scale, and then establish a linear relationship using regression), and then combine them to model the wetlands WSA of the entire PPR or any small sections more accurately. The last drawback concerning spatial scale is, due to their coarse resolution (30m), it is difficult for TM/ETM+ images to detect wetlands smaller than 0.40-0.8 ha (Ozesmi and Bauer 2002) and water areas close to lakeshore, but those small wetlands or edge area are biologically important. Therefore, as shown in table 2, the WSA derived from our Landsat dataset slightly underestimated the actual wetlands WSA (Table 3.2) though very high accuracies were achieved.

The third potential error source is about wetland variation caused by direct human activities. Since European settlement, pothole wetlands have been drained for agricultural use, resulting in a significant loss of wetlands. On the other hand, recently programs have been implemented to restore wetlands (Johnson et al. 2008), through the gains from them are minor compared to the ongoing loss due to agricultural conversion. Such wetland changes caused by direct human activities are detectable when Landsat records are used; however, PDSI is a drought index and clearly does not have the ability to capture this information. Thus, the variation of wetland WSA caused by direct human activities would not be able to predicted and reflected by our model. Nevertheless, it is not the goal for our PDSI model to account for direct human impact, and another equation could add to our model to account for them if users want to consider it. For example, investigations can be done to survey the proportion or exact area of wetlands WSA created or destroyed by human activities.

Lastly, notice the model predicts WSA only. The actual wetlands may decline with a different rate as the decline rate of WSA. The resilience of wetlands to the loss of WSA must be considered in further studies. Moreover, with a linear model, a simple and linear profile of the bathymetry of each pothole is assumed.

3.7 Conclusions

Temperature and precipitation are the most important climatic factors in determining the wetland water surface extent in the PPR. The PDSI, which is based on supply-and-demand concept of water balance and thus can comprehensively reflect climate change information in terms of temperature and precipitation, is very useful for modeling the PPR wetlands WSA change. WSA of current year is not only influenced by its current climatic condition, but is more severely influenced by climatic condition of previous years especially the prior year. PDSI as far back as three years can have influence on the current year WSA. However, only the current year PDSI ($PDSI_{t-0}$) and the PDSI two years prior ($PDSI_{t-2}$) were included in our final linear model (Equation 2) due to significant auto-correlation between PDSI series with one year separation. The model has R^2 that measures up to 0.79 with steep slope of each independent variable, reflecting the high sensitivity of the PPR wetlands to climate change. Based on my prediction, WSA of the PPR wetlands will decrease more than half by 2050s and more than two-thirds by 2080s as a result of drought from climate warming. This considerable future wetland loss caused only by climate change must be considered in future wetland management and climate adaptation policy. Nevertheless, due to some inherent drawbacks of PDSI, the scale related problems, and the inability to capture WSA variation caused by direct human activities, my model cannot explain 100% of the wetland WSA temporal change over the PPR and cannot reflect the short-term change caused by short-term weather events. To improve the scale-up prediction over the PPR region, future work is to establish individual models for each climate division contained by the PPR according to our conceptual model and combine them together for simulation.

3.8 Acknowledgements

This project was supported by the University Of Toledo Office Of Undergraduate Research through the Undergraduate Summer Research and Creative Activity Program (USRCAP). We thank Doctor Aiguo Dai from the National Center for Atmospheric Research for providing simulated monthly PDSI data. We thank the thorough review and input from an anonymous reviewer which improved this paper. We also thank our colleagues working in the Environmental Remote Sensing Laboratory of the University of Toledo for help revising this paper.

CHAPTER 4 RELATING ALGAL BLOOMS TO CO_2 FLUX IN WESTERN LAKE ERIE

Abstract

Lakes are important components in regulating carbon cycling within a landscape, yet reliable measurements of CO_2 flux within lakes especially large lakes at sufficient time and spatial scales are scarce and the current understanding of its various drivers are poor. Algal blooms have caused many environmental problems, but their relationships to ecosystem-scale CO_2 flux have never been examined. I integrated Eddy Covariance (EC) and remote sensing techniques to investigate how algal blooms may affect CO_2 flux in the western basin of Lake Erie, which is infamous for algal blooms. Three years (2012-2014) of long-term EC data at two sites were used. I found that no meteorological variables were significantly related to CO_2 flux under both high and low chlorophyll-a (a proxy of algal biomass) conditions at a 30-min scale; at daily scale, CO_2 flux was only correlated with some meteorological variables during algal bloom periods; and that chlorophyll-a concentrations were directly correlated with CO_2 flux at monthly scale at 1-2 month lag, depending on site location. My analysis suggests that growth/algal blooms may directly and indirectly influence CO_2 flux in Lake Erie and the relationship between algal growth/algal blooms and CO_2 flux varies spatially and temporally. However, considering the complexity of processes that drive CO_2 flux within large lakes and that some uncertainties remain in our estimations of both CO_2 flux and chlorophyll-a, more studies are needed to confirm our findings as well as extend our application to other large inland waters.

Keywords: Carbon Flux, Lake, Algal bloom, Eddy Covariance

4.1 Introduction

Lakes are important regulators in regional and global carbon cycling (Cole et al. 1994, Jonsson et al. 2003, Jonsson et al. 2007, Buffam et al. 2011, Hanson et al. 2014). Carbon produced within lakes or imported from upstream ecosystems may be stored in water, transported downstream, released via outgassing to the atmosphere, and/or deposited to the sediment (Battin et al. 2009, Tranvik et al. 2009). Many lakes in terrestrial landscapes are sources of CO_2(Cole et al. 1994), and if integrated into climate models, may shift these landscapes to become greater sources of CO_2. Failure to consider lake components from any up-scaling efforts on carbon pools and fluxes (Jung et al. 2011, Sun et al. 2011, Xiao et al. 2011) may add uncertainties to the derived products. To successfully integrate lakes into up-scaled products and climate models, one needs to understand the major carbon pools in lakes, the major fluxes to/from lakes, and the drivers and regulators of these pools and fluxes. The pools of key constituents of the lake carbon budget can be readily measured, but discerning the fluxes tends to be more problematic (Hanson et al. 2014).

NEE (net exchange of CO_2 between the lake and atmosphere) is one of the key fluxes within lakes, yet the current understanding of its various drivers is poor as reliable, large scale, and long-term measurements are scarce. Traditionally, CO_2 emissions from lakes have been measured via floating chambers with CO_2 sensors (Eugster et al. 2003) or estimated from measured CO_2 concentrations and gas transfer coefficients (Cole and Caraco 1998). Such methods have their own advantages but are insufficient for continuous long-term and relatively larger spatial scale (e.g., > 1 km) observation. NEE or CO_2 concentration/partial pressure in water was found to be vaguely correlated with phytoplankton primary production

and respiration, sediment respiration, climate, land use/land cover in watershed, etc., by using these methods (Sellers et al. 1995, Rantakari and Kortelainen 2005, Kortelainen et al. 2006, Finlay et al. 2009). However, these previous studies often used samples taken from one or a few locations to represent a whole lake, or samples taken from a few days to represent monthly or annual flux. Because of this, all correlative relationships previously found are worth careful re-examining within a longer term and larger scale context. Eddy covariance (EC) towers, which continuously and directly measure the ecosystem-level net exchange between the earth surface and the atmosphere, have provided us new opportunities to understand NEE in lakes. EC have been extensively applied in various terrestrial ecosystems to quantify NEE and study its drivers and regulators across multiple spatial and temporal scales (Baldocchi et al. 2001, Baldocchi and Wilson 2001, Stoy et al. 2009, Yi et al. 2010, Ouyang et al. 2014), but have been rarely applied in lakes especially in large lakes. Notably, only a few published articles have reported EC measurements of CO_2 fluxes over lakes, and these exclusively measured small lakes (Anderson et al. 1999, Eugster et al. 2003, Vesala et al. 2006, Jonsson et al. 2008, Huotari et al. 2011). These few studies focused on reporting the magnitude and temporal change of CO_2 fluxes, or comparing EC to traditional methods, but again the various drivers and regulators were rarely examined.

Algal blooms in lakes, especially harmful algal blooms (HAB), have been associated to a range of environmental problems worldwide (Anderson et al. 2002, Davies and Nugegoda 2012, Steffen et al. 2014); however, its association to NEE has been poorly understood in many large lakes that are susceptible for HABs (e.g., Lake Erie). Small lakes have limited pelagic zones and algae may not be the dominant primary producer, but in larger trophic

lakes algae are one of the most important biological features to solely determine the magnitude of primary productivity in open water. However, the potential effects of algal growth on NEE in open water areas of large lakes have never been carefully investigated at sufficient temporal and spatial scales due to various technical challenges. One such challenge is the continuous ecosystem-scale measurement of NEE and the other is the consecutive in situ measurement of algal biomass at the similar scale. In this study, the EC technique was used to measure NEE over western Lake Erie, the 12th largest lake on Earth by surface area, and the chlorophyll-a concentration was estimated from remote sensing to indicate algal growth. Many satellites (e.g. CZCS, SeaWiFS, and MODIS Aqua) have collected spatially continuous data repeatedly at high temporal resolution, and have provided us large scale data to study the underlying drivers of CO_2 flux between lake water and the atmosphere. These satellites record radiometric information of light reflected from water columns, and retrieval algorithms convert the radiometric measurements into interpretable physical properties (e.g., chlorophyll-a) based on the assumption that unique relationships exist between the spectral content of the scattered sunlight measured by the satellite-borne sensor and color producing agents (i.e., CPAs: chlorophyll-a and other pigments, colored dissolved organic matter (CDOM), and non-algal particulates) in the water, which all interact with sunlight (Lesht et al., 2012).

One important finding from EC-related work in terrestrial ecosystems is that vegetation properties and meteorological conditions are the main drivers of NEE. As a result, biotic measurements, such as chlorophyll-a related vegetation index (e.g., LAI (Leaf Area Index), NDVI (Normalized Difference Vegetation Index)), and meteorological measurements (e.g.,

air/soil temperatures, PAR, precipitation, etc.) are highly correlated with and/or co-vary with NEE at multiple time scales. Usually, meteorological variables are strong drivers of daily NEE cycles during growing seasons, and LAI/NDVI only co-varies with NEE at seasonal to annual cycles (Baldocchi et al. 2001, Stoy et al. 2009, Ouyang et al. 2014). Algae is the "vegetation" in the pelagic zone of Lake Erie. Algal photosynthesis takes in CO_2 dissolved in the water, which reduce the water's CO_2 concentration and has the potential to disturb the CO_2 equilibrium between the water and the atmosphere interface to cause a downward CO_2 flux. The eutrophic status of Lake Erie varies both spatially and temporally, with the western Lake Erie infamous for having HABs and being trophic (Commission 1980). Therefore, productivity along with algal growth likely comprises an important internal carbon process in western Lake Erie. According to what I have learned about NEE in terrestrial ecosystems, I hypothesize that (1) stronger relationships between daily mean values of meteorological variables and NEE would be observed during algal bloom periods than non-algal bloom periods, and (2) mean chlorophyll-a would be negatively related to mean NEE (the greater the chlorophyll-a, the lower the CO2 emission) at some longer time scales (e.g., monthly)

In this study, I aim to investigate the effect of algal growth/blooms on regulating NEE within western Lake Erie. In sum, I examined the relationship between chlorophyll-a and NEE at long time scales (i.e., 8-day, and monthly), and how algal blooms can affect the relationship between meteorological variables and NEE at shorter time scales (i.e., 30-min, and daily). This is the first study to research the biotic drivers of CO_2 flux over western Lake Erie, and also one of the few to investigate the underlying drivers of CO_2 flux for large inland lakes. This investigation could be well adapted to other big inland lakes and coastal waters.

4.2 Methodologies

4.2.1 Study Area

Our study area is the western basin of Lake Erie. Lake Erie is the fourth largest lake in North America by surface area and is well known for harmful algae bloom (HAB) events and or its history of cultural eutrophication, especially in the shallow western basin (Figure 4.1). The western basin comprises about one fifth of Lake Erie's total surface area and is naturally-delimitated from the deeper central basin by bedrock islands, reefs, and shoals (Herdendorf and Monaco 1988). Following the Great Lakes Water Quality Agreement (GLWQA) in 1972 that set maximum target phosphorus (P) loads, western Lake Erie experienced a period of improvement of algal blooms from the late 1970s through the mid-1990s, but has since returned to eutrophic conditions and HABs with a change in dominant species (Bridgeman et al. 2013). Western Lake Erie is strongly influenced by the inflow of the Maumee River, which brings in high loadings of suspended sediments and nutrients from the agriculturally-dominated watersheds and results in high turbidity (Paul et al. 1982) and abundant alga growth (Bertram 1993).

In this investigation, I installed two permanent EC flux stations in October 2011 in western Lake Erie. The first was located on top of the NOAA No.2 light buoy (41.8314N, 83.2006W, termed the Light site) and the second at the city of Toledo water intake crib (41.7167 N, 83.2667W, termed the Crib site) (Figure 4.1). The Light site is located 12km away from the lake coast while the Crib site is 4km from the coast. The water at the Light site is deeper and usually clearer than the Crib site (Figure 4.1). The equipment at the two sites have been routinely maintained by us and has been in continual operation since late 2011.

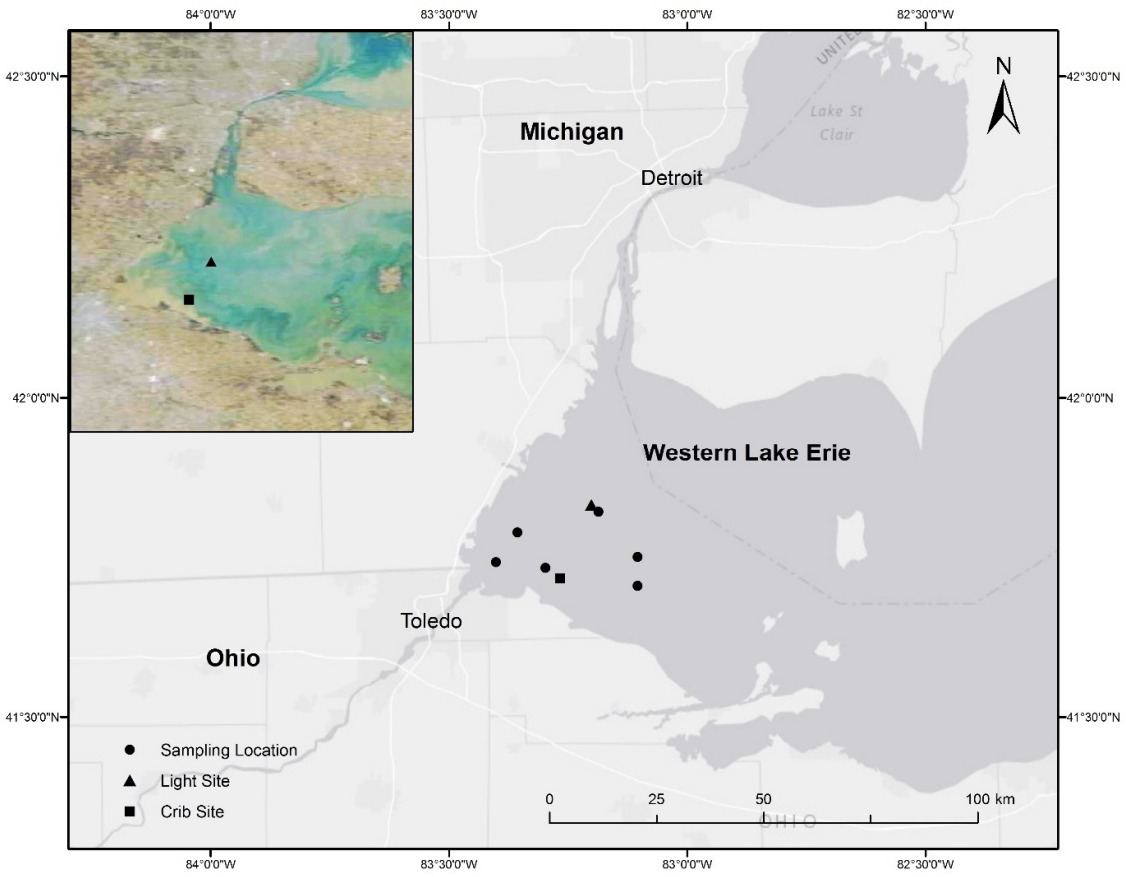

Figure 4.1, The study area- western Lake Erie. The EC towers were marked as a black triangle and rectangle respectively. The black circles represents where water samples were taken for chlorophyll-a extraction at 10-14 days interval. On the left-top is a MODIS true color image showing that western Lake Erie is high turbidity water especially at the Maumee River mouth.

4.2.2 NEE and meteorological measurements

An open-path EC system was installed at both sites at ~15 m above to measure NEE between the water surface and the atmosphere the lake at 30-min intervals. I utilized data collected in 2012, 2013, and 2014 for analysis in this study. Each EC system consists of an

infrared gas analyzer (IRGA, Model LI-7500A, LI-COR, Lincoln, NE, USA) that measures high-frequency (10 Hz) CO_2 and water vapor concentrations and a CSAT3 three-dimensional sonic anemometer (Campbell Scientific Inc. CSI, Logan, UT, USA) that measures three dimensional wind velocities and sonic temperatures. The IRGA was calibrated annually starting with deployment in October, 2011. Raw data spikes were removed; wind coordinates were rotated to the mean streamline plane calculated from wind data over an entire year (Wilczak et al. 2001) and temperature was corrected for changes in atmospheric humidity and pressure (Schotanus et al. 1983). Each 30-min mean NEE then was calculated as the covariance of vertical wind velocity, air temperature, and CO_2 and water vapor concentrations with the Webb-Pearman-Leuning correction (Webb et al. 1980, Massman and Lee 2002). The self-heating effect of the IRGA during winter was corrected to 30-min fluxes (Grelle and Burba 2007). The diagnostic signals from the CSAT3 and LI-7500A were used to detect and filter out periods having instrument malfunction. Additionally, stationarity of each 30-min flux was calculated to filter out data with poor turbulent conditions (Foken and Wichura 1996). Micrometeorological variables including photosynthetically active radiation (PAR) (LI-190, LI-COR), horizontal wind speed (U), relative humidity (RH), and air temperature (Ta) (HMP45C, CSI) were also measured at the same height as the EC system. Vapor pressure deficit (VPD), another important meteorological variable, was computed from Ta and RH as well. Additionally, footprint analysis (Kormann and Meixner 2001) of the 30-min CO_2 flux suggested that the 2 km radius centered at our tower contributed accumulatively more than 75% of the measured flux(Shao et al. 2015).

4.2.3 NEE at different temporal scales

After the data quality control was conducted as stated in 4.2.2, gaps were left in the 30-min CO_2 flux time series that reached 60% per year for the three year time series. This gap percentage is similar to that for other terrestrial EC sites in this area (Chu et al. 2014a, Chu et al. 2014b, Ouyang et al. 2014). EC related work in terrestrial ecosystems often use certain gap filling approaches (Reichstein et al. 2005, Moffat et al. 2007) to fill these gaps. Short gaps are usually replaced with values from nearby observation with similar meteorological conditions, while longer gaps are filled with some established relationship between NEE and meteorological drivers (Moffat et al. 2007). I did not fill all the gaps since good methods for gap-filling EC measurement in lakes does not exist except when calculating daily mean NEE. Instead, I employed the following strategy. First, I used only 30-min data that passed data quality control. I then calculated 8-day mean NEE for those 8-day windows having at least half of the 30-min NEE available, and monthly mean NEE for the months with at least one third of the 30-min NEE available. Daily mean NEE was calculated for those days where the number of gaps was less than half after gap-filling, i.e., I filled 30-min gaps for screened days using two steps: 1) linear interpolation was applied to gaps less than 1.5 hours and 2) the remaining gaps were filled with the mean of nearby 30-min values from similar periods within ± 1days. This method of gap-filling was validated by verifying that 30-min NEE are auto-correlated within 1-3 steps, and 30-min NEE at the same time during consecutive days was auto-correlated with only one-day lag (Figure 4.2). I carried out gap-filling to compute daily means, since both daily NEE and 30-min NEE are at high frequencies that are variable,therefore reliable daily mean estimation is dependent on having most of the 48 30-

min data points within a day being available. Even so, applying a strict criteria that two thirds of the 30-min data points must be available would retain only a few days of the daily NEE data.

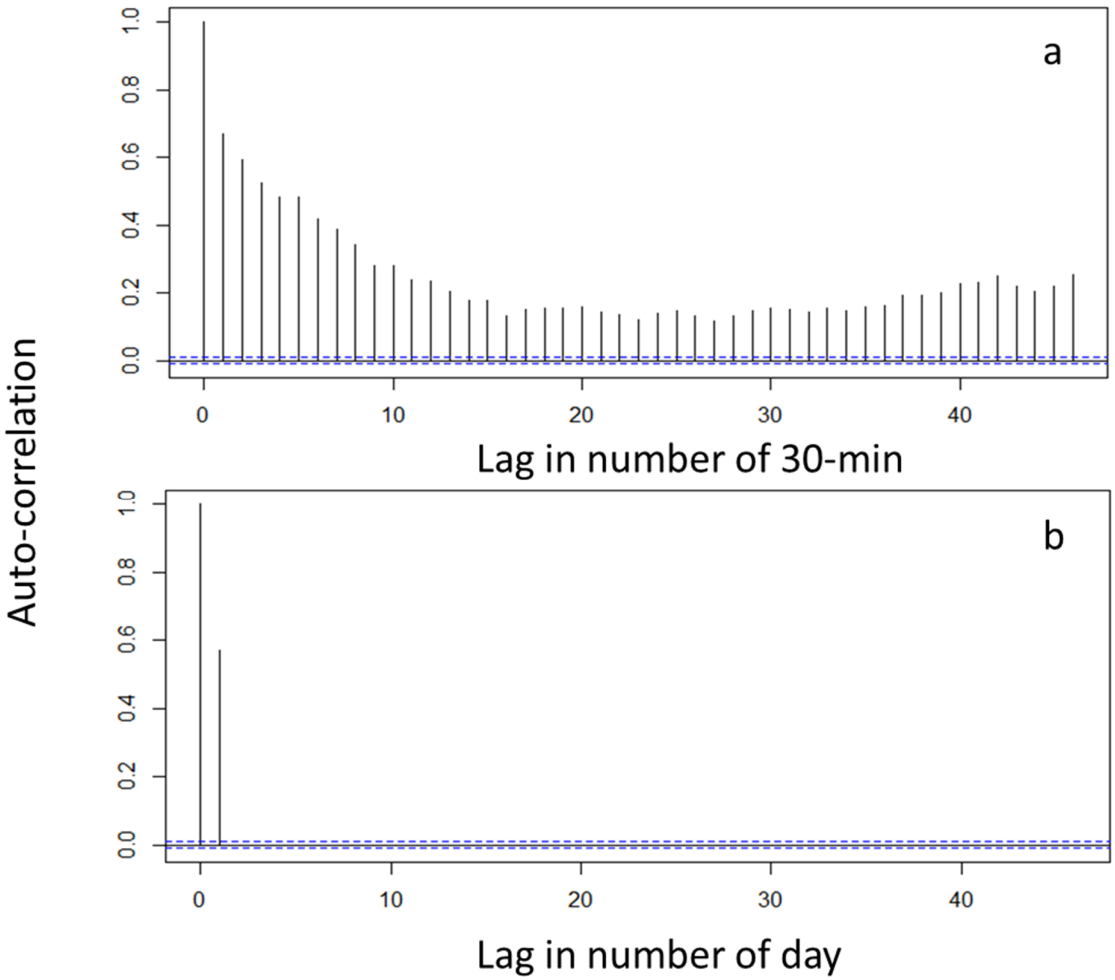

Figure 4.2, Example of autocorrelation tests of 30-minNEE. 30-min NEE at 30-min interval at the Crib site (a), and 30-min NEE of the 20th 30-min (i.e., the second half hour of 10 am) at daily interval (b).

4.2.4 Chlorophyll-a measurement and estimation

Water was sampled for chlorophyll-a at six locations in western Lake Erie (Figure 4.1) at 10-14 day intervals between April and October in 2012 and 2013. At each sampling site, two 50 ml replicates of water samples were collected, one at the depth of 1m and another at the surface in each sampling trip. Water samples were filtered after being brought back to the

lab using glass-fiber filters (GF/F). The filters were desiccated and stored in an ultra-cold freezer (-70 °C). Chlorophyll-a then was extracted from the filters using dimethylformamide and analyzed fluorometrically on a Turner fluorometer (Moorhead et al. 2003). These field sampling data were used to validate estimation of chlorophyll-a with remote sensing.

Chlorophyll-a for analysis in this study was retrieved from remote sensing radiative measurements determined by the MODIS sensor on NASA's Aqua MODIS satellite with a OC3 algorithm (O'Reilly 2000). Existing retrieval algorithms can be categorized into two groups: (1) semi-analytical models that first model water-leaving radiance with the multiple interacting CPAs from their inherent optical properties and then invert the model to calculate the concentrations of considered CPAs from satellite recorded radiometric information, and (2) the empirical algorithms which are based on the assumption that a single CPA (e.g. chlorophyll-a) is dominant and that a relationship (usually linear) exists between this single CPA and some function of the radiometric measurements. Both groups of algorithms have been widely applied in the Laurentian Great Lakes, and empirical algorithms performed even better than semi-analytical algorithms in many cases (Lesht et al. 2012). OC3 is an empirical band ratio algorithm that is of greatest value in regions where the concentrations of non-algal interfering substances are minimal (e.g., the open ocean). In coastal and inland waters where the optical properties are complex, OC3 performs relatively poorly. Semi-analytical algorithms are designed to have advantages over conventional empirical algorithms for optically complex water, but the development of an accurate semi-analytical model is complex and difficult (Maritorena et al. 2002), and requires accurate measurements of inherent optical properties. In fact, previous studies in the Great Lakes have shown that the

empirical band ratio retrieval algorithms produced chlorophyll-a concentrations that were proportional to observed concentrations, and only tended to overestimate concentrations at lower values and underestimate them at higher values (Lesht et al. 2012). NASA provides standard 1-km resolution chlorophyll-a products (Level-2) computed by OC3, but the NASA standard products exclusively use ocean bands that were designed to have high sensitivity over the dynamic range of reflectance typical over open oceans (Franz et al. 2006). Since western Lake Erie contains highly turbid inland water, it is possible for such ocean bands to be saturated (Franz et al. 2006). The inclusion of other land/cloud bands from MODIS data, with both increased spatial resolution and reduced sensitivity over a broader dynamic spectral range, may improve the retrieval of chlorophyll-a over inland waters (Franz et al. 2006). Thus, I included such land/cloud bands to compute 250m resolution chlorophyll-a (Level-2) from MODIS Level-1 reflectance data. Because OC3 is determined empirically with a global dataset in which the chlorophyll-a distribution range is approximately 0.008-90 μg/L, I excluded values outside of the range 0.01 to 100μg/L. Quality flags that indicated cloudy conditions, atmospheric correction failure, severe sun glint, and saturation of bands, etc., were used to mask out bad quality pixels. Our validation suggests that our Level-2 MODIS chlorophyll-a estimation using OC3 is accurate for correlation analysis (Figure 4.3).

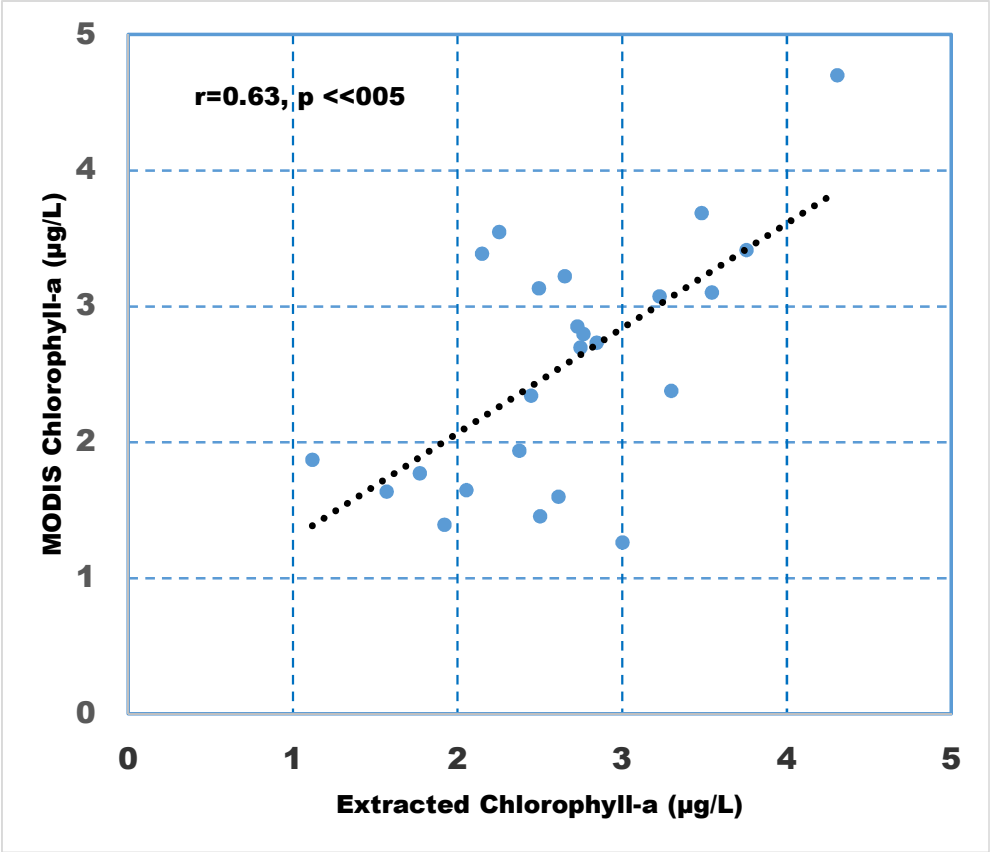

Figure 4.3, Comparison of estimated Chlorophyll-a concentrations by MODIS to extracted Chlorophyll-a concentrations from water samples. Data are plotted in log scale.

Aqua MODIS covers western Lake Erie at least once a day, but as a result of data quality control, our Level-2 MODIS chlorophyll-a had considerable spatial and temporal gaps. Spatial and temporal binning algorithms (Campbell et al. 1995) thus were used to determine daily, 8-day, and monthly composites products (Level-3) at 4×4 km2 spatial resolution to match the footprint of the EC towers. One advantage of remote sensed chlorophyll-a is that it measures the portion of a water column that transmits light and can better spatially match the footprints of EC towers than extracted chlorophyll-a from site

specific sampling. All remote sensing data processes were conducted in SeaDAS 7.1 and ENVI 5.1.

4.2.5 Statistical Analysis

Regression analysis was used to test for significant relationships between the mean values of a meteorological variable (i.e., PAR, Ta, WD, RH, and VPD), and/or chlorophyll-a and NEE at four time scales (i.e., 30-min, daily, weekly, and monthly means). Ideally, exploring relationship at high frequencies/short time scales requires de-trending to remove any trends and/or variation at low frequencies/long time scales. The NEE measurements in this study show no daily trends and only a very weak seasonal trend (APPENDIXC, Figure C.4 and C.5), thus negating the need for a de-trending analysis. To examine whether algal blooms can affect how meteorological conditions drive NEE at high frequencies, the relationship between 30-min meteorological variables (i.e., PAR, Ta, WD, RH and VPD) and 30-min NEE was compared under both high chlorophyll-a (>=10 μg/L) and low chlorophyll-a (< 10 μg/L) conditions, and the relationship between daily mean meteorological variables (i.e., par, Ta, WD, RH and VPD) and daily mean NEE was compared between periods with and without algal blooms. Based on observed chlorophyll-a variations, algal bloom periods were defined as August and September in 2012 and 2014, and August, September, and October in 2013. To examine whether chlorophyll-a drives a change in NEE at low frequency/long time scales (i.e., seasonal and annual cycles), the relationship between 8-day and monthly means of chlorophyll-a and NEE was explored using regression analysis. Unlike in terrestrial ecosystems, algae first consumes CO_2 dissolved in water, and water then exchanges CO_2 with the atmosphere; thus I also conducted regression analysis between the 8-

day/month chlorophyll-a and the following 1st or 2nd 8-day/month NEE to examine temporally lagged relationships. The same analysis was applied to Light and Crib EC stations separately. Though chlorophyll-a concentrations are usually log-normally distributed within a large sample, I did not apply log-transformation because it did not improve normality, potentially due to our smaller data size. All statistical analysis was performed using the R platform (R Development Core Team, 2014, version 3.1.1). I did not examine the relationship between chlorophyll-a and NEE at the higher frequency 30-min means and daily means due to limited data and increased data uncertainty at high frequencies.

4.3 Results

4.3.1 Seasonal changes of Algal bloom and NEE

Western Lake Erie experienced similar seasonal patterns of algal blooms in the three sampling years (i.e., 2012, 2013, and 2014). Based on the temporal and spatial distribution of chlorophyll-a measurements, the algae bloom began to grow quickly in late summer with blooms initiating near the coast (Figure 4.3). In 2012 and 2014, the largest algae (in both concentration and area) bloom mainly occurred in August and September, while in 2013, the bloom continued from August through to October. Algal growth followed apparent seasonality in all three years, with a higher concentration of chlorophyll-a occurring in late summer and fall and with lower concentrations chlorophyll-a occurring at other times.

NEE only showed only a weak seasonality with more negative NEE values in late fall and more positive or neutral NEE values in late summer (Figure 3, APPENDIX Figure C.3) at both EC sites. In the spring, the Light site tended to have negative or neutral NEE, while the Crib site tended to have positive or neutral NEE. August is the month when algal bloom reached the peak, however, NEE at both sites in August were either positive (e.g., in 2012 and 2014) or neutral (e.g., 2013). The seasonal patterns of algal blooms and NEE indicated a lagged relationship between the two.

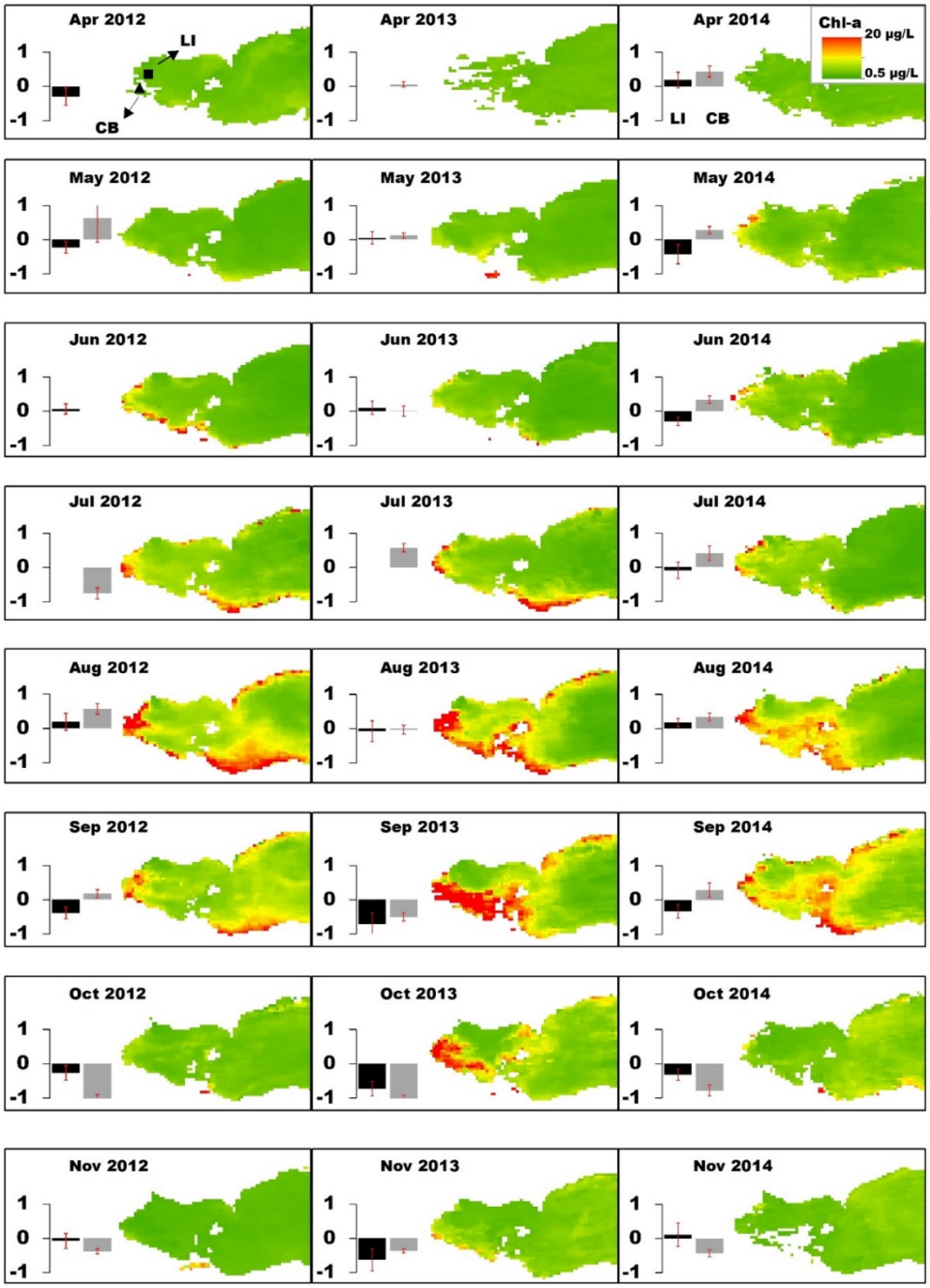

Figure 4.4, The monthly mean chlorophyll-a distribution in western Lake Erie and the monthly mean NEE (µ mol m^{-2} s^{-1}) at both the Light and Crib sites, with standard errors shown by red bars

4.3.2 Meteorological variables and NEE

The relationships between the 30-min means of meteorological variables and NEE were similar under both high chlorophyll-a (chlorophyll-a >= 10 μg/L) and low chlorophyll-a conditions (chlorophyll-a <10 μg/L). At 30-min frequency, NEE was not correlated to any of the meteorological variables (i.e., PAR, Ta, U, VPD, and RH) during either nighttime or daytime at both the Light and the Crib site (Figure 4.5). The 30-min mean NEE under high chlorophyll-a (chlorophyll-a >= 10 μg/L) and low chlorophyll-a conditions (chlorophyll-a <10 μg/L) at both sites also did not significantly differ under varying PAR and Ta conditions (Figures 4.6 and 4.7). However, the relationships between daily means of meteorological variables and NEE were different during algal blooms (August and September in 2012, 2014, and August, September, and October in 2013) versus non-algal bloom seasons (i.e., other months) (Figure 5). PAR, Ta, and U were significantly correlated with daily average NEE during the algal bloom seasons at both sites (Figure 4.8). VPD and RH were linearly correlated with NEE at the Light site but not at the Crib site, however, VPD may be non-linearly related to NEE at the Crib Site based on local regression fitting (Figure 4.8).

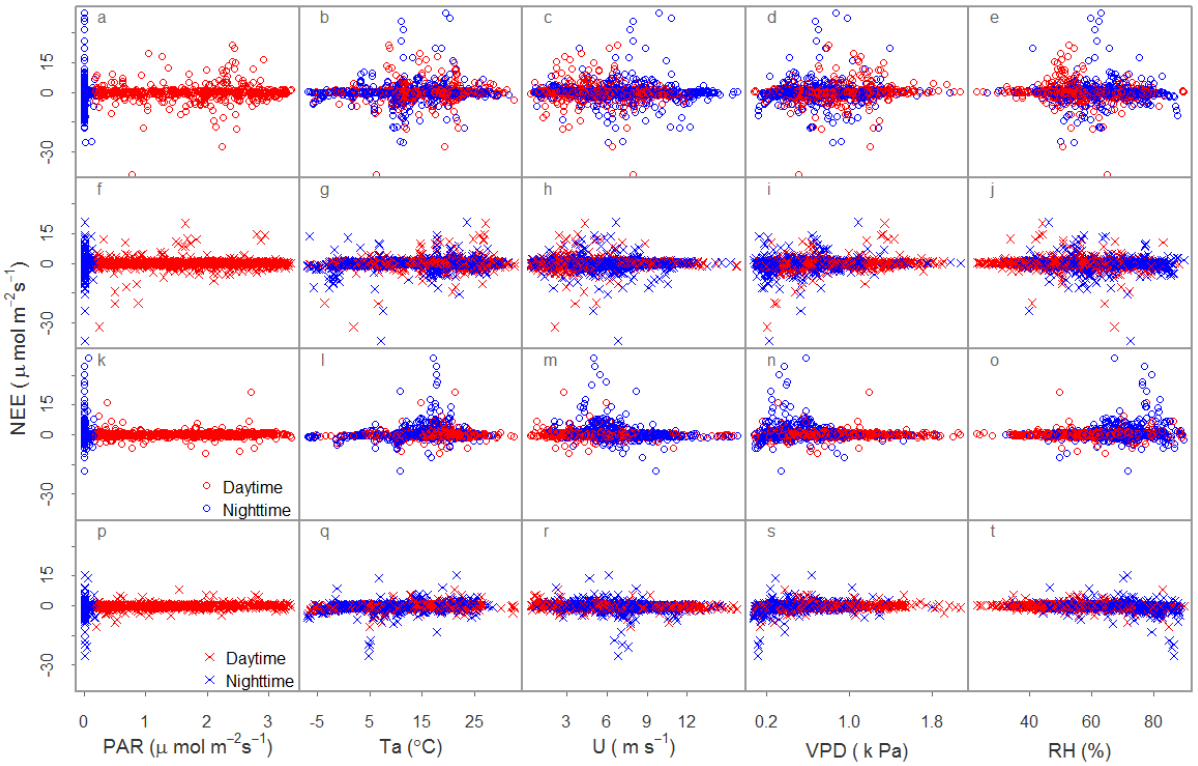

Figure 4.5, Scatter plot of NEE versus meteorological variables at both the Light site under high chlorophyll-a condition (>=10 mg/L, a, b, c, d, and e) and low chlorophyll-a condition (<10 mg/L ,f, g, h, I, and j), and the Crib site under high chlorophyll-a condition(k, l, m, n, o) and low chlorophyll-a conditions (p, q, r, s and t). High chlorophyll-a conditions are drawn by circles, while low chlorophyll-conditions are drawn by crosses.

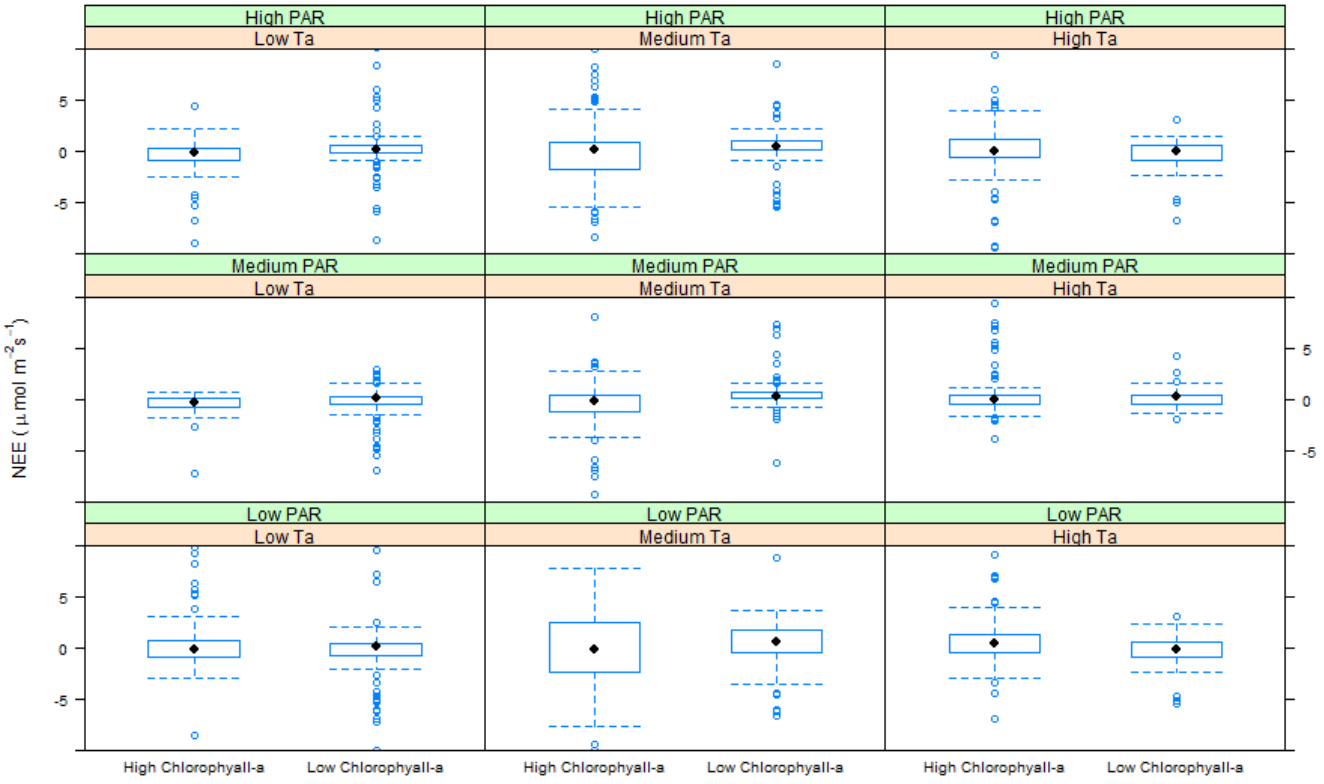

Figure 4.6, Boxplot comparisons of NEE between high chlorophyll-a conditions (>=10 mg/L) and low chlorophyll-a condition at the Light site . Low, medium, and high PAR and Ta were determined by one third and two thirds quantiles of each variable respectively. There are NEE values beyond the limits of the y-axis , which are not shown.

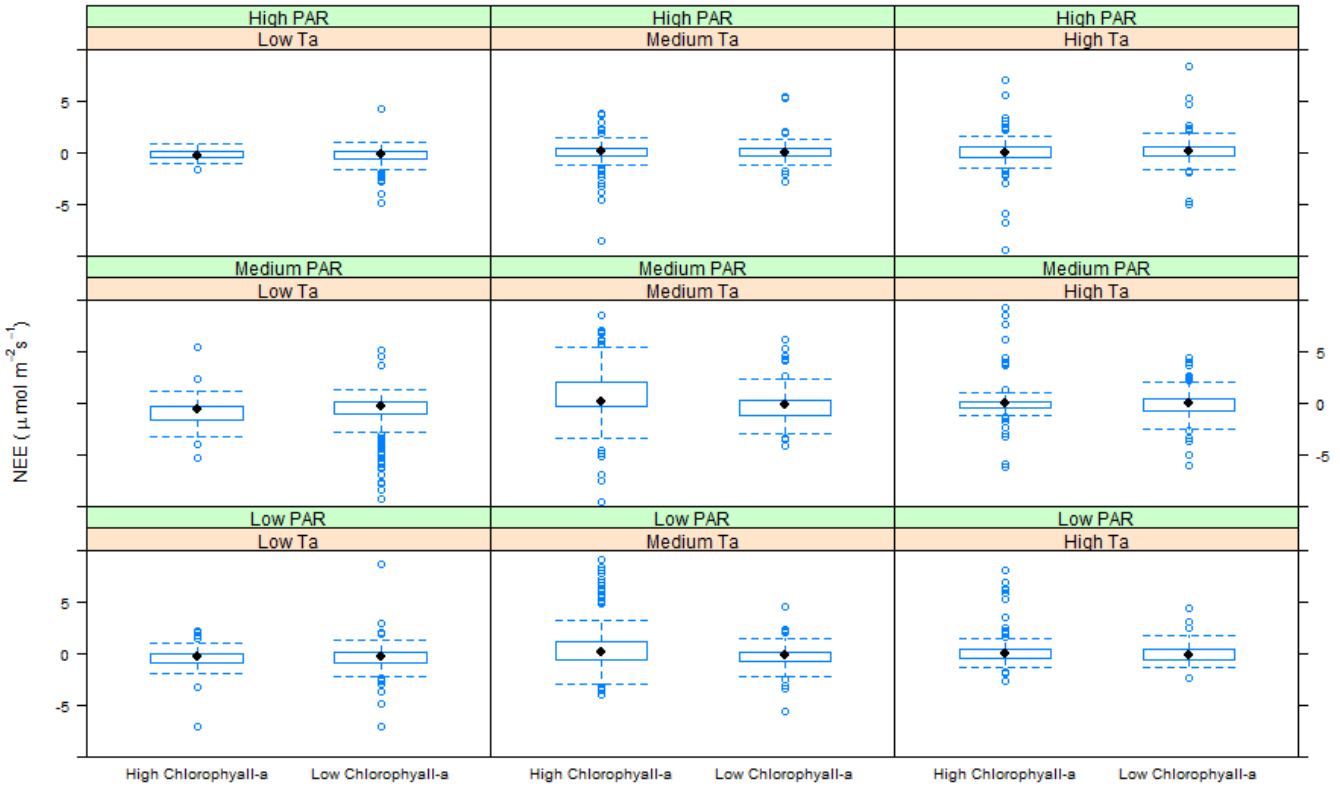

Figure 4.7, Boxplot comparison of NEE between the high chlorophyll-a conditions (>=10 mg/L) and low chlorophyll-a condition at the Crib site. Low, medium, and high PAR and Ta were determined by one third and tow thirds quantiles of each variable, respectively. There are NEE beyond the limis of the vertical axix , which are not shown.

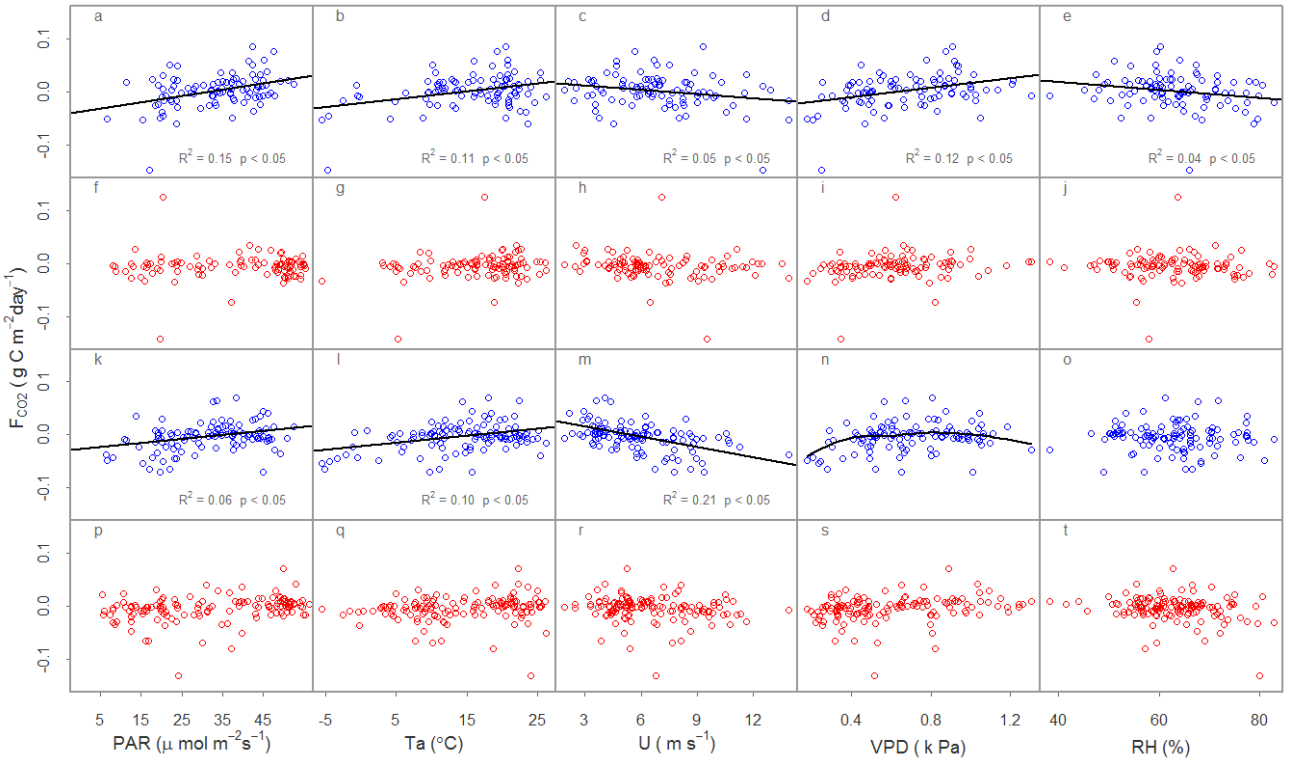

Figure 4.8, Scatter plot of NEE versus meteorological variables at both the Light site during algal bloom seasons (a, b, c, d, and e) and non-algal bloom seasons (f, g, h, i, and j), and the Crib site during algal bloom seasons (k, l, m, n, and o) and non-algal bloom seasons (p, q, r, s, and t). Linear lines were fitted by regression when there was a significantly linear relationship. A *loess* local regression smoothing line was fitted to plot n at the Crib site.

4.3.3 Chlorophyll-a and NEE

No significant correlation was found between the 8-day mean NEE and chlorophyll-a when there was no temporal lag between the two phenomenon (Table 4.1). However, when NEE was temporally lagging behind chlorophyll-a by one 8-day period, the correlation increased and became significant at the Light site, When NEE was lagging behind chlorophyll-a by two 8-day periods, the correlation also increased and the p-value (0.07) was substantially decreased (Table 4.1). Mean NEE and mean chlorophyll-a values during the same month were also not correlated, but a significantly negative correlation was obtained between monthly mean NEE and monthly mean chlorophyll-a at the Light site when NEE lagged behind one month compared to chlorophyll-a, and at Crib site when NEE lagged behind by two months compared to chlorophyll-a (Figure 4.9). Although the two sites had similar meteorological conditions in each year (Table 4.2) aside from wind velocity, the site (Crib in 2012 and 2014, Light in 2013) that had a higher chlorophyll-a in August, September, and October also had a more negative NEE in the following September, October, and November (Figure 4.10). Result show that 2013 had the highest chlorophyll-a concentration, following 2012 and 2014 for both sites. Examining each site, the year that had higher chlorophyll-a a in August, September, and October also had a more negative NEE in the following September, October, and November (Figure 4.10). A strong linear relationship (R^2=0.91) existed for average chlorophyll-a in August, September, and October with average NEE in September, October, and November (i.e. one month lagged effect) (Figure 4.10). Mean 8-day NEE and chlorophyll-a values were more likely (e.g., smaller p-value) to be correlated when temporal delays were considered (Table1).

Table 4.1, Linear correlations between chlorophyll-a and NEE over an 8-day scale (i.e., 8-day means) and their corresponding p-value.

	Light Site		Crib Site	
	Correlation	p-value	Correlation	p-value
No lag	0.24	0.27	0.13	0.66
NEE lagged chlorophyll-a by one 8-day period	0.48	0.04*	0.06	0.82
NEE lagged chlorophyll-a by two months	0.28	0.17	0.47	0.07

Table 4.2, Average meteorological conditions at the Light and Crib sites during different periods. The PAR values used in this study are cross validated by each other from both sites and only one value is reported here.

			Ta (°C)	U (ms^{-1})	VPD (kPa)	RH (%)	PAR ($mol\ m^{-2}\ (30min)^{-1}$)
Aug. Sept. Oct.	2012	Light	17.7	5.1	0.60	68.3	0.58
		Crib	17.4	6.2	0.64	66.2	
	2013	Light	18.2	4.9	0.54	71.5	0.60
		Crib	18.3	5.6	0.62	68.3	
	2014	Light	17.6	4.8	0.52	71.3	0.54
		Crib	17.9	5.8	0.57	69.5	
Sep. Oct. Nov.	2012	Light	11.8	5.1	0.42	69.3	0.41
		Crib	11.7	6.2	0.46	66.4	
	2013	Light	12.2	6.0	0.40	70.7	0.43
		Crib	12.4	6.9	0.45	68.0	
	2014	Light	14.0	5.1	0.45	69.7	0.44
		Crib	14.3	6.5	0.49	67.9	

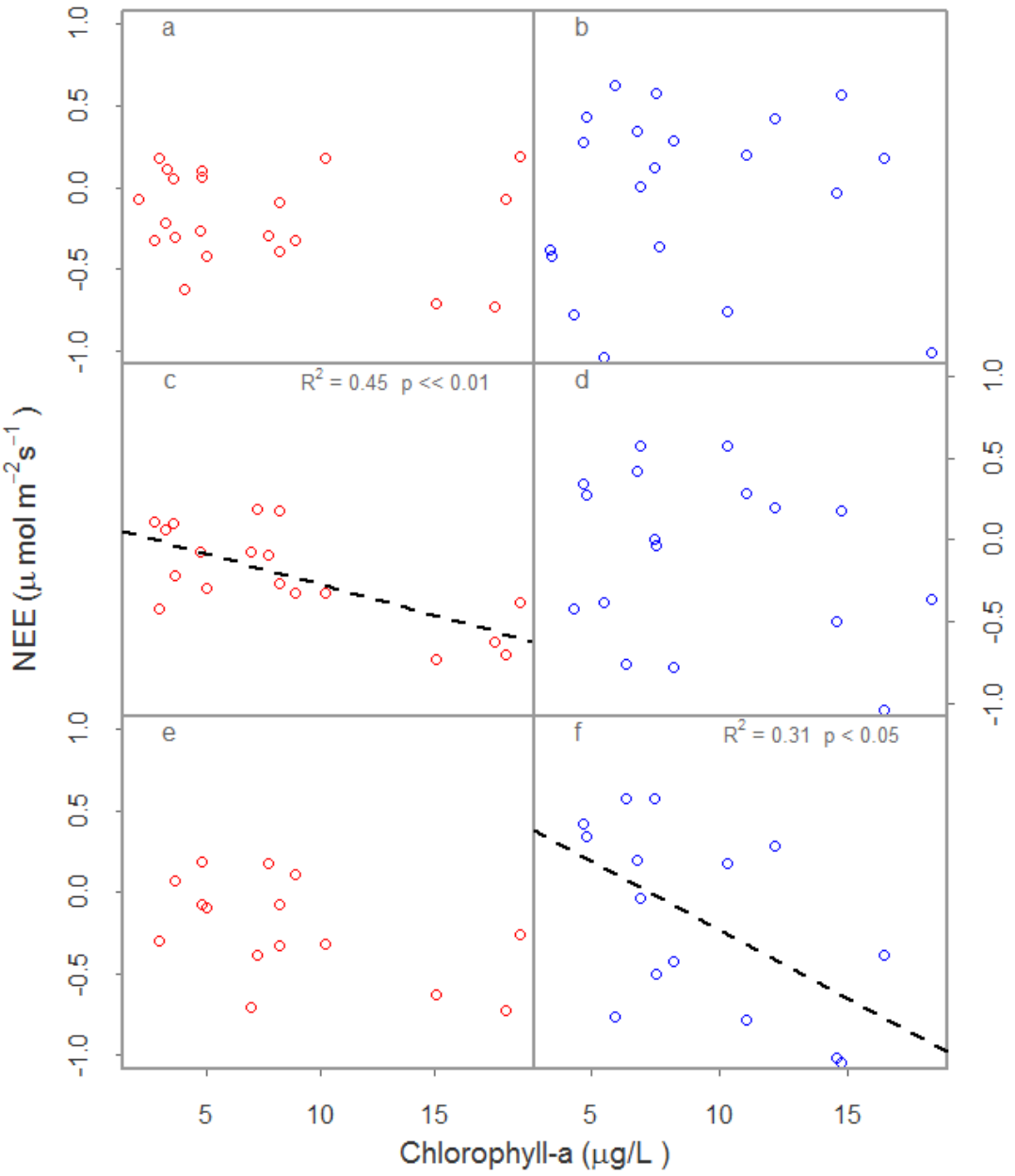

Figure 4.9, The scatter plots of monthly mean NEE and chlorophyll-a at the Light (red) and Crib (blue) sites when there is no lag (a and b); NEE lagged behind chlorophyll-a by one month (c and d) and NEE lagged behind chlorophyll-a by two month (e and f). Lines were fitted by regression only when there is a significant linear relationship.

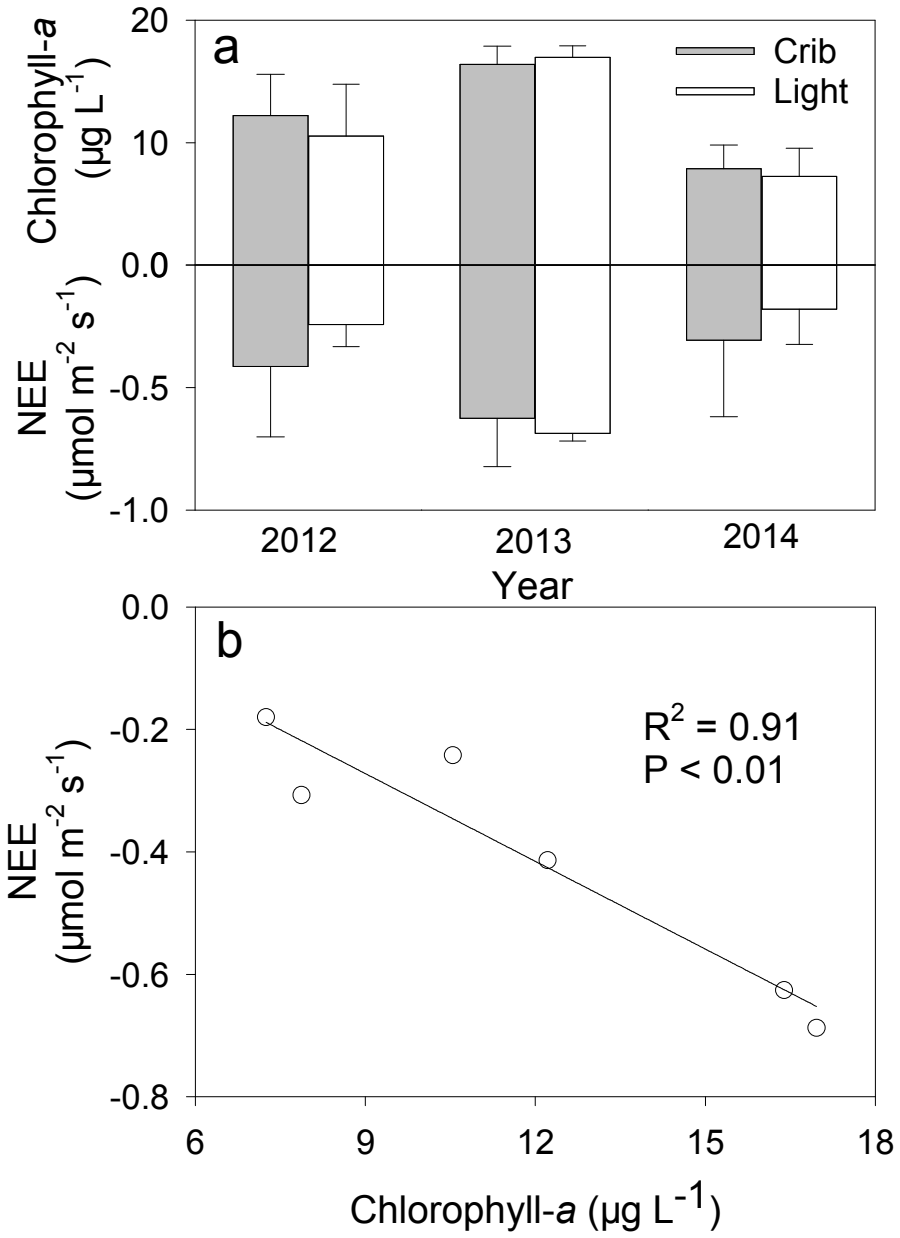

Figure 4.10, Bar comparisons of mean chlorophyll-a in August–October with mean NEE in September–November across EC sites and years(a); and the correlation between mean chlorophyll-a in August–October with mean NEE in September–November (b).

4.4 Discussions

4.4.1 The effect of chlorophyll-a on NEE

Chlorophyll-a concentrations were indirectly related to NEE during algal blooms, suggesting algal blooms may have indirect effects on NEE. No relationship between 30-min meteorological variables and NEE existed under either high or low chlorophyll-a conditions in western Lake Erie. This suggests that at such a high frequency, neither chlorophyll-a concentrations nor any meteorological variable alone significantly influences NEE. This finding is consistent with those from productive terrestrial ecosystems, showing that no single meteorological variable or biotic variable dominated as a driver altering NEE at similar time scales (Baldocchi et al. 2001, Stoy et al. 2009, Ouyang et al. 2014). However, algal blooms can change the relationship between daily mean meteorological variables and NEE. Due to limited data and high uncertainty in both NEE measurements by EC and chlorophyll-a estimations from remote sensing at high frequencies, I was not able to examine the direct relationship between mean values of NEE measurement and chlorophyll-a at 30-min and daily scales. However, during late summer and fall of 2013 (the period during the three years with the most abundant algal blooms), I collected 30-min chlorophyll-a data with a YSI 6600 water quality sonde at 1-m water depth at the Crib site for wavelet coherence analysis (APPENDIX C,C1.1). There were no co-varying relationship (APPENDIX C,Figure C.1) between chlorophyll-a and NEE at scales less than a week. The daily mean NEE, however, was significantly correlated with some important meteorological variables during algal blooms. This suggests that stronger internal processes (e.g., primary productivity and respiration) during periods of algal blooms, and meteorological variables may drive change in

NEE. Indeed, both primary productivity and respiration have previously been reported to be related with PAR, temperature, winds, and chlorophyll- a (Coloso et al. 2011, Solomon et al. 2013). It should be noted that PAR was positively rather than negatively correlated with NEE at both sites (i.e., higher PAR, more CO_2 emission), which also suggests absorption of CO_2 by chlorophyll-a. Although enough PAR is essential for a high photosynthesis rate in algae, increased water temperature occurring at the same time may also cause higher respiration to offset CO_2 absorption by algae. The growth as well as the resultant decomposition of algae could increase CDOM substantially in water simultaneously (Bade et al. 2007). CDOM not only lowers productivity by absorbing the blue portion of PAR (Branco and Kremer 2006), but also promotes respiration by providing materials for bacterial consumption under higher temperatures. At the beginning of bloom periods (i.e., August) when PAR was at the highest level, the lake actually acted as stronger source of CO_2, which may be attributable to high respiration caused by higher temperatures and higher CDOM concentrations. In August, nearby terrestrial ecosystems and the lake were close to peak biomass status, which can produce high CDOM in the lake. Conversely, more negative or smaller NEE levels are more likely to occur late in the algal bloom season (i.e., September or October) when light and temperature are optimal for photosynthesis but not high enough to spur strong respiration.

Monthly mean chlorophyll-a values were correlated with temporally lagged NEE, suggesting that chlorophyll-a may directly affect NEE at monthly scales and co-vary with NEE at seasonal and annual cycles with a phrase shift. Comparison of NEE between the Light and Crib site over the same period, or between NEE measurements from different years at the same site also suggests that the higher the chlorophyll-a in August, September, and

October, the more negative the NEE is in later months (i.e., September, October, and November) following the algal blooms. Studies using various approaches have previously reported that in terrestrial ecosystems where primary productivity is substantially greater than community respiration, the chlorophyll-a related vegetation index (e.g., LAI, NDVI) and NEE either was highly correlated with their monthly means or co-varied at seasonal/annual cycles (Baldocchi et al. 2001, Stoy et al. 2009, Ouyang et al. 2014, Xie et al. 2014b). However, the relationship between chlorophyll-a and NEE that we found in western Lake Erie, is weak and shows a time lag. Western Lake Erie receives abundant allochthonous organic materials from its watersheds that may be used by its bacterial community, thus algal primary productivity does not exceed community respiration seasonally or annually. In fact, over these three years, western Lake Erie annually acted as a small CO_2 source (Figure S4), suggesting heterotrophy. Therefore, the eutrophic status of western Lake Erie (i.e., the ratio of community heterotrophic respiration to net primary productivity) likely contributed to this observed weak relationship. The exact mechanism underlying this lagged relationship could not be addressed in this study with limited data and analysis, however some possible reasons can be hypothesized. First, the direct response of monthly NEE to chlorophyll-a may lag by 1-2 months, but this lag may reflect accumulation at shorter time scales. An examination of Table 4.1 reveals that when an 8-day NEE was compared with 8-day mean chlorophyll-a by an 8-day period lag at the Light site, a significant correlation was found, and when 8-day NEE lagged behind chlorophyll-a at Crib site by two 8-day periods, the observed correlation had a $p=0.07$. Second, this large water body may act as a mediator to buffer the response. CO_2 is dissolved in the water and usually exists in dynamic equilibrium with the atmosphere.

To cause downward CO_2 flux, algae must first consume CO_2 in the water until the partial CO_2 pressure becomes lower than the atmosphere, resulting in diffusion. Depending on the saturation status, temperature, and other conditions, the NEE measured by the flux tower may be delayed at different degrees to reflect the consumption of CO_2 by algae. Third, to produce the observed negative effects on NEE, algal productivity may first have to offset community respiration. A previous study in western Lake Erie found that 28 days are required for a gram of phytoplankton to produce an additional gram of glucose to be available for reproduction (Verduin 1956). Finally, chlorophyll-a solely represents biomass but peak biomass does not equal peak productivity, and chlorophyll-a concentration obviously is not the sole factor that can influence NEE. Meteorological conditions may directly or indirectly drive changes of NEE at many time scales. Directly, these factors might regulate respiration and photosynthesis in the lake and affect physical processes such as diffusion and turbulence. Indirectly, they take affect when the algae begin to bloom and when the lake water begins to stratify or mix. The dissolved organic carbon in the lake, both autochthonous and allochthonous, often may become a dominant driver of carbon processes in lakes as well (Hanson et al. 2014). As a result of so many complex processes that could affect NEE, peak chlorophyll-a does not necessarily coincide with the least NEE. During and after late algal blooms algae continue using up CO_2 while lower temperature lessen respiration and result in more CO_2 being dissolved in the water; these factors lead to the observed small and negative NEE values.

The effect of chlorophyll-a on NEE may also vary spatially and temporally. Notably, our study found that the relationships among chlorophyll-a, NEE, and meteorological variables

vary across temporal scales (i.e., 30-min, daily, 8-day, and monthly) and between the two sites. Between the two sampling sites over three sampling years, different NEE values were obtained along with different magnitudes of algal blooms. These differed both spatially (between the two sites for the same year) as well as temporally (among the years at a given site). Due to varying intensities of algae blooms, and with difference in turbidity, eutrophic status, water stratification, and etc., the relationship between chlorophyll-a and NEE thus varies spatially as well as temporally across short and long time scales.

4.4.2 Uncertainties

Uncertainties stem from both chlorophyll-a concentrations and CO_2 flux measurements. Remote sensing of chlorophyll-a remains poorly understood in inland waters (Bukata 2005). Although, applications in the Great Lakes suggested that estimated concentrations are proportional to observed concentrations, the first could vary from the latter by as much as an order of magnitude (Lesht et al. 2012). This might affect the calculated relationship between chlorophyll-a and NEE. Usually, the higher or the lower actual chlorophyll-a is, the greater degree of overestimation or underestimation. Uncertainties of NEE comprise both random and systematic errors (which could stem from the flux calculations, flux calibrations, and/or gap-filling), and quantification of such errors remains a challenge in EC communities. Conventional QA/QC protocols for processing EC data following procedures (such as the Webb-Pearman-Leuning corrections) suggested by Fluxnet, solely focus on system errors as followed in this study. Although random errors cannot be corrected,the influence of random errors can be largely reduced when NEE is aggregated into long time scales (Richardson et al.

2006), increasing confidence in the reliability of our finding of a significant correlation between monthly mean chlorophyll-a and NEE. Spatial mismatch of NEE and chlorophyll-a also might be a concern, since chlorophyll-a was measured at a fixed footprint defined by MODIS pixels, but the actual footprint contributing to the NEE measurements at the EC towers was inconsistent in both direction and total area. Thus, I used 4×4 km spatially averaged MODIS chlorophyll-a to alleviate this problem as an average of >75% of NEE was contributed by the 4×4 km water area surrounding each tower.

4.5 Conclusions

This article is our first step understanding the driving mechanisms of NEE in western Lake Erie. It constitutes a pioneer study of the relationship between algal growth/blooms and NEE at an ecosystem scale in large lakes. Our results suggest that the mean values of algal chlorophyll-a and NEE are negatively correlated in western Lake Erie at a monthly scale with a time lag, suggesting that the two may co-vary at seasonal/annual cycles. This relationship between chlorophyll-a and NEE may vary spatially and temporally. I also found that in algal bloom seasons with high chlorophyll-a, the daily means of many important meteorological variables (e.g., Ta, PAR, and wind speed) were significantly related to daily NEE. My findings indicate that chlorophyll-a may be directly related to NEE over long time scales, and could alter the relationship between meteorological variables and NEE at short time scales. My findings are also consistent with findings from terrestrial ecosystems, which show that chlorophyll-a related vegetation indexes and NEE co-vary at seasonal to annual scales, and that meteorological variables are a more important and active driver during growing seasons than non-growing seasons. However, considering the complexity of processes that drive NEE and that some uncertainties remain in our estimations of both and chlorophyll-a, our results should be interpreted as illustrative rather than definitive. I need to better characterize the Lake ecosystem, investigate/model the complex processes of NEE , and document accurate algal bloom/chlorophyll-a data to further quantify the relationship between NEE and chlorophyll-a at multiple spatial and temporal scales.

4.6 Acknowledgements

This study is contribution #2015-XX from the Lake Erie Research Center. I thank Michael Deal, Yahn-Jauh Su, Cody Kish, Butch Berger, Andrew McClure, Brenda Snyder, and others from the City of Toledo Division of Water Treatment for building and maintaining the site infrastructure and assisting in the data collection and management. Our site was aided by support from NOAA Great Lakes Environmental Research Laboratory (GLERL), for which I especially thank help from Steve Ruberg. This study was supported by the National Science Foundation (NSF1034791) Field Station and Marine Labs (FSML), the NASA-NEWS Program (NN-H-04-Z-YS-005-N), and the USCCC.

CHAPTER 5 CONCLUSIONS

5.1 Lessons learned

The studies in this dissertation highlight the spatial and temporal changes of important ecosystem characteristics. Large spatial scale remote sensing observations and long-term EC and weather station observations were combined to study spatial and temporal variations of NEE and WSA in three contrasting ecosystems. First, I quantified the variation of NEE in a rare terrestrial ecosystem, Ohio's Oak Openings, at time scales ranging from 30-min to multiple years, and investigated how Ta and PAR drive these changes at different time scales. Second, by selecting Kidder County, North Dakota as a proxy, I was able to quantify the inter-annual changes of WSA and their response to drought in the PPR by establishing a regression model. Lastly, the spatial-temporal changes of chlorophyll-a and NEE and its possible drivers were thoroughly investigated in western Lake Erie. Overall, the studies supported the conclusion that targeted ecosystem characteristics demonstrated significant spatial and temporal variation and that they were related to pertinent drivers at certain time/spatial scales.

Lessons learned from the three studies in this dissertation include:

1. Ecosystem characteristics are non-stationary phenomenon; they uniquely change at different time scales and time periods. NEE in Ohio Oak Openings, varied most at daily, seasonal, and annual scales and significant daily oscillation only happened during growing seasons. WSA in the PPR presented strong inter-annual and intra-annual variations. NEE in western Lake Erie, on the other hand, presented a weak seasonal pattern, but no significant oscillating patterns at other shorter scales.

2. Climate/meteorology could be both low and high frequency drivers of these ecosystem characteristics, and different variables may play different roles at certain time scales/ frequencies. WSA of potholes in the PPR over the last few decades presented significant seasonal and annual variations, which were derived by precipitation, temperature, and drought. NEE in both Oak Openings and western Lake Erie was correlated to PAR and Ta around daily scales during growing and algal bloom seasons, respectively. Seasonal and annual variations of NEE in both Oak Openings and western Lake Erie were related to Ta. Also, by analyzing Oak Openings and by removing the confounding effects, PAR was shown as the more important driver of NEE for high frequency variation and Ta was shown as the more important driver for low frequency variations. There was no direct result in Lake Erie showing that meteorological variables drive the change of NEE at seasonal and annual scales, but results did show that algal growth might have forced seasonal and annual changes of NEE. Because algal growth is largely determined by temperature and then PAR, climate/meteorology could also play an important role in driving these low frequency variations and temperature may be more important than PAR.

3. Lagged correlation is common between ecosystem characteristics and their possible drivers; and lagged or lasting effects must be considered in understanding drivers of spatial-temporal changes. In the PPR region, lagged correlation was found between WSA and PDSI as far as three years ago. Lagged correlation between Ta/PAR and NEE was found across many scales. The chlorophyll-a was only correlated with NEE when time lag was included in western Lake Erie, which was useful for judging driving mechanisms. PDSI leads WSA in PPR, chlorophyll-a leads NEE in western Lake Erie, and PAR synchronizes NEE at the daily

scale in Oak Openings. Therefore, they could be important drivers. However, Ta lags behind NEE at the daily scale in Oak Openings, and is thus not likely a driver of NEE at that time scale.

4. Spatial scale and location matters when understanding the changes of ecosystem characteristics. I measured NEE at ecosystem scales with footprints at a few kilometers, and as a result the variations and the corresponding driving mechanisms observed are different from other studies at micro scales (e.g., leaf scale, algae cells). The temporal changes of NEE also differed very much in Oak Openings and in western Lake Erie. Even within the same ecosystem, NEE and its correlations to other driving variables differ at the two locations we investigated in western Lake Erie. The model we built from PDSI to predict WSA will also change when we move to different scales and locations.

5.2 Recommendation for future research

The spatial and temporal changes of ecosystem characteristics is a very broad topic, but can be easily focused as seen in my three studies presented in chapters 2–4. These investigations increased the understanding of NEE in temperate forests, water dynamics in wetlands, and of NEE and algal blooms in large lakes. Environmentalists, policy makers, and the public are eager to know more on these various ecosystem characteristics from different ecosystems as well. By discovering additional ecosystem processes, we may better structure future adaptations and mitigations in response to global change. Future research could extend beyond my dissertation and further fill the knowledge gaps.

In my research, I have analyzed phase shifts among Ta, PAR, and NEE at daily and annual scales; and have then concluded that between Ta and PAR, PAR is the major driver for NEE oscillations at short time scales (e.g. daily) while Ta is the major driver for NEE oscillations at long time scales (e.g., seasonal and annual). These findings and analysis were, however, limited to our targeted ecosystems only. Future studies should expand into other ecosystems. One can further examine whether the magnitude of a phase shift between Ta and NEE at the daily scale and between PAR and NEE at the annual scale are either consistent or changing among similar ecosystem types (e.g., temperate forests) from different climate zones and across different ecosystem types from the same climate zone. The correlating dynamics of vegetation might change among different climate zones and ecosystems as the diurnal and seasonal cycles of Ta and PAR vary. These differences may be related to both the macro-scale climate conditions as well as the meso-scale ecosystem characteristics. Also, ecosystem functions often respond non-linearly to many environmental drivers. While

wavelets are good tools for detecting local linear relationships, they are not the best tools for analyzing non-linear responses. New methods should be developed in order to investigate non-linear relationships between important ecosystem characteristics and the various potential drivers at multiple temporal and spatial scales. The Hilbert–Huang transform (HHT), for example, could be developed for a scale-dependent non-linear relationship among a few variables. I demonstrated that wavelet tools have a strong ability to detect scale-dependent relationships locally and reveal the overall patterns of NEE and of the related drivers Ta and PAR. However, I also mentioned that some possible responses of NEE to climate anomalies have been detected by wavelets. Wavelet transformation and analysis are also one of the best methods to detect anomalies among different phenomenon. Climate anomalies have occurred in the last few years in the Midwestern US, and climate anomalies are projected to increase in the future. Future studies should detect how NEE responds to climate extremes and anomalies using various wavelet analyses. On the other hand, Ta and PAR are not the only important drivers of NEE, and thus more studies are needed to disentangle the confounding effects of other coupled influential factors on NEE as well.

Wetlands, while precious ecosystems, are shrinking worldwide. More studies are needed to understand their changes. In my wetland study, the change of WSA was found to be related to drought/wet conditions, which was represented by the drought index PDSI. As precipitation, temperature, and other factors could change drought/wet conditions, the detailed physical processes, which drive the change of WSA in PPR, remain unclear. Therefore, future studies could focus on establishing a more detailed model where physical variables (e.g. temperature, precipitation, and evapotranspiration) could be included to

explain the change of WSA. This is very important for increasing the confidence in future predictions, since two areas with the same PDSI are very likely to have different temperature, receive different amount of precipitation, and so on. Additionally, the same relationship between PDSI and wetland areas, or between other physical variables (such as temperature and precipitation) and wetland areas may change across the PPR and over time. Future studies should develop hierarchical models where the same model structure could be applied in all sub-regions and the entire PPR, but with values of coefficients that vary to fit local relationships. Such hierarchical models could be developed in a Bayesian framework, with more data and information added as they increase, thereby improving the models gradually. In my study, WSA was used to represent the change of wetland areas. However, it may improve if water mass, or the combination of water mass and water area, could be used. The GRACE satellites that measure Earth's gravitational field may be able to monitor the water mass change in the PPR. Future research should try to explore the application of GRACE to monitor the water mass change in the PPR and how this change is related to other wetland area changes. Changes in the PPR's wetlands may also be caused by human activities. In future research, social and economic data should be included to explain the proportion of changes that are not related to climate change, but rather to human activities.

Direct long-term and large spatial scale measurements of NEE in inland lakes are still scarce today and, more efforts are needed to collect these. At the same time, possible drivers of NEE, such algal biomass, water temperature profiles, pH, CDOM, partial pressure of carbon dioxide (pCO_2) and other water quality variables and meteorological variables, etc., should be observed and collected for examining drivers of NEE change at multiple temporal

and spatial scales. Aside from algae, my studies have also suggested that the climate and meteorological conditions are likely important drivers of the carbon process in Lake Erie. Therefore, future studies must further investigate how NEE may respond to climate and weather change at related time and spatial scales. We have observed NEE and meteorological conditions for more than three years, but still lack long-term continuous water quality data to understand their potential influences on NEE. It is considered that pCO_2 is the physical variable that is most important and directly related to the exchange of CO_2 between surface water and the upper atmosphere. Unfortunately, I did not have pCO_2 data in my study. This variable should be measured at sufficient temporal scales in the future to examine how physical diffusion directly drives the change of NEE, and to examine how biological processes such as algal blooms can affect this physical process. Algal blooms are an environmental phenomenon in many other lakes and their possible influence on NEE may differ due to different ecosystem characteristics; but these possible influences have never been examined in those lakes at sufficient spatial scales. Therefore, future studies should focus on extending the spatial and temporal scales and on expanding the diversity of lakes under investigation. Remote sensing has proved to be an important tool in collecting chlorophyll-a, CDOM, and other water quality data at large spatial scales repeatedly (e.g., daily, monthly, and annually). Future studies, thus, should take advantage of both remote sensing techniques and EC techniques to investigate the spatial and temporal changes of many important ecosystem characteristics in not only Lake Erie, but in other large lakes as well. Also, after the major drivers of NEE have been well understood, models relying on

remote sensing data should be applied to an up-scale NEE estimation of the whole lake in order to better understand the spatial and temporal variation of NEE and make a prediction.

In light of my findings, the future direction of research should focus on: 1) expanding into multiple ecosystems/locations to study the lagged correlation/effects between NEE/WSA and their corresponding drivers in order to check the relationship's consistency and differentiation within time and space; 2) developing an advanced methodology, other than wavelets and linear regression, to understand non-linear responses of NEE/WSA to climate drivers since not all causal relationship are necessarily linear; 3) building hierarchical models to explain variations of NEE/WSA as the underlying driving mechanisms vary across spatial scales and locations; 4) and observing an array of diverse inland water ecosystems, and including them into the landscape as a whole to understand water and carbon cycles.

APPENDICES

APPENDIX A: Supplementary materials for Chapter 2

A.1, Non-linear relationships between Ta/PAR and NEE

NEE, Ta, and PAR may all have nonlinear characteristics and for these non-linear attributes, wavelet analysis has some issues dealing with them directly. However, I addressed this issue through data transformations to tackle with some well-known nonlinear characteristics among NEE, Ta, and PAR. For example, one component of NEE, respiration is well-known to respond exponentially to Ta, and the other component of NEE, GPP oftentimes responds as a parabolic function to PAR. I thus made a log-transform and root-square transform of NEE respectively (which would address the nonlinearity issues), ran CWT on transformed NEE, and conducted XWT(Ta, NEE) and CWT(Ta, NEE) with log-transformed NEE, and XWT(PAR, NEE) and CWT(PAR, NEE) with root-square transformed NEE. The results of these analyses are included here (Figures A.1 and A.2). We actually found that any nonlinearity has negligible influences on our general conclusion.

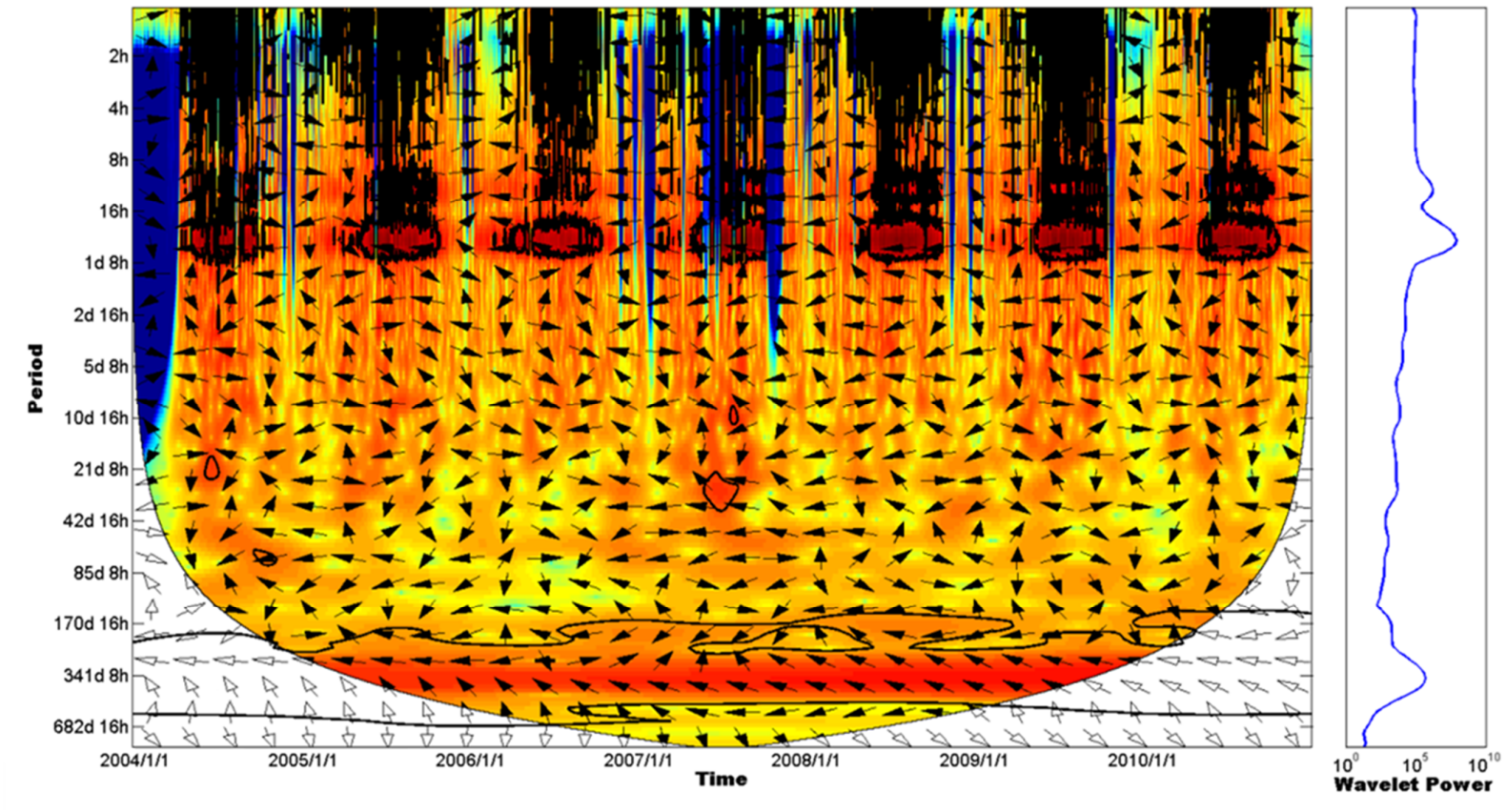

Figure A.1, XWT between PAR and square root of NEE. The 5% significance level against red noise is shown as a thick contour. The cone of influence (COI) is shown as a thin line. The significant PWC for Ta and NEE at long scales was not centered at a year, which might be an influence of gap-filling techniques.

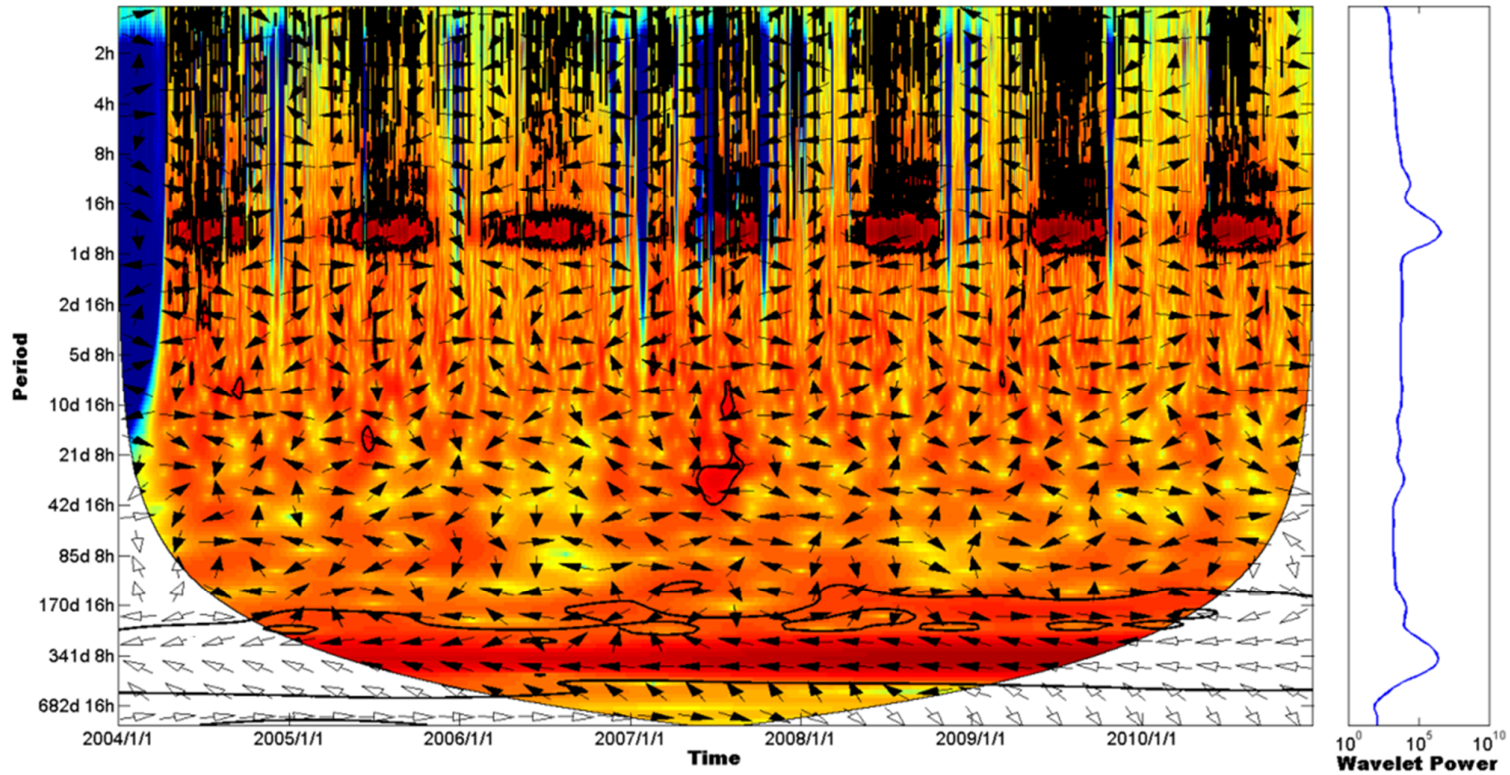

Figure A.2, XWT between Ta and log-transformed NEE (b). The 5% significance level against red noise is shown as a thick contour. The cone of influence (COI) is shown as a thin line. The significant PWC for Ta and NEE at long scales was not centered at a year, which might be an influence of gap-filling techniques.

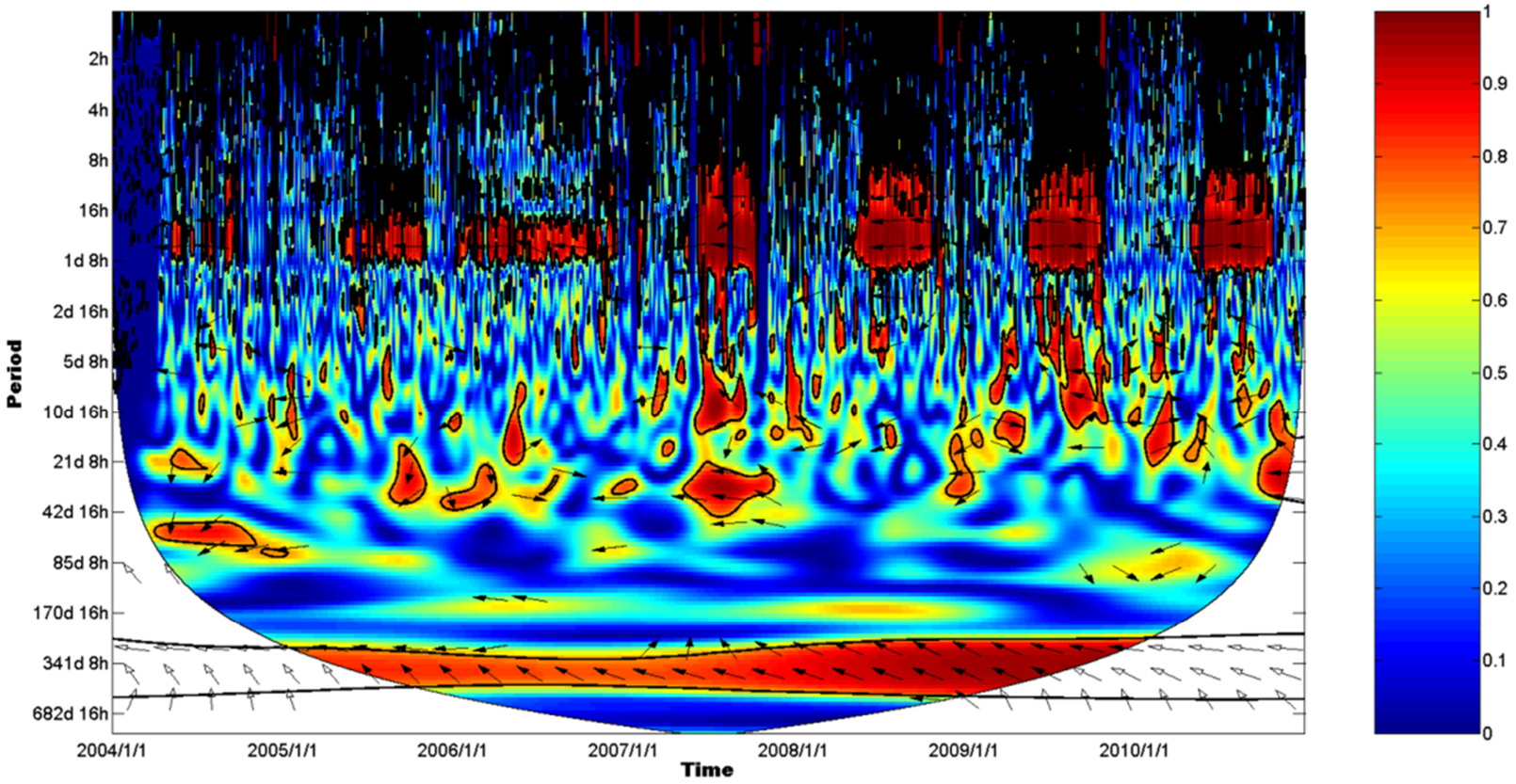

Figure A.3, WTC between Fc and square root of NEE. The 5% significance level against red noise is shown as a thick contour. The cone of influence (COI) is shown as a thin line.

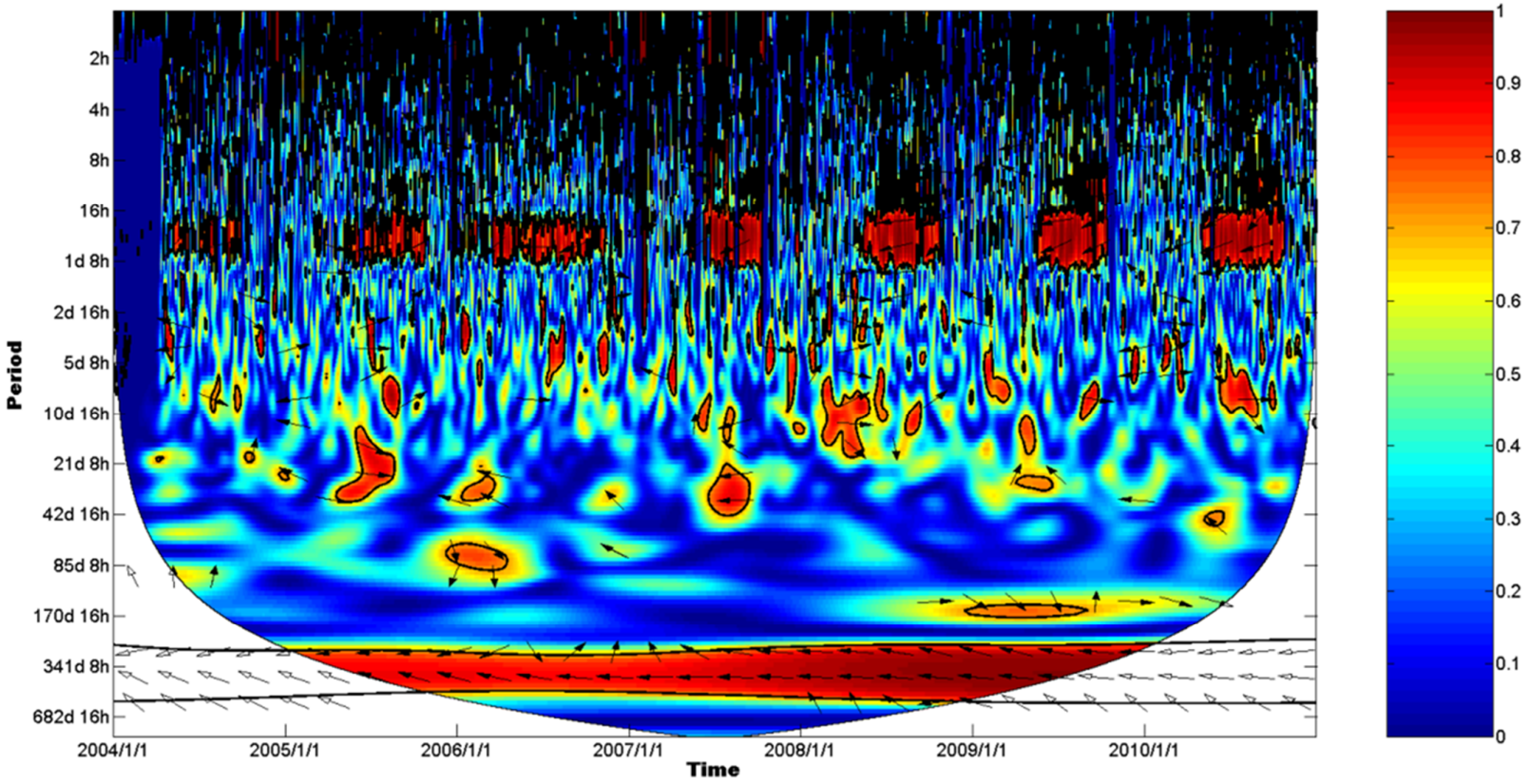

Figure A.4, WTC between Ta and log transformed NEE. The 5% significance level against red noise is shown as a thick contour. The cone of influence (COI) is shown as a thin line.

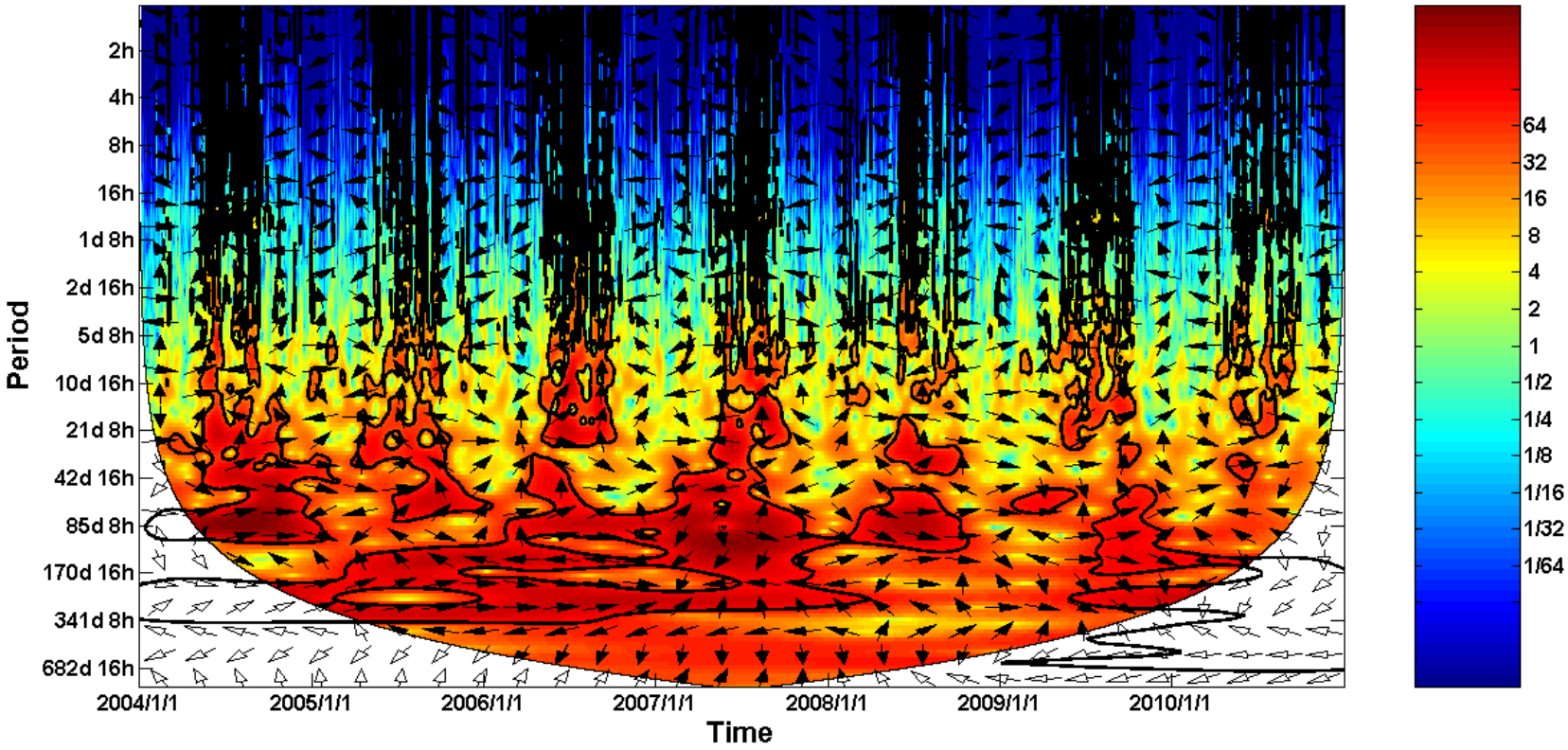

Figure A.5, XWT between SWC (soil water content) and NEE. The 5% significance level against red noise is shown as a thick contour. The cone of influence (COI) is shown as a thin line.

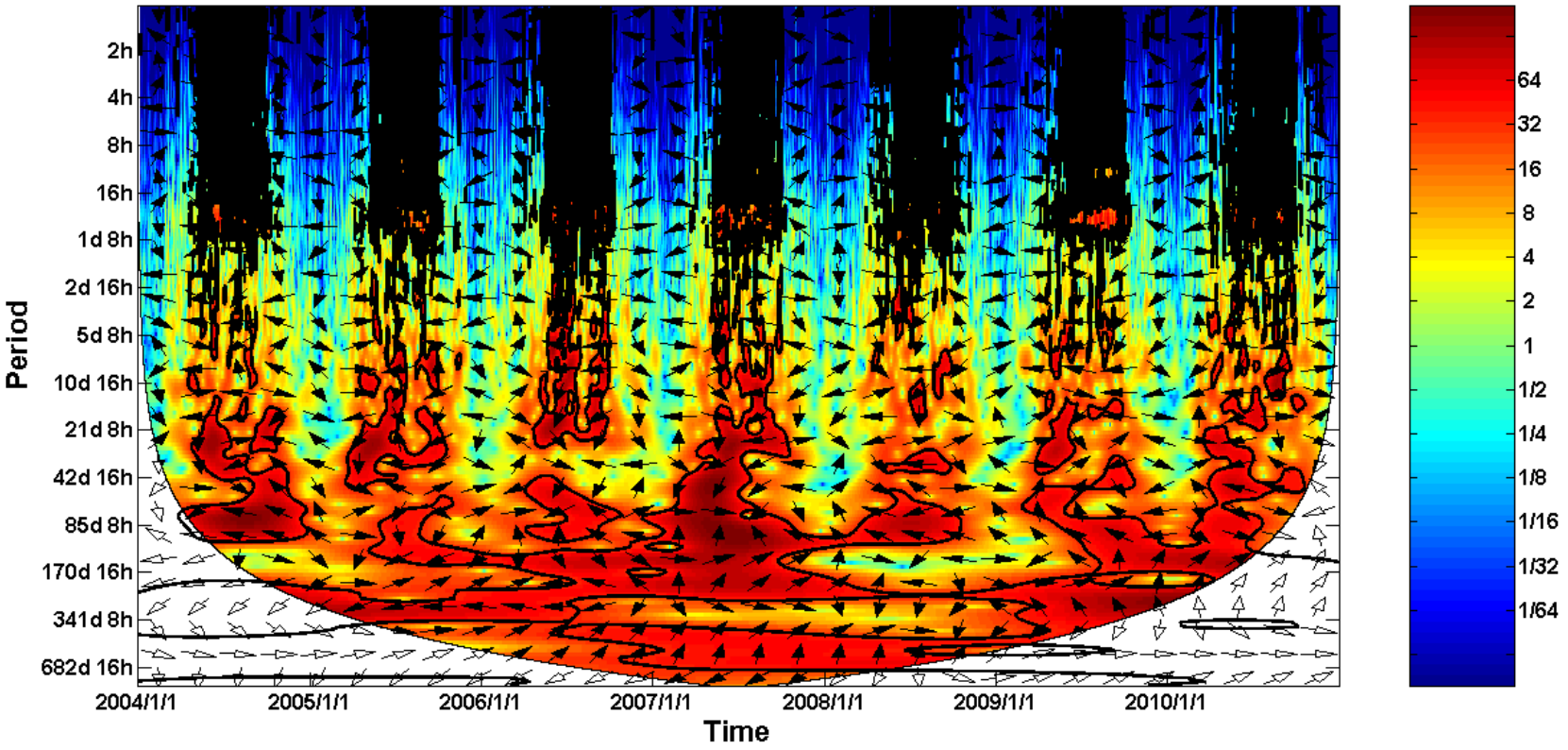

Figure A.6, XWT between VPD (vapor pressure deficit) and NEE. The 5% significance level against red noise is shown as a thick contour. The cone of influence (COI) is shown as a thin line.

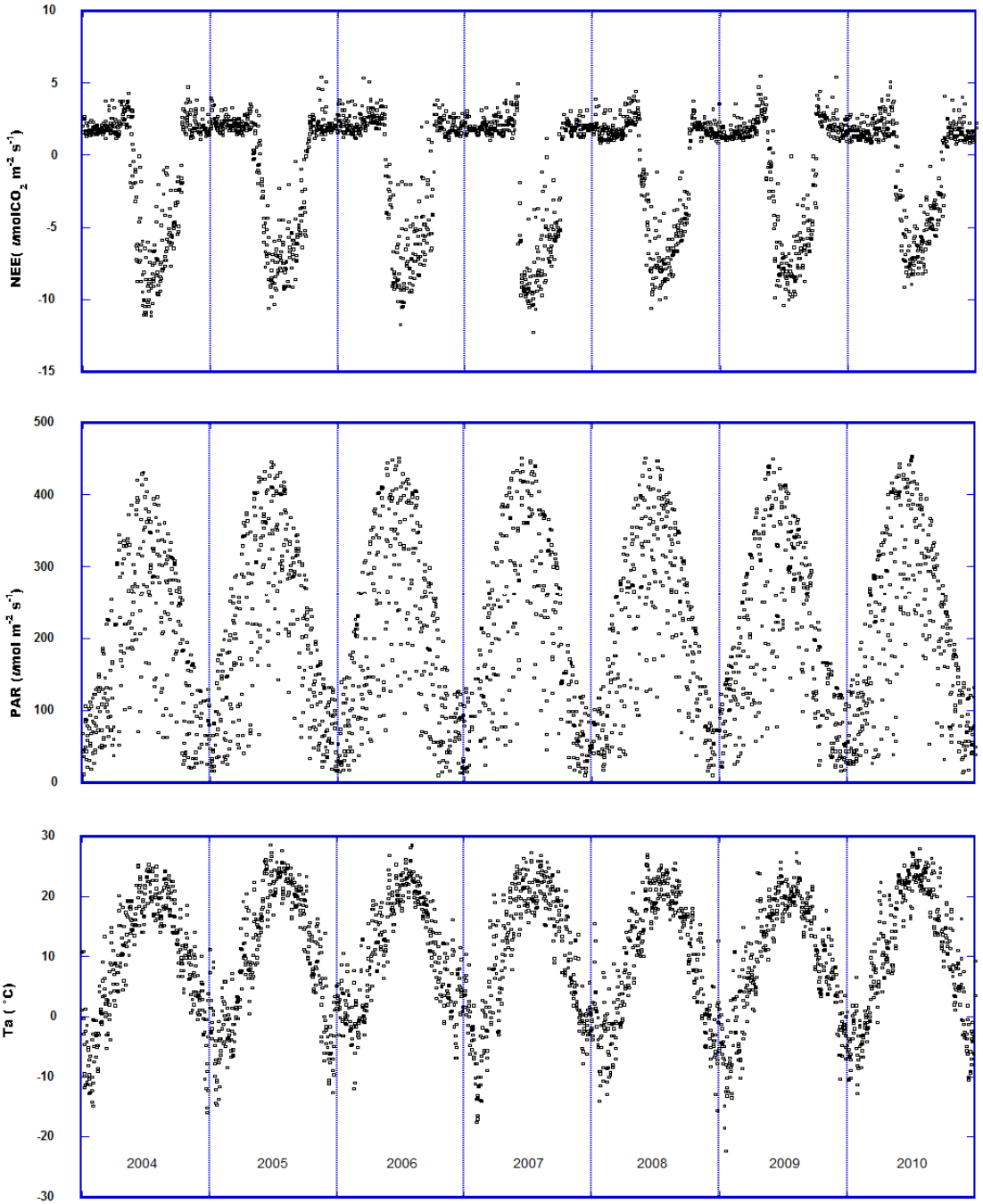

Figure A.7, Seven years of time series NEE, PAR, and Ta show significant seasonal and annual cycles.

APPENDIX B: Supplementary materials for Chapter 3

B.1, The influences of precipitation and temperature on WSA

In Chapter 3, we studied the sensitivity of WSA in PPR to the drought index PDSI. However, key biophysical properties like temperature, precipitation, evapotranspiration, soil moisture, vegetation, and ground water can all affect the drought condition of an area. As a result, we are still unclear what biophysical variables caused the actual loss of WSA. Among those potential variables, temperature and precipitation are obviously the most important two. Thus, I examined the relationship between WSA and temperature/precipitation separately using simple regression. I excluded multiple linear regressions because high degrees of multicollinearity invalidate the model. WSA was significantly correlated to temperature and precipitation of the past instead of the current time. Current year WSA was significantly correlated with air temperature and precipitation of the year before last (Ta_{t-2} and $Precipitation_{t-1}$), and precipitation of last year ($Precipitation_{t-1}$) (Figure B.1). The air temperature and the precipitation of the current year ($Ta_{t-0\ and}\ Precipitation_{t-0}$), were not correlated to WSA of the current year (Figure B.1).

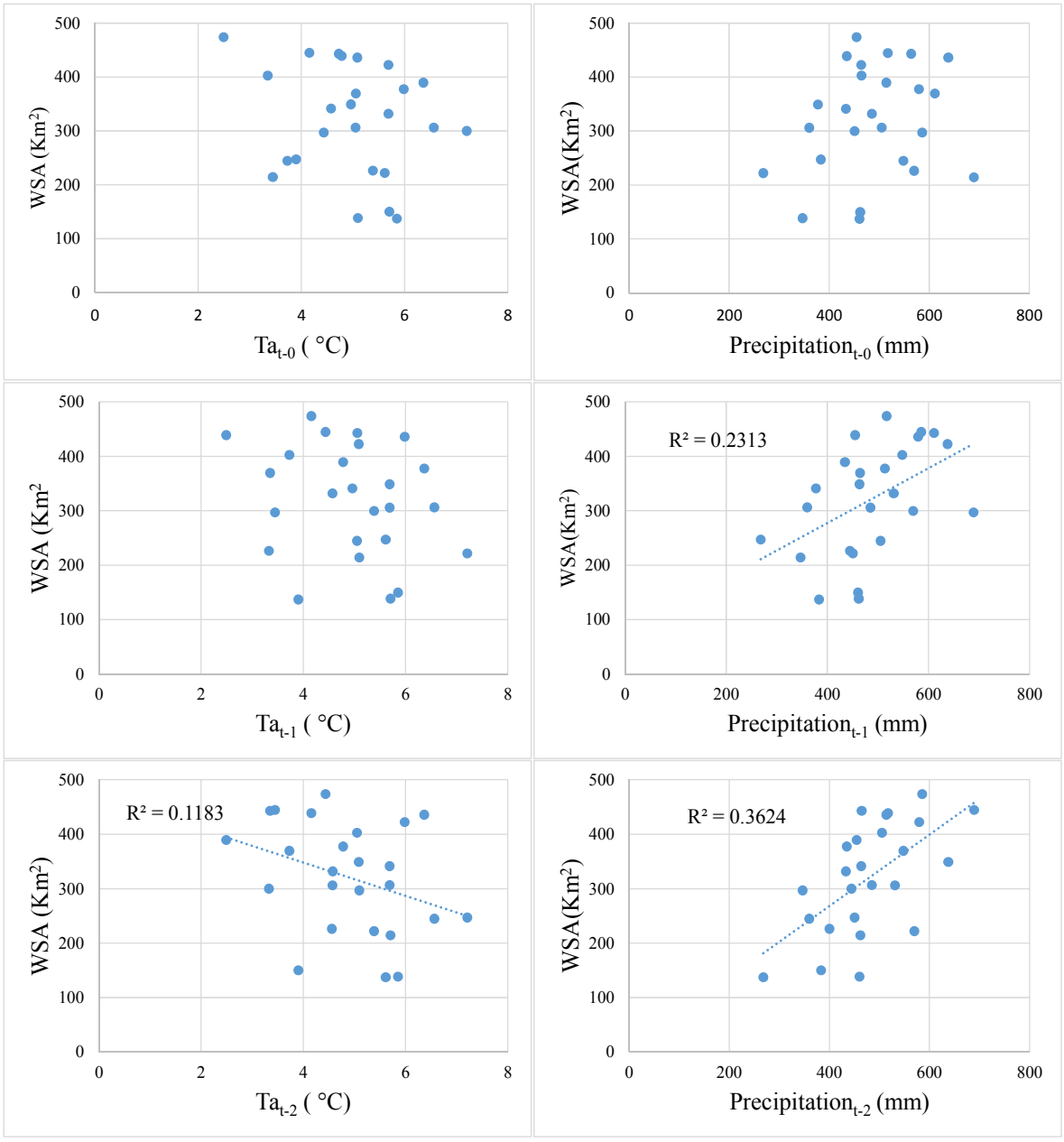

Figure B.1, The relationship between WSA and air temperature/precipitation of current year (t-0), last year (t-1), and the previous 2nd year (t-2). Regression lines were fitted when the relationship was statistically significant at $p < 0.05$.

APPENDIX C: Supplementary materials for Chapter 4

C.1 Chlorophyll-a sampling by YSI 6600

A time series of chlorophyll-a concentrations (hereafter YSI chlorophyll-a) at 30-min temporal resolution was sampled from 1-m depth at the Crib site with an YSI 6600 water quality sonde from July 8–Oct. 29, 2013, when the highest chlorophyll-a concentration was observed in 2012–2014. If no relationships could be found between chlorophyll-a concentration and NEE during this period, it likely was absent at other times. The YSI measured chlorophyll-a by quantifying the fluorescent characteristics of the chlorophyll. Calibration was necessary for the YSI chlorophyll-a readings to provide meaningful chlorophyll-a values for specific types of water. The calibration required a standard with known amounts of phytoplankton. We were not able to do such calibration, which did not affect wavelet coherence analysis or correlation analysis.

C.2 Wavelet coherence analysis

Wavelet coherence (WTC) is a tool for identifying possible relationships between two processes by searching frequency bands and time intervals during which they co-vary (Ng and Chan 2012). The WTC square of two time series X and Y is defined as:

$$R_n^2(x,y) = \frac{|S(s^{-1}W_n^{XY}(s)|^2}{S(s^{-1}|W_n^X(s)|^2)\cdot S(s^{-1}|W_n^Y(s)|^2)}$$

where S is a smoothing operator, s is the set of wavelet scales, and W is the continuous wavelet transform CWT operator as defined in Eq. 4 in chapter 2. The Morlet wavelet was

chosen as the mother wavelet because it provides a good balance between the localization of time and frequency. The S operator can have varying forms and produce a large impact on a significant level. We followed the form of S operator from Torrence and Webster (1998)for the Morlet wavelet. The definition of WTC closely resembles the traditional correlation coefficient, and it is useful to think of the WTC as a localized correlation coefficient in time frequency space (Grinsted et al. 2004). Wavelet coherence between two phenomena was also tested at a 5% significance level against red noises through a Monte Carlo simulation because it is well known that the random error of CO_2 flux is not normally distributed, but is linearly scaled with the magnitudes of fluxes (Richardson et al. 2006).

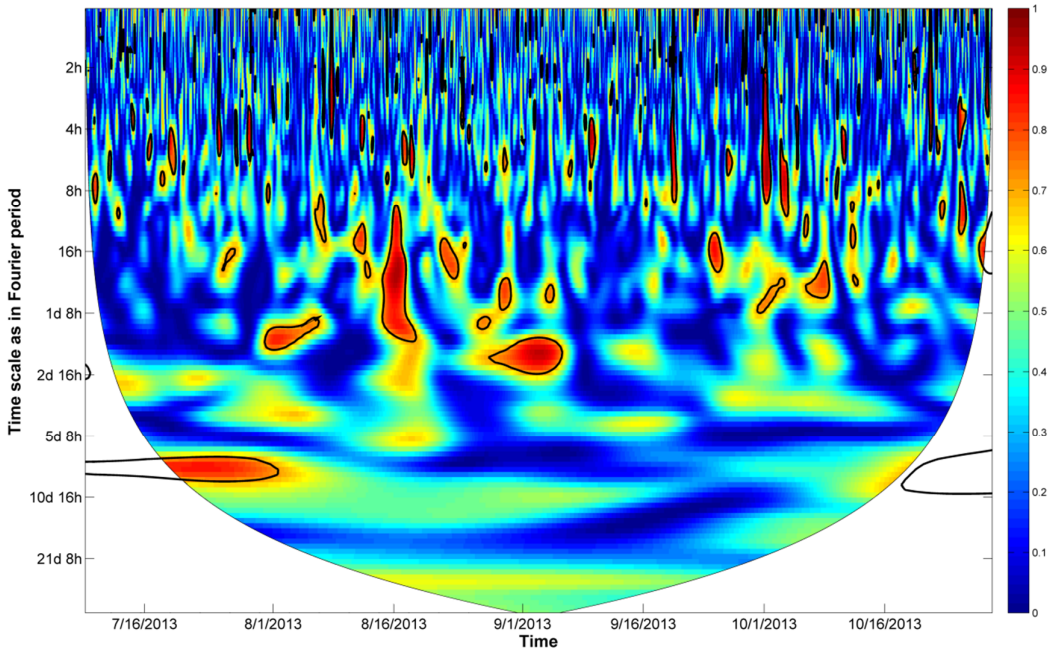

Figure C.1, Wavelet coherence analysis of chlorophyll-a measured by a YSI 6600 water quality sonde and EC NEE at the Crib site. The 5% significance level against red noise is shown as a thick contour. The cone of influence (COI) is shown as a thin line. Both chlorophyll-a NEE were standarized to have zero means and a variation equal to 1. Gaps of NEE were filled using the marginal distribution sampling (MDS) method.

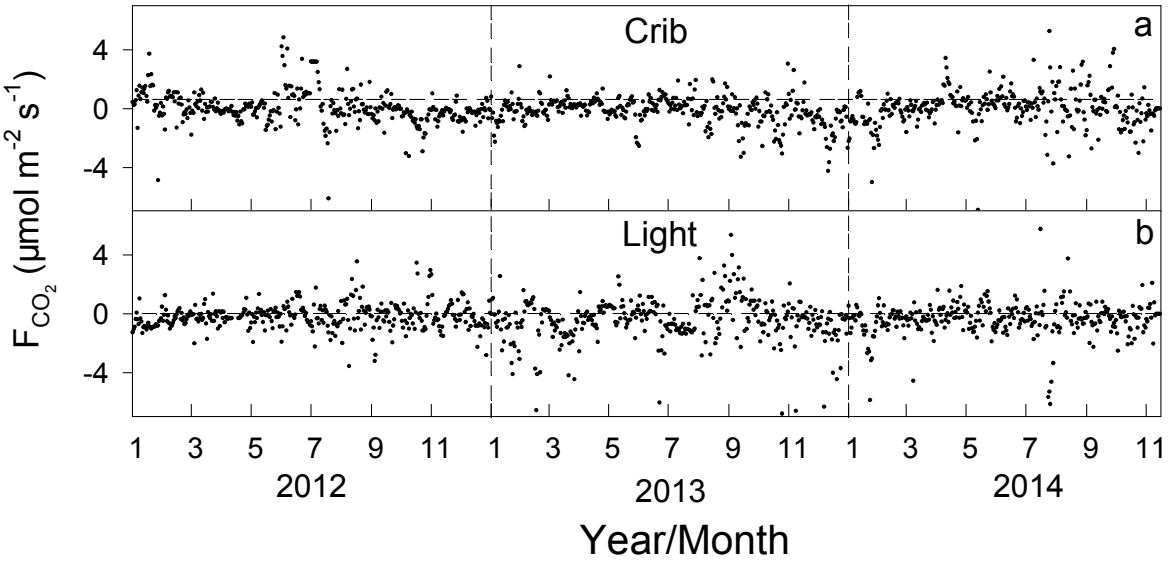

Figure C.2, Daily NEE at the Crib and Light sites. Daily NEE were calculated for the mean values of the 48, 30-min data based on the gap-filled NEE time series. The marginal distribution sampling (MDS) method used for terrestrial ecosystems was adopted here for gap-filling.

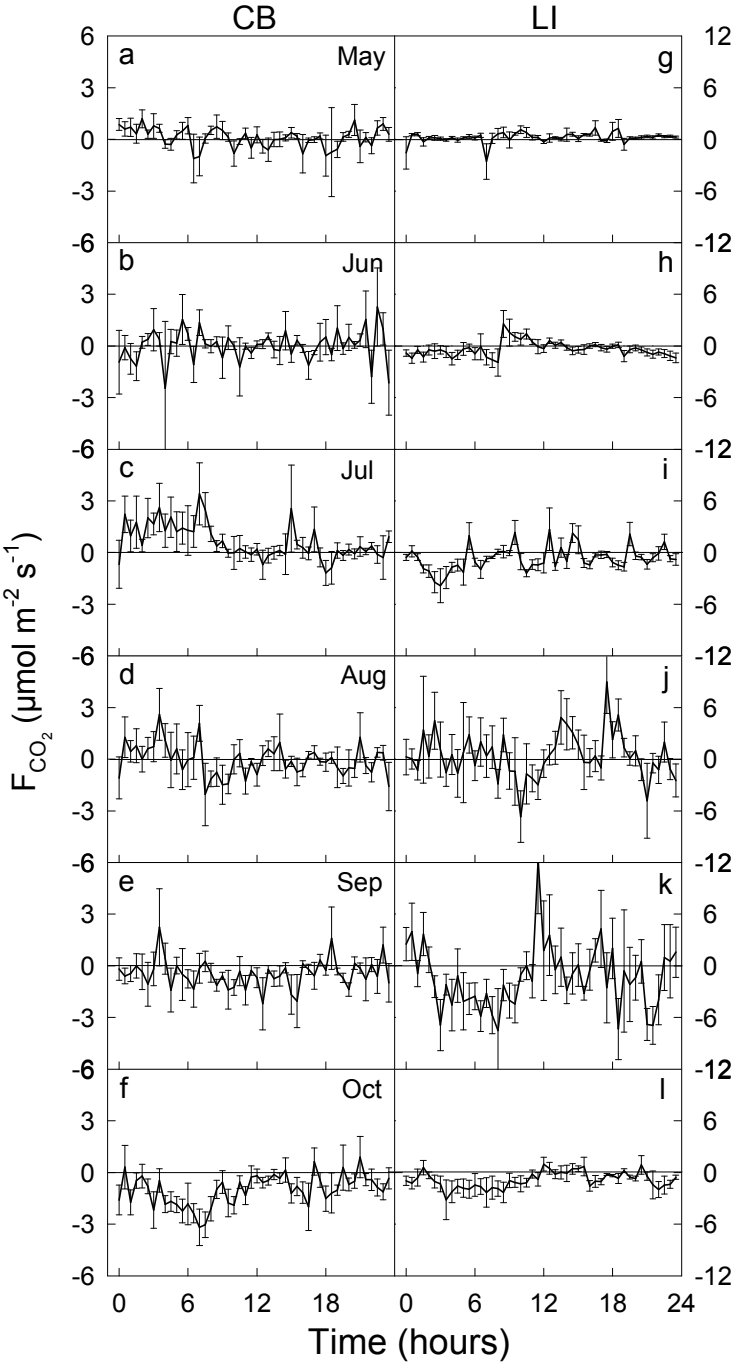

Figure C.3, Daily NEE cycles per month from May–October in 2013(Changliang et al. unpublished)(Changliang et al. unpublished) at the Crib (a-f) and the Light site (g-i). The daily cycles were calculated by averaging the 30-min, non-gap-filled NEE measurement taken at the same time per day within each month.

BIBLIOGRAPHY

BIBLIOGRAPHY

Ahmadi, S. H., and A. Sedghamiz. 2007. Geostatistical analysis of spatial and temporal variations of groundwater level. Environmental Monitoring and Assessment **129**:277-294.

Akaike, H. 1981. Citation classic - a new look at the statistical-mode identification. Current Contents/Engineering Technology & Applied Sciences:22-22.

Ali, K., D. Witter, and J. Ortiz. 2014. Application of empirical and semi-analytical algorithms to MERIS data for estimating chlorophyll a in Case 2 waters of Lake Erie. Environmental Earth Sciences **71**:4209-4220.

Anderson, D., P. Glibert, and J. Burkholder. 2002. Harmful algal blooms and eutrophication: Nutrient sources, composition, and consequences. Estuaries **25**:704-726.

Anderson, D. E., R. G. Striegl, D. I. Stannard, C. M. Michmerhuizen, T. A. McConnaughey, and J. W. LaBaugh. 1999. Estimating lake-atmosphere CO2 exchange. Limnology and Oceanography **44**:988-1001.

Assouline, S., and Y. Mahrer. 1996. Spatial and temporal variability in microclimate and evaporation over lake kinneret: Experimental evaluation. Journal of Applied Meteorology **35**:1076-1084.

Avila, L. F., C. R. de Mello, J. M. de Mello, and A. M. da Silva. 2011. Spatial and temporal patterns of soil moisture in a watershed with predominance of oxisols. Revista Brasileira De Ciencia Do Solo **35**:1801-1810.

Bade, D. L., S. R. Carpenter, J. J. Cole, M. L. Pace, E. Kritzberg, M. C. Van de Bogert, R. M. Cory, and D. M. McKnight. 2007. Sources and fates of dissolved organic carbon in lakes as determined by whole-lake carbon isotope additions. Biogeochemistry **84**:115-129.

Baldocchi, D., E. Falge, and K. Wilson. 2001. A spectral analysis of biosphere-atmosphere trace gas flux densities and meteorological variables across hour to multi-year time scales. Agricultural and Forest Meteorology **107**:1-27.

Baldocchi, D. D., and K. B. Wilson. 2001. Modeling CO2 and water vapor exchange of a temperate broadleaved forest across hourly to decadal time scales. Ecological Modelling **142**:155-184.

Batt, B. D. J., M. G. Anderson, C. D. ANDERSON, and F. D. CASWELL. 1989. The use of prairie potholes by North American ducks, IOWA State University Press: AMES, IOWA, USA.

Battin, T. J., S. Luyssaert, L. A. Kaplan, A. K. Aufdenkampe, A. Richter, and L. J. Tranvik. 2009. The boundless carbon cycle. Nature Geoscience **2**:598-600.

Beeri, O., and R. L. Phillips. 2007. Tracking palustrine water seasonal and annual variability in agricultural wetland landscapes using Landsat from 1997 to 2005. Global Change Biology **13**:897-912.

Bernstein, L. S., S. M. Adler-Golden, R. L. Sundberg, R. Y. Levine, T. C. Perkins, A. Berk, A. J. Ratkowski, G. Felde, and M. L. Hoke. 2005. Validation of the Quick Atmospheric Correction (QUAC) algorithm for VNIR-SWIR multi-and hyperspectral imagery. Pages 668-678 *in* S. S. Shen and P. E. Lewis, editors. Algorithms and Technologies for Multispectral, Hyperspectral, and Ultraspectral Imagery XI. Spie-Int Soc Optical Engineering, Bellingham.

Bertram, P. E. 1993. Total phosphorus and dissolved-oxygen trends in the central basin of Lake Erie, 1970-1991. Journal of Great Lakes Research **19**:224-236.

Branco, A. B., and J. N. Kremer. 2006. The relative importance of chlorophyll and colored dissolved organic matter (CDOM) to the prediction of the diffuse attenuation coefficient in shallow estuaries (vol 28, pg 643, 2006). Estuaries and Coasts **29**:530-530.

Brander, L. M., R. Florax, and J. E. Vermaat. 2006. The empirics of wetland valuation: A comprehensive summary and a meta-analysis of the literature. Environmental & Resource Economics **33**:223-250.

Braswell, B. H., W. J. Sacks, E. Linder, and D. S. Schimel. 2005. Estimating diurnal to annual ecosystem parameters by synthesis of a carbon flux model with eddy covariance net ecosystem exchange observations. Global Change Biology **11**:335-355.

Brewer, L. G., and J. L. Vankat. 2004. Description of vegetation of the Oak Openings of northwestern Ohio at the time of Euro-American settlement. Ohio Journal of Science **104**:76-85.

Bridgeman, T. B., J. D. Chaffin, and J. E. Filbrun. 2013. A novel method for tracking western Lake Erie Microcystis blooms, 2002-2011. Journal of Great Lakes Research **39**:83-89.

Buffam, I., M. G. Turner, A. R. Desai, P. C. Hanson, J. A. Rusak, N. R. Lottig, E. H. Stanley, and S. R. Carpenter. 2011. Integrating aquatic and terrestrial components to construct a complete carbon budget for a north temperate lake district. Global Change Biology **17**:1193-1211.

Bukata, R. P. 2005. Satellite monitoring of inland and coastal water quality. CRC, New York, USA.

Burke, E. J., S. J. Brown, and N. Christidis. 2006. Modeling the recent evolution of global drought and projections for the twenty-first century with the hadley centre climate model. Journal of Hydrometeorology **7**:1113-1125.

Campbell, J. W., J. M. Blaisdell, and M. Darzi. 1995. Volume 32, Level-3 SeaWiFS Data Products: Spatial and Temporal Binning Algorithms. NASA, Greenbelt, Maryland.

Cazelles, B., M. Chavez, D. Berteaux, F. Menard, J. O. Vik, S. Jenouvrier, and N. C. Stenseth. 2008. Wavelet analysis of ecological time series. Oecologia **156**:287-304.

Changliang, S., C. Jiquan, S. Carol A., C. Housen, O. Zutao, B. Thomas B., C. Kevin P., B. Richard H., and J. Ranjeet. unpublished. Diurnal to annual changes in latent, sensible heat and CO2 fluxes over a Laurentian Great Lake: A case study in western Lake Erie

Chapin, F. S., III, P. Matson, H. A. Mooney, F. S. Chapin, III, P. Matson, and H. A. Mooney. 2002. Principles of terrestrial ecosystem ecology. Springer-Verlag.

Chen, J. Q., M. Falk, E. Euskirchen, K. T. P. U, T. H. Suchanek, S. L. Ustin, B. J. Bond, K. D. Brosofske, N. Phillips, and R. C. Bi. 2002. Biophysical controls of carbon flows in three successional Douglas-fir stands based on eddy-covariance measurements. Tree Physiology **22**:169-177.

Chu, H., J. Chen, J. F. Gottgens, Z. Ouyang, R. John, K. Czajkowski, and R. Becker. 2014a. Net ecosystem methane and carbon dioxide exchanges in a Lake Erie coastal marsh and a nearby cropland. Journal of Geophysical Research: Biogeosciences **119**:2013JG002520.

Chu, H., J. F. Gottgens, J. Chen, G. Sun, A. R. Desai, Z. Ouyang, C. Shao, and K. Czajkowski. 2014b. Climatic variability, hydrologic anomaly, and methane emission can turn productive freshwater marshes into net carbon sources. Global Change Biology:n/a-n/a.

Cole, J. J., and N. F. Caraco. 1998. Atmospheric exchange of carbon dioxide in a low-wind oligotrophic lake measured by the addition of SF6. Limnology and Oceanography **43**:647-656.

Cole, J. J., N. F. Caraco, G. W. Kling, and T. K. Kratz. 1994. Carbon-dioxide supersaturation in the surface waters of lakes. Science **265**:1568-1570.

Coloso, J. J., J. J. Cole, and M. L. Pace. 2011. Difficulty in Discerning Drivers of Lake Ecosystem Metabolism with High-Frequency Data. Ecosystems **14**:935-948.

Commission, I. J. 1980. Phosphorus Management for the Great Lakes. Windsor, Ontario.

Coppin, P., I. Jonckheere, K. Nackaerts, B. Muys, and E. Lambin. 2004. Digital change detection methods in ecosystem monitoring: a review. International Journal of Remote Sensing **25**:1565-1596.

Council, N. R. 1982. Impacts of emerging agricultural trends on fish and wildlife habitat. National Academy Press, Washington, DC, USA.

Dahl, T. E. 1990. Wetland losses in the United States 1780's to 1980's. U.S. Fish and Wildlife Service.

Dai, A. G. 2011. Drought under global warming: a review. Wiley Interdisciplinary Reviews-Climate Change **2**:45-65.

Daubechies, I. 1990. The wavelet transform, time-frequency localization and signal analysis. IEEE Transactions on Information Theory **36**:961-1005.

Davies, W., and D. Nugegoda. 2012. Harmful algal blooms in the Gippsland Lakes, Victoria: a review. Proceedings of the Royal Society of Victoria **124**:179-192.

Dietze, M. C., R. Vargas, A. D. Richardson, P. C. Stoy, A. G. Barr, R. S. Anderson, M. A. Arain, I. T. Baker, T. A. Black, J. M. Chen, P. Ciais, L. B. Flanagan, C. M. Gough, R. F. Grant, D. Hollinger, R. C. Izaurralde, C. J. Kucharik, P. Lafleur, S. G. Liu, E. Lokupitiya, Y. Q. Luo, J. W. Munger, C. H. Peng, B. Poulter, D. T. Price, D. M. Ricciuto, W. J. Riley, A. K. Sahoo, K. Schaefer, A. E. Suyker, H. Q. Tian, C. Tonitto, H. Verbeeck, S. B. Verma, W. F. Wang, and E. S. Weng. 2011. Characterizing the performance of ecosystem models across time scales: A spectral analysis of the North American Carbon Program site-level synthesis. Journal of Geophysical Research-Biogeosciences **116**.

Dodson, S. 2004. Introduction to Limnology McGraw-Hill Science/Engineering/Math, New York.

Dracup, J. A. 1991. Drought monitoring. Stochastic Hydrology and Hydraulics **5**:261-266.

Epron, D., Y. Nouvellon, O. Roupsard, W. Mouvondy, A. Mabiala, L. Saint-Andre, R. Joffre, C. Jourdan, J. M. Bonnefond, P. Berbigier, and O. Hamel. 2004. Spatial and temporal variations of soil respiration in a Eucalyptus plantation in Congo. Forest Ecology and Management **202**:149-160.

Eugster, W., G. Kling, T. Jonas, J. P. McFadden, A. Wuest, S. MacIntyre, and F. S. Chapin. 2003. CO2 exchange between air and water in an Arctic Alaskan and midlatitude Swiss lake: Importance of convective mixing. Journal of Geophysical Research-Atmospheres **108**.

Falge, E., D. Baldocchi, R. Olson, P. Anthoni, M. Aubinet, C. Bernhofer, G. Burba, R. Ceulemans, R. Clement, H. Dolman, A. Granier, P. Gross, T. Grünwald, D. Hollinger, N.-O. Jensen, G. Katul, P. Keronen, A. Kowalski, C. T. Lai, B. E. Law, T. Meyers, J. Moncrieff, E. Moors, J. W. Munger, K. Pilegaard, Ü. Rannik, C. Rebmann, A. Suyker, J. Tenhunen, K. Tu, S. Verma, T. Vesala, K. Wilson, and S. Wofsy. 2001. Gap filling strategies for defensible annual sums of net ecosystem exchange. Agricultural and Forest Meteorology **107**:43-69.

Fang, H., S. Wei, and S. Liang. 2012. Validation of MODIS and CYCLOPES LAI products using global field measurement data. Remote Sensing of Environment **119**:43-54.

Finlay, K., P. R. Leavitt, B. Wissel, and Y. T. Prairie. 2009. Regulation of spatial and temporal variability of carbon flux in six hard-water lakes of the northern Great Plains. Limnology and Oceanography **54**:2553-2564.

Foken, T., and B. Wichura. 1996. Tools for quality assessment of surface-based flux measurements. Agricultural and Forest Meteorology **78**:83-105.

Folke, C. 2006. Resilience: The emergence of a perspective for social-ecological systems analyses. Global Environmental Change-Human and Policy Dimensions **16**:253-267.

Franz, B. A., P. J. Werdell, G. Meister, E. J. Kwiatkowska, S. W. Bailey, Z. Ahmad, and C. R. McClain. 2006. MODIS Land Bands for Ocean Remote Sensing Applications.*in* Proc. Ocean Optics XVIII, Montreal, Canada.

Frazier, P. S., and K. J. Page. 2000. Water body detection and delineation with Landsat TM data. Photogrammetric Engineering and Remote Sensing **66**:1461-1467.

Garrity, S. R., G. Bohrer, K. D. Maurer, K. L. Mueller, C. S. Vogel, and P. S. Curtis. 2011. A comparison of multiple phenology data sources for estimating seasonal transitions in deciduous forest carbon exchange. Agricultural and Forest Meteorology **151**:1741-1752.

Gleason, R. A., N. H. Euliss, B. A. Tangen, M. K. Laubhan, and B. A. Browne. 2011. USDA conservation program and practice effects on wetland ecosystem services in the Prairie Pothole Region. Ecological Applications **21**:S65-S81.

Goulden, M. L., S. D. Miller, H. R. da Rocha, M. C. Menton, H. C. de Freitas, A. Figueira, and C. A. D. de Sousa. 2004. Diel and seasonal patterns of tropical forest CO2 exchange. Ecological Applications **14**:S42-S54.

Grelle, A., and G. Burba. 2007. Fine-wire thermometer to correct CO2 fluxes by open-path analyzers for artificial density fluctuations. Agricultural and Forest Meteorology **147**:48-57.

Griffis, T. J., T. A. Black, K. Morgenstern, A. G. Barr, Z. Nesic, G. B. Drewitt, D. Gaumont-Guay, and J. H. McCaughey. 2003. Ecophysiological controls on the carbon balances of three southern boreal forests. Agricultural and Forest Meteorology **117**:53-71.

Grinsted, A., J. C. Moore, and S. Jevrejeva. 2004. Application of the cross wavelet transform and wavelet coherence to geophysical time series. Nonlinear Processes in Geophysics **11**:561-566.

Guttman, N. B., and R. G. Quayle. 1996. A historical perspective of US climate divisions. Bulletin of the American Meteorological Society **77**:293-303.

Hanson, P. C., I. Buffam, J. A. Rusak, E. H. Stanley, and C. Watras. 2014. Quantifying lake allochthonous organic carbon budgets using a simple equilibrium model. Limnology and Oceanography **59**:167-181.

Hayal, D., L. Brook, and F. Aramde. 2012. Aspects of climate change and its associated impacts on wetland ecosystem functions - a review. The Journal of American Science **8**:582-596.

Herdendorf, C. E., and M. E. Monaco. 1988. Physical and chemical limnology of the island region of Lake Erie. Ohio State University.

Huang, N. E., and Z. H. Wu. 2008. A review on Hilbert-Huang transform: method and its applications to geophysical studies. Reviews of Geophysics **46**.

Huang, S. L., D. Dahal, C. Young, G. Chander, and S. G. Liu. 2011. Integration of Palmer Drought Severity Index and remote sensing data to simulate wetland water surface from 1910 to 2009 in Cottonwood Lake area, North Dakota. Remote Sensing of Environment **115**:3377-3389.

Huotari, J., A. Ojala, E. Peltomaa, A. Nordbo, S. Launiainen, J. Pumpanen, T. Rasilo, P. Hari, and T. Vesala. 2011. Long-term direct CO2 flux measurements over a boreal lake: Five years of eddy covariance data. Geophysical Research Letters **38**:5.

Huxman, T. E., K. A. Snyder, D. Tissue, A. J. Leffler, K. Ogle, W. T. Pockman, D. R. Sandquist, D. L. Potts, and S. Schwinning. 2004. Precipitation pulses and carbon fluxes in semiarid and arid ecosystems. Oecologia **141**:254-268.

Jacobs, C. M. J., A. F. G. Jacobs, F. C. Bosveld, D. M. D. Hendriks, A. Hensen, P. S. Kroon, E. J. Moors, L. Nol, A. Schrier-Uijl, and E. M. Veenendaal. 2007. Variability of annual CO2 exchange from Dutch grasslands. Biogeosciences **4**:803-816.

Jarvis, P. G., J. M. Massheder, S. E. Hale, J. B. Moncrieff, M. Rayment, and S. L. Scott. 1997. Seasonal variation of carbon dioxide, water vapor, and energy exchanges of a boreal black spruce forest. Journal of Geophysical Research-Atmospheres **102**:28953-28966.

Johnson, R. R., F. T. Oslund, and D. R. Hertel. 2008. The past, present, and future of prairie potholes in the United States. Journal of Soil and Water Conservation **63**:84A-87A.

Johnson, W. C., B. V. Millett, T. Gilmanov, R. A. Voldseth, G. R. Guntenspergen, and D. E. Naugle. 2005. Vulnerability of northern prairie wetlands to climate change. Bioscience **55**:863-872.

Johnson, W. C., B. Werner, G. R. Guntenspergen, R. A. Voldseth, B. Millett, D. E. Naugle, M. Tulbure, R. W. H. Carroll, J. Tracy, and C. Olawsky. 2010. Prairie wetland complexes as landscape functional units in a changing climate. Bioscience **60**:128-140.

Jones, R. 2002. Landscape ecology: In theory and practice, pattern and process. Geography **87**:369-370.

Jonsson, A., J. Aberg, A. Lindroth, and M. Jansson. 2008. Gas transfer rate and CO(2) flux between an unproductive lake and the atmosphere in northern Sweden. Journal of Geophysical Research-Biogeosciences **113**:13.

Jonsson, A., G. Algesten, A. K. Bergstrom, K. Bishop, S. Sobek, L. J. Tranvik, and M. Jansson. 2007. Integrating aquatic carbon fluxes in a boreal catchment carbon budget. Journal of Hydrology **334**:141-150.

Jonsson, A., J. Karlsson, and M. Jansson. 2003. Sources of carbon dioxide supersaturation in clearwater and humic lakes in northern Sweden. Ecosystems **6**:224-235.

Jung, M., M. Reichstein, H. A. Margolis, A. Cescatti, A. D. Richardson, M. A. Arain, A. Arneth, C. Bernhofer, D. Bonal, J. Q. Chen, D. Gianelle, N. Gobron, G. Kiely, W. Kutsch, G. Lasslop, B. E. Law, A. Lindroth, L. Merbold, L. Montagnani, E. J. Moors, D. Papale, M. Sottocornola, F. Vaccari, and C. Williams. 2011. Global patterns of land-atmosphere fluxes of carbon dioxide, latent heat, and sensible heat derived from eddy covariance, satellite, and meteorological observations. Journal of Geophysical Research-Biogeosciences **116**:16.

Kantrud, H. A., G. L. Krapu, and G. A. Swanson. 1989. Prairie Basin wetlands of the Dakotas USA a Community profile. U S Fish and Wildlife Service Biological Report **85**:I.

Katul, G., C. T. Lai, K. Schafer, B. Vidakovic, J. Albertson, D. Ellsworth, and R. Oren. 2001. Multiscale analysis of vegetation surface fluxes: from seconds to years. Advances in Water Resources **24**:1119-1132.

Khomik, M., M. A. Arain, and J. H. McCaughey. 2006. Temporal and spatial variability of soil respiration in a boreal mixedwood forest. Agricultural and Forest Meteorology **140**:244-256.

Knutsen, G. A., and N. H. Euliss. 2001. Wetland restoration in the Prairie Pothole Region of North America: a literature review. U.S. Geological Survey, Reston, Virginia, USA.

Kormann, R., and F. X. Meixner. 2001. An analytical footprint model for non-neutral stratification. Boundary-Layer Meteorology **99**:207-224.

Kortelainen, P., M. Rantakari, J. T. Huttunen, T. Mattsson, J. Alm, S. Juutinen, T. Larmola, J. Silvola, and P. J. Martikainen. 2006. Sediment respiration and lake trophic state are important predictors of large CO2 evasion from small boreal lakes. Global Change Biology **12**:1554-1567.

Kull, O., and B. Kruijt. 1998. Leaf photosynthetic light response: a mechanistic model for scaling photosynthesis to leaves and canopies. Functional Ecology **12**:767-777.

Kwon, H., E. Pendall, B. E. Ewers, M. Cleary, and K. Naithani. 2008. Spring drought regulates summer net ecosystem CO2 exchange in a sagebrush-steppe ecosystem. Agricultural and Forest Meteorology **148**:381-391.

Landres, P. B., P. Morgan, and F. J. Swanson. 1999. Overview of the use of natural variability concepts in managing ecological systems. Ecological Applications **9**:1179-1188.

Larson, D. L. 1995. Effects of climate on number of northern prairie wetlands. Climatic Change **30**:169-180.

Law, B. E., E. Falge, L. Gu, D. D. Baldocchi, P. Bakwin, P. Berbigier, K. Davis, A. J. Dolman, M. Falk, J. D. Fuentes, A. Goldstein, A. Granier, A. Grelle, D. Hollinger, I. A. Janssens, P. Jarvis, N. O. Jensen, G. Katul, Y. Mahli, G. Matteucci, T. Meyers, R. Monson, W. Munger, W. Oechel, R. Olson, K. Pilegaard, K. T. Paw, H. Thorgeirsson, R. Valentini, S. Verma, T. Vesala, K. Wilson, and S. Wofsy. 2002. Environmental controls over carbon

dioxide and water vapor exchange of terrestrial vegetation. Agricultural and Forest Meteorology **113**:97-120.

Lee, X., W. Massman, and B. Law. 2004. Handbook in micrometeorology: A guide for surface flux measurement and analysis. Kluwer Academic Publishers, Dordrecht, the Netherlands.

Lesht, B. M., R. P. Barbiero, and G. J. Warren. 2012. Satellite ocean color algorithms: A review of applications to the Great Lakes. Journal of Great Lakes Research **38**:49-60.

Liu, J., J. M. Chen, J. Cihlar, and W. M. Park. 1997. A process-based boreal ecosystem productivity simulator using remote sensing inputs. Remote Sensing of Environment **62**:158-175.

Liu, Y. F., X. Song, G. R. Yu, X. M. Sun, X. F. Wen, and Y. R. Chen. 2005. Seasonal variation of CO2 flux and its environmental factors in evergreen coniferous plantation. Science in China Series D-Earth Sciences **48**:123-132.

Livingston, R. J., and A. Prasad. 1997. Blue green algae blooms in a north Florida lake: Long-term response to nutrient loading and interspecific competition. Phycologia **36**:65-65.

Mainuddin, M., and M. Kirby. 2009. Spatial and temporal trends of water productivity in the lower Mekong River Basin. Agricultural Water Management **96**:1567-1578.

Maritorena, S., D. A. Siegel, and A. R. Peterson. 2002. Optimization of a semianalytical ocean color model for global-scale applications. Applied Optics **41**:2705-2714.

Maselli, F., M. Chiesi, M. Moriondo, L. Fibbi, M. Bindi, and S. W. Running. 2009. Modelling the forest carbon budget of a Mediterranean region through the integration of ground and satellite data. Ecological Modelling **220**:330-342.

Massel, S. R. 2001. Wavelet analysis for processing of ocean surface wave records. Ocean Engineering **28**:957-987.

Massman, W. J., and X. Lee. 2002. Eddy covariance flux corrections and uncertainties in long-term studies of carbon and energy exchanges. Agricultural and Forest Meteorology **113**:121-144.

Meng, J., X. Du, and B. Wu. 2013. Generation of high spatial and temporal resolution NDVI and its application in crop biomass estimation. International Journal of Digital Earth **6**:203-218.

Mihanovic, H., M. Orlic, and Z. Pasaric. 2009. Diurnal thermocline oscillations driven by tidal flow around an island in the Middle Adriatic. Journal of Marine Systems **78**:S157-S168.

Mitsch, W. J., and J. G. Gosselink. 2007. Wetlands. John Wiley & Sons, Hoboken, NJ.

Moffat, A. M., D. Papale, M. Reichstein, D. Y. Hollinger, A. D. Richardson, A. G. Barr, C. Beckstein, B. H. Braswell, G. Churkina, A. R. Desai, E. Falge, J. H. Gove, M. Heimann, D. F. Hui, A. J. Jarvis, J. Kattge, A. Noormets, and V. J. Stauch. 2007. Comprehensive comparison of gap-filling techniques for eddy covariance net carbon fluxes. Agricultural and Forest Meteorology **147**:209-232.

Moorhead, D. L., T. B. Bridgeman, and J. Morris. 2003. Changes in water quality of Maumee Bay, Lake Erie: 1974 - 2002. IAGLR Conference Program and Abstracts **46**:129-130.

Mueller, K. L., V. Yadav, P. S. Curtis, C. Vogel, and A. M. Michalak. 2010. Attributing the variability of eddy-covariance CO2 flux measurements across temporal scales using geostatistical regression for a mixed northern hardwood forest. Global Biogeochemical Cycles **24**.

Ng, E. K. W., and J. C. L. Chan. 2012. Geophysical applications of partial wavelet coherence and multiple wavelet coherence. Journal of Atmospheric and Oceanic Technology **29**:1845-1853.

Niemuth, N. D., B. Wangler, and R. E. Reynolds. 2010. Spatial and Temporal Variation in Wet Area of Wetlands in the Prairie Pothole Region of North Dakota and South Dakota. Wetlands **30**:1053-1064.

Noormets, A., S. G. McNulty, J. L. DeForest, G. Sun, Q. Li, and J. Chen. 2008. Drought during canopy development has lasting effect on annual carbon balance in a deciduous temperate forest. New Phytologist **179**:818-828.

O'Reilly, J. E. 2000. Ocean Color Chlorophyll a Algorithms for SeaWiFS, OC2 and OC4: Version 4. NOAA, National Marine Fisheries Service, Narragansett, Rhode Island.

Ouyang, Z., J. Chen, R. Becker, H. Chu, J. Xie, C. Shao, and R. John. 2014. Disentangling the confounding effects of PAR and air temperature on net ecosystem exchange at multiple time scales. Ecological Complexity **19**:46-58.

Ozesmi, S. L., and M. E. Bauer. 2002. Satellite remote sensing of wetlands. Wetlands Ecology and Management **10**:381-402.

Pachauri, R. K., R. A. Myles, R. B. Vicente, and B. John. 2014. Climate Change 2014 Synthesis Report.

Palmer, W. C. 1965. Meteorological drought. U.S. Department of Commerce Weather Bureau, Washington DC.

Parry, M. L., O. F. Canziani, J. P. Palutikof, P. J. v. d. Linden, and C. E. Hanson. 2007. Contribution of working group II to the fourth assessment report of the Intergovernmental Panel on Climate Change, 2007. Cambridge University Press, Cambridge,United Kingdom and New York, NY, USA.

Paul, J. F., R. Kasprzyk, and W. Lick. 1982. Turbidity in the western basin of Lake Erie. Journal of Geophysical Research-Oceans and Atmospheres **87**:5779-5784.

Peng, Z. K., M. R. Jackson, J. A. Rongong, F. L. Chu, and R. M. Parkin. 2009. On the energy leakage of discrete wavelet transform. Mechanical Systems and Signal Processing **23**:330-343.

Penuelas, J., and I. Filella. 2001. Phenology - Responses to a warming world. Science **294**:793

Rantakari, M., and P. Kortelainen. 2005. Interannual variation and climatic regulation of the CO2 emission from large boreal lakes. Global Change Biology **11**:1368-1380.

Reichstein, M., E. Falge, D. Baldocchi, D. Papale, M. Aubinet, P. Berbigier, C. Bernhofer, N. Buchmann, T. Gilmanov, A. Granier, T. Grunwald, K. Havrankova, H. Ilvesniemi, D. Janous, A. Knohl, T. Laurila, A. Lohila, D. Loustau, G. Matteucci, T. Meyers, F. Miglietta, J. M. Ourcival, J. Pumpanen, S. Rambal, E. Rotenberg, M. Sanz, J. Tenhunen, G. Seufert, F. Vaccari, T. Vesala, D. Yakir, and R. Valentini. 2005. On the separation of net ecosystem exchange into assimilation and ecosystem respiration: review and improved algorithm. Global Change Biology **11**:1424-1439.

Reis, S., and H. M. Yilmaz. 2008. Temporal monitoring of water level changes in Seyfe Lake using remote sensing. Hydrological Processes **22**:4448-4454.

Richardson, A. D., D. Y. Hollinger, J. D. Aber, S. V. Ollinger, and B. H. Braswell. 2007. Environmental variation is directly responsible for short- but not long-term variation in forest-atmosphere carbon exchange. Global Change Biology **13**:788-803.

Richardson, A. D., D. Y. Hollinger, G. G. Burba, K. J. Davis, L. B. Flanagan, G. G. Katul, J. W. Munger, D. M. Ricciuto, P. C. Stoy, A. E. Suyker, S. B. Verma, and S. C. Wofsy. 2006. A multi-site analysis of random error in tower-based measurements of carbon and energy fluxes. Agricultural and Forest Meteorology **136**:1-18.

Richardson, A. D., D. Y. Hollinger, D. B. Dail, J. T. Lee, J. W. Munger, and J. O'Keefe. 2009. Influence of spring phenology on seasonal and annual carbon balance in two contrasting New England forests. Tree Physiology **29**:321-331.

Rosenberry, D. O., D. I. Stannard, T. C. Winter, and M. L. Martinez. 2004. Comparison of 13 equations for determining evapotranspiration from a prairie wetland, Cottonwood Lake Area, North Dakota, USA. Wetlands **24**:483-497.

Ryu, Y., J. Verfaillie, C. Macfarlane, H. Kobayashi, O. Sonnentag, R. Vargas, S. Ma, and D. D. Baldocchi. 2012. Continuous observation of tree leaf area index at ecosystem scale using upward-pointing digital cameras. Remote Sensing of Environment **126**:116-125.

Schmer, M. R., R. B. Mitchell, K. P. Vogel, W. H. Schacht, and D. B. Marx. 2010. Spatial and Temporal Effects on Switchgrass Stands and Yield in the Great Plains. Bioenergy Research **3**:159-171.

Schot, P. P., and S. M. Pieber. 2012. Spatial and temporal variations in shallow wetland groundwater quality. Journal of Hydrology **422**:43-52.

Schotanus, P., F. T. M. Nieuwstadt, and H. A. R. Bruin. 1983. Temperature measurement with a sonic anemometer and its application to heat and moisture fluxes. Boundary-Layer Meteorology **26**:81-93.

Sellers, P., R. H. Hesslein, and C. A. K. Kelly. 1995. Continuous measurement of CO2 for estimation of air-water fluxes in lakes: An in situ technique. Limnology and Oceanography **40**:575-581.

Shao, C., J., C. A. Chen, C. Stepien, H. Chu, Ouyang, T. Bridgeman, K. P. Czajkowski, r. Becker, and R. John. 2015. iurnal to annual changes in latent, sensible heat and CO2 fluxes over a Laurentian Great Lake: A case study in western Lake Erie. Journal of Geographic Research – Biogeosciences.

Siqueira, M. B., G. G. Katul, D. A. Sampson, P. C. Stoy, J. Y. Juang, H. R. McCarthy, and R. Oren. 2006. Multiscale model intercomparisons of CO2 and H2O exchange rates in a maturing southeastern US pine forest. Global Change Biology **12**:1189-1207.

Solomon, C. T., D. A. Bruesewitz, D. C. Richardson, K. C. Rose, M. C. Van de Bogert, P. C. Hanson, T. K. Kratz, B. Larget, R. Adrian, B. L. Babin, C. Y. Chiu, D. P. Hamilton, E. E. Gaiser, S. Hendricks, V. Istvanovics, A. Laas, D. M. O'Donnell, M. L. Pace, E. Ryder, P. A. Staehr, T. Torgersen, M. J. Vanni, K. C. Weathers, and G. W. Zhu. 2013. Ecosystem respiration: Drivers of daily variability and background respiration in lakes around the globe. Limnology and Oceanography **58**:849-866.

Solomon, S., M. Qin, M. Manning, M. Marquis, K. Averyt, M. M. B. Tignor, H. L. Miller, and Z. Chen. 2007. Climate change 2007. Cambridge Univeristy Press, Cambridge, UK.

Sorenson, L. G., R. Goldberg, T. L. Root, and M. G. Anderson. 1998. Potential effects of global warming on waterfowl populations breeding in the Northern Great Plains. Climatic Change **40**:343-369.

Steffen, M. M., B. S. Belisle, S. B. Watson, G. L. Boyer, and S. W. Wilhelm. 2014. Status, causes and controls of cyanobacterial blooms in Lake Erie. Journal of Great Lakes Research **40**:215-225.

Stoy, P. C., M. C. Dietze, A. D. Richardson, R. Vargas, A. G. Barr, R. S. Anderson, M. A. Arain, I. T. Baker, T. A. Black, J. M. Chen, R. B. Cook, C. M. Gough, R. F. Grant, D. Y. Hollinger, R. C. Izaurralde, C. J. Kucharik, P. Lafleur, B. E. Law, S. Liu, E. Lokupitiya, Y. Luo, J. W. Munger, C. Peng, B. Poulter, D. T. Price, D. M. Ricciuto, W. J. Riley, A. K. Sahoo, K. Schaefer, C. R. Schwalm, H. Tian, H. Verbeeck, and E. Weng. 2013. Evaluating the agreement between measurements and models of net ecosystem exchange at different times and timescales using wavelet coherence: an example using data from the North American Carbon Program Site-Level Interim Synthesis. Biogeosciences **10**:6893-6909.

Stoy, P. C., G. G. Katul, M. B. S. Siqueira, J. Y. Juang, H. R. McCarthy, H. S. Kim, A. C. Oishi, and R. Oren. 2005. Variability in net ecosystem exchange from hourly to inter-annual time scales at adjacent pine and hardwood forests: a wavelet analysis. Tree Physiology **25**:887-902.

Stoy, P. C., A. D. Richardson, D. D. Baldocchi, G. G. Katul, J. Stanovick, M. D. Mahecha, M. Reichstein, M. Detto, B. E. Law, G. Wohlfahrt, N. Arriga, J. Campos, J. H. McCaughey, L. Montagnani, K. T. P. U, S. Sevanto, and M. Williams. 2009. Biosphere-atmosphere exchange of CO2 in relation to climate: a cross-biome analysis across multiple time scales. Biogeosciences **6**:2297-2312.

Sun, G., P. Caldwell, A. Noormets, S. G. McNulty, E. Cohen, J. M. Myers, J. C. Domec, E. Treasure, Q. Z. Mu, J. F. Xiao, R. John, and J. Q. Chen. 2011. Upscaling key ecosystem functions across the conterminous United States by a water-centric ecosystem model. Journal of Geophysical Research-Biogeosciences **116**:16.

Sun, Z. G., X. H. Long, C. M. Sun, W. Zhou, W. M. Ju, and J. L. Li. 2013. Evaluation of net primary productivity and its spatial and temporal patterns in southern China's grasslands. Rangeland Journal **35**:331-338.

Tang, J. W., D. D. Baldocchi, and L. Xu. 2005. Tree photosynthesis modulates soil respiration on a diurnal time scale. Global Change Biology **11**:1298-1304.

Tjoelker, M. G., J. Oleksyn, and P. B. Reich. 2001. Modelling respiration of vegetation: evidence for a general temperature-dependent Q(10). Global Change Biology **7**:223-230.

Tong, L. G., X. L. Xu, Y. Fu, and S. Li. 2014. Wetland Changes and Their Responses to Climate Change in the "Three-River Headwaters" Region of China since the 1990s. Energies **7**:2515-2534.

Torrence, C., and G. P. Compo. 1998. A practical guide to wavelet analysis. Bulletin of the American Meteorological Society **79**:61-78.

Torrence, C., and P. J. Webster. 1998. The annual cycle of persistence in the El Nino Southern Oscillation. Quarterly Journal of the Royal Meteorological Society **124**:1985-2004.

Tranvik, L. J., J. A. Downing, J. B. Cotner, S. A. Loiselle, R. G. Striegl, T. J. Ballatore, P. Dillon, K. Finlay, K. Fortino, L. B. Knoll, P. L. Kortelainen, T. Kutser, S. Larsen, I. Laurion, D. M. Leech, S. L. McCallister, D. M. McKnight, J. M. Melack, E. Overholt, J. A. Porter, Y. Prairie, W. H. Renwick, F. Roland, B. S. Sherman, D. W. Schindler, S. Sobek, A. Tremblay, M. J. Vanni, A. M. Verschoor, E. von Wachenfeldt, and G. A. Weyhenmeyer. 2009. Lakes and reservoirs as regulators of carbon cycling and climate. Limnology and Oceanography **54**:2298-2314.

Urbanski, S., C. Barford, S. Wofsy, C. Kucharik, E. Pyle, J. Budney, K. McKain, D. Fitzjarrald, M. Czikowsky, and J. W. Munger. 2007. Factors controlling CO2 exchange on timescales from hourly to decadal at Harvard Forest. Journal of Geophysical Research-Biogeosciences **112**.

van der Valk, A. G. 2005. Water-level fluctuations in North American prairie wetlands. Hydrobiologia **539**:171-188.

van Dijk, A., A. J. Dolman, and E. D. Schulze. 2005. Radiation, temperature, and leaf area explain ecosystem carbon fluxes in boreal and temperate European forests. Global Biogeochemical Cycles **19**.

Verduin, J. 1956. Primary Production in Lakes. Limnology and Oceanography **1**:85-91.

Vesala, T., J. Huotari, U. Rannik, T. Suni, S. Smolander, A. Sogachev, S. Launiainen, and A. Ojala. 2006. Eddy covariance measurements of carbon exchange and latent and sensible heat fluxes over a boreal lake for a full open-water period. Journal of Geophysical Research-Atmospheres **111**:12.

Webb, E. K., G. I. Pearman, and R. Leuning. 1980. Correction of flux measurements for density effects due to heat and water-vapor transfer. Quarterly Journal of the Royal Meteorological Society **106**:85-100.

Wetzel, R. G. 2001. Limnology: Lake and River Ecosystems. Acedemic Press, New York.

Wilczak, J. M., S. P. Oncley, and S. A. Stage. 2001. Sonic anemometer tilt correction algorithms. Boundary-Layer Meteorology **99**:127-150.

Wilson, D. J., A. W. Western, and R. B. Grayson. 2004. Identifying and quantifying sources of variability in temporal and spatial soil moisture observations. Water Resources Research **40**.

Winter, T. C., and D. O. Rosenberry. 1998. Hydrology of prairie pothole wetlands during drought and deluge: A 17-year study of the Cottonwood Lake wetland complex in North Dakota in the perspective of longer term measured and proxy hydrological records. Climatic Change **40**:189-209.

Withey, P., and G. C. van Kooten. 2011. The effect of climate change on optimal wetlands and waterfowl management in Western Canada. Ecological Economics **70**:798-805.

Xiao, J. F., K. J. Davis, N. M. Urban, K. Keller, and N. Z. Saliendra. 2011. Upscaling carbon fluxes from towers to the regional scale: Influence of parameter variability and land cover representation on regional flux estimates. Journal of Geophysical Research-Biogeosciences **116**:15.

Xiao, X. M., Q. Y. Zhang, B. Braswell, S. Urbanski, S. Boles, S. Wofsy, M. Berrien, and D. Ojima. 2004. Modeling gross primary production of temperate deciduous broadleaf forest using satellite images and climate data. Remote Sensing of Environment **91**:256-270.

Xie, J., J. Chen, G. Sun, H. Chu, A. Noormets, Z. Ouyang, R. John, S. Wan, and W. Guan. 2014a. Long-term variability and environmental control of the carbon cycle in an oak-dominated temperate forest. Forest Ecology and Management **313**:319-328.

Xie, J., J. Q. Chen, G. Sun, H. S. Chu, A. Noormets, Z. T. Ouyang, R. John, S. Q. Wan, and W. B. Guan. 2014b. Long-term variability and environmental control of the carbon cycle in an oak-dominated temperate forest. Forest Ecology and Management **313**:319-328.

Xu, F. L., K. C. Lam, R. W. Dawson, S. Tao, and Y. D. Chen. 2004. Long-term temporal-spatial dynamics of marine coastal water quality in the Tolo Harbor, Hong Kong, China. Journal of Environmental Sciences-China **16**:161-166.

Xu, H. Q. 2006. Modification of normalised difference water index (NDWI) to enhance open water features in remotely sensed imagery. International Journal of Remote Sensing **27**:3025-3033.

Yi, C. X., D. Ricciuto, R. Li, J. Wolbeck, X. Y. Xu, M. Nilsson, L. Aires, J. D. Albertson, C. Ammann, M. A. Arain, A. C. de Araujo, M. Aubinet, M. Aurela, Z. Barcza, A. Barr, P. Berbigier, J. Beringer, C. Bernhofer, A. T. Black, P. V. Bolstad, F. C. Bosveld, M. S. J. Broadmeadow, N. Buchmann, S. P. Burns, P. Cellier, J. M. Chen, J. Q. Chen, P. Ciais, R. Clement, B. D. Cook, P. S. Curtis, D. B. Dail, E. Dellwik, N. Delpierre, A. R. Desai, S. Dore, D. Dragoni, B. G. Drake, E. Dufrene, A. Dunn, J. Elbers, W. Eugster, M. Falk, C. Feigenwinter, L. B. Flanagan, T. Foken, J. Frank, J. Fuhrer, D. Gianelle, A. Goldstein, M. Goulden, A. Granier, T. Grunwald, L. Gu, H. Q. Guo, A. Hammerle, S. J. Han, N. P. Hanan, L. Haszpra, B. Heinesch, C. Helfter, D. Hendriks, L. B. Hutley, A. Ibrom, C. Jacobs, T. Johansson, M. Jongen, G. Katul, G. Kiely, K. Klumpp, A. Knohl, T. Kolb, W. L. Kutsch, P. Lafleur, T. Laurila, R. Leuning, A. Lindroth, H. P. Liu, B. Loubet, G. Manca, M. Marek, H. A. Margolis, T. A. Martin, W. J. Massman, R. Matamala, G. Matteucci, H. McCaughey, L. Merbold, T. Meyers, M. Migliavacca, F. Miglietta, L. Misson, M. Moelder, J. Moncrieff, R. K. Monson, L. Montagnani, M. Montes-Helu, E. Moors, C. Moureaux, M. M. Mukelabai, J. W. Munger, M. Myklebust, Z. Nagy, A. Noormets, W. Oechel, R. Oren, S. G. Pallardy, T. P. U. Kyaw, J. S. Pereira, K. Pilegaard, K. Pinter, C. Pio, G. Pita, T. L. Powell, S. Rambal, J. T. Randerson, C. von Randow, C. Rebmann, J. Rinne, F. Rossi, N. Roulet, R. J. Ryel, J. Sagerfors, N. Saigusa, M. J. Sanz, G. S. Mugnozza, H. P. Schmid, G. Seufert, M. Siqueira, J. F. Soussana, G. Starr, M. A. Sutton, J. Tenhunen, Z. Tuba, J. P. Tuovinen, R. Valentini, C. S. Vogel, J. X. Wang, S. Q. Wang, W. G. Wang, L. R. Welp, X. F. Wen, S. Wharton, M. Wilkinson, C. A. Williams, G. Wohlfahrt, S. Yamamoto, G. R. Yu, R. Zampedri, B. Zhao, and X. Q. Zhao. 2010. Climate control of terrestrial carbon exchange across biomes and continents. Environmental Research Letters **5**.

Yu, G. R., X. J. Zhu, Y. L. Fu, H. L. He, Q. F. Wang, X. F. Wen, X. R. Li, L. M. Zhang, L. Zhang, W. Su, S. G. Li, X. M. Sun, Y. P. Zhang, J. H. Zhang, J. H. Yan, H. M. Wang, G. S. Zhou, B. R. Jia, W. H. Xiang, Y. N. Li, L. Zhao, Y. F. Wang, P. L. Shi, S. P. Chen, X. P. Xin, F. H. Zhao, Y. Y. Wang, and C. L. Tong. 2013. Spatial patterns and climate drivers of carbon fluxes in terrestrial ecosystems of China. Global Change Biology **19**:798-810.

Yuan, W. P., S. G. Liu, G. R. Yu, J. M. Bonnefond, J. Q. Chen, K. Davis, A. R. Desai, A. H. Goldstein, D. Gianelle, F. Rossi, A. E. Suyker, and S. B. Verma. 2010. Global estimates

of evapotranspiration and gross primary production based on MODIS and global meteorology data. Remote Sensing of Environment **114**:1416-1431.

Zedler, J. B., and S. Kercher. 2005. Wetland resources: Status, trends, ecosystem services, and restorability. Pages 39-74 Annual Review of Environment and Resources. Annual Reviews, Palo Alto.

Zhang, B., F. W. Schwartz, and G. Liu. 2009. Systematics in the size structure of prairie pothole lakes through drought and deluge. Water Resources Research **45**:W04421.